doi:10.1093/brain/awx350 BRAIN 2018: 0; 1–37 | 1

BRAIN
A JOURNAL OF NEUROLOGY

Concussion, microvascular injury, and early tauopathy in young athletes after impact head injury and an impact concussion mouse model

Chad A. Tagge,[1,2,*] Andrew M. Fisher,[1,2,*] Olga V. Minaeva,[1,2,3,*] Amanda Gaudreau-Balderrama,[1,2] Juliet A. Moncaster,[1,3,4] Xiao-Lei Zhang,[5] Mark W. Wojnarowicz,[1,4] Noel Casey,[1,6] Haiyan Lu,[7] Olga N. Kokiko-Cochran,[7,†] Sudad Saman,[8] Maria Ericsson,[9] Kristen D. Onos,[10] Ronel Veksler,[11] Vladimir V. Senatorov, Jr,[12] Asami Kondo,[13] Xiao Z. Zhou,[13] Omid Miry,[5] Linnea R. Vose,[5] Katisha R. Gopaul,[5] Chirag Upreti,[5] Christopher J. Nowinski,[4,14] Robert C. Cantu,[4,14,15] Victor E. Alvarez,[14,16] Audrey M. Hildebrandt,[16] Erich S. Franz,[1,2] Janusz Konrad,[2] James A. Hamilton,[4] Ning Hua,[4] Yorghos Tripodis,[14,17] Andrew T. Anderson,[18] Gareth R. Howell,[10] Daniela Kaufer,[12,19] Garth F. Hall,[8] Kun P. Lu,[13] Richard M. Ransohoff,[7,‡] Robin O. Cleveland,[20] Neil W. Kowall,[4,14,16] Thor D. Stein,[4,14,16] Bruce T. Lamb,[7,§] Bertrand R. Huber,[4,14,16,21] William C. Moss,[18] Alon Friedman,[11,22] Patric K. Stanton,[5] Ann C. McKee,[4,14,16] Lee E. Goldstein[1,2,3,4,6,14]

*These authors contributed equally to this work.

The mechanisms underpinning concussion, traumatic brain injury, and chronic traumatic encephalopathy, and the relationships between these disorders, are poorly understood. We examined post-mortem brains from teenage athletes in the acute-subacute period after mild closed-head impact injury and found astrocytosis, myelinated axonopathy, microvascular injury, perivascular neuroinflammation, and phosphorylated tau protein pathology. To investigate causal mechanisms, we developed a mouse model of lateral closed-head impact injury that uses momentum transfer to induce traumatic head acceleration. Unanaesthetized mice subjected to unilateral impact exhibited abrupt onset, transient course, and rapid resolution of a concussion-like syndrome characterized by altered arousal, contralateral hemiparesis, truncal ataxia, locomotor and balance impairments, and neurobehavioural deficits. Experimental impact injury was associated with axonopathy, blood–brain barrier disruption, astrocytosis, microgliosis (with activation of triggering receptor expressed on myeloid cells, TREM2), monocyte infiltration, and phosphorylated tauopathy in cerebral cortex ipsilateral and subjacent to impact. Phosphorylated tauopathy was detected in ipsilateral axons by 24 h, bilateral axons and soma by 2 weeks, and distant cortex bilaterally at 5.5 months post-injury. Impact pathologies co-localized with serum albumin extravasation in the brain that was diagnostically detectable in living mice by dynamic contrast-enhanced MRI. These pathologies were also accompanied by early, persistent, and bilateral impairment in axonal conduction velocity in the hippocampus and defective long-term potentiation of synaptic neurotransmission in the medial prefrontal cortex, brain regions distant from acute brain injury. Surprisingly, acute neurobehavioural deficits at the time of injury did not correlate with blood–brain barrier disruption, microgliosis, neuroinflammation, phosphorylated tauopathy, or electrophysiological dysfunction. Furthermore, concussion-like deficits were observed after impact injury, but not after blast exposure under experimental conditions matched for head kinematics. Computational modelling showed that impact injury generated focal point loading on the head and seven-fold greater peak shear stress in the brain compared to blast exposure. Moreover, intracerebral shear stress peaked before onset of gross head motion. By comparison, blast induced distributed force loading on the head and diffuse, lower magnitude shear

Received March 27, 2017. Revised October 2, 2017. Accepted October 29, 2017

stress in the brain. We conclude that force loading mechanics at the time of injury shape acute neurobehavioural responses, structural brain damage, and neuropathological sequelae triggered by neurotrauma. These results indicate that closed-head impact injuries, independent of concussive signs, can induce traumatic brain injury as well as early pathologies and functional sequelae associated with chronic traumatic encephalopathy. These results also shed light on the origins of concussion and relationship to traumatic brain injury and its aftermath.

1 Molecular Aging and Development Laboratory, Boston University School of Medicine, Boston, MA 02118, USA
2 Boston University College of Engineering, Boston, MA 02215, USA
3 Boston University Photonics Center, Boston University, Boston, MA 02215, USA
4 Boston University School of Medicine, Boston, MA 02118, USA
5 Department of Cell Biology and Anatomy, New York Medical College, Valhalla, NY 10595, USA
6 The Center for Biometals and Metallomics, Boston University School of Medicine, Boston, MA 02118, USA
7 Lerner Research Institute, Cleveland Clinic, 9500 Euclid Ave., Cleveland, OH 44195, USA
8 Department of Biological Sciences, University of Massachusetts Lowell, Lowell, MA 01854, USA
9 Electron Microscope Facility, Harvard Medical School, Boston, MA 02115, USA
10 The Jackson Laboratory, Bar Harbor, ME 04609, USA
11 Departments of Brain and Cognitive Sciences, Physiology and Cell Biology, Zlotowski Center for Neuroscience, Ben-Gurion University of the Negev, Beer-Sheva 84105, Israel
12 Helen Wills Neuroscience Institute, University of California, Berkeley, Berkeley, CA 94720, USA
13 Department of Medicine, Beth Israel Deaconess Medical Center, Harvard Medical School, Boston, MA 02215, USA
14 Alzheimer's Disease Center, CTE Program, Boston University School of Medicine, Boston, MA 02118, USA
15 Department of Neurosurgery, Emerson Hospital, Concord, MA 01742, USA
16 VA Boston Healthcare System, Boston, MA 02130, USA
17 Department of Biostatistics, Boston University School of Public Health, Boston, MA 02118, USA
18 Lawrence Livermore National Laboratory, Livermore, CA 94551, USA
19 Department of Integrative Biology, University of California, Berkeley, Berkeley, CA 94720, USA
20 Institute of Biomedical Engineering, University of Oxford, Oxford OX3 7DQ, UK
21 National Center for PTSD, VA Boston Healthcare System, Boston, MA 02130, USA
22 Department of Medical Neuroscience, Brain Repair Center, Dalhousie University, Halifax, B3H 4R2, Canada

[†]Present address: Department of Neuroscience, The Ohio State University, Columbus, OH 43210, USA

[‡]Present address: Biogen Idec, Cambridge, MA 02142, USA

[$]Present address: Stark Neurosciences Research Institute, Indiana University School of Medicine, Indianapolis, IN 46202, USA

Correspondence to: Lee E. Goldstein, MD, PhD
Boston University School of Medicine, 670 Albany Street, Boston, MA 02118, USA
E-mail: lgold@bu.edu

Keywords: concussion; traumatic brain injury; chronic traumatic encephalopathy; tau protein; TREM2

Abbreviations: CTE = chronic traumatic encephalopathy; LTP = long-term potentiation; TBI = traumatic brain injury

Introduction

Closed-head impact injuries are a common cause of concussion (Ropper and Gorson, 2007; Harmon *et al.*, 2013; McCrory *et al.*, 2013; Sharp and Jenkins, 2015) and traumatic brain injury (TBI) (Langlois *et al.*, 2006; Menon *et al.*, 2010; Jordan, 2013; Sharp *et al.*, 2016). These injuries are also associated with post-traumatic sequelae (Guskiewicz *et al.*, 2007*a*; Ropper and Gorson, 2007; Blennow *et al.*, 2012; Smith *et al.*, 2013*b*), including late-life cognitive decline, neurodegenerative disease, and dementia (Guskiewicz *et al.*, 2005; Gavett *et al.*, 2010; Lehman *et al.*, 2012; Stamm *et al.*, 2015; Stein *et al.*, 2015*b*; Montenigro *et al.*, 2017). Emerging evidence implicates repetitive neurotrauma, including sports-related closed-head impact injuries, as a major risk factor for later development of chronic traumatic encephalopathy (CTE), a progressive tau protein neurodegenerative disease (McKee *et al.*, 2013, 2016; Mez *et al.*, 2017).

An association between sports-related head injuries and chronic neuropsychiatric disturbances was first described by Martland as the 'punch-drunk syndrome' of pugilists (Martland, 1928). Parker and later Millspauch variously dubbed the same condition 'traumatic encephalopathy' (Parker, 1934) and 'dementia pugilistica' (Millspaugh, 1937). Critchley proposed the name 'chronic traumatic encephalopathy' (Critchley, 1949, 1957) to capture the progressive long-term nature of the disorder. CTE is now recognized as a distinct tau protein neurodegenerative disease that is neuropathologically defined by perivascular

accumulation of abnormally phosphorylated tau protein in the depths of cortical sulci (McKee *et al.*, 2016). Based on the presence of this distinctive lesion, CTE has been confirmed in post-mortem brains from individuals across a wide age range, including teenagers and young adults (McKee *et al.*, 2013; Bieniek *et al.*, 2015; Mez *et al.*, 2017). Modern case series have documented CTE neuropathology in contact sport athletes with repetitive concussive and subconcussive head injuries (Omalu *et al.*, 2005; McKee *et al.*, 2009, 2013; Mez *et al.*, 2017) as well as military veterans with combat-related blast exposure (Omalu *et al.*, 2011; Goldstein *et al.*, 2012; Shively *et al.*, 2016). In addition, deep sulcal tau pathology has been reported in long-term TBI survivors of single-episode neurotrauma (Johnson *et al.*, 2012). While the preponderance of reported CTE cases include a history of repeated mild TBI, a subset (~20% of cases) is notable for absence of prior concussion (McKee *et al.*, 2014; Bieniek *et al.*, 2015; Stein *et al.*, 2015*a*). This observation suggests that repeated head injuries, even in the absence of frank concussion, may induce brain pathologies associated with CTE.

Mild forms of TBI (Kay *et al.*, 1993; Carroll *et al.*, 2004; Ruff *et al.*, 2009; Menon *et al.*, 2010; Katz *et al.*, 2014; Kristman *et al.*, 2014) account for the majority of head injuries worldwide (Roozenbeek *et al.*, 2013; Bazarian *et al.*, 2014; Gardner and Yaffe, 2015). While the pathogenesis of CTE is unknown, emerging evidence points to a putative causal association with neurotrauma (Omalu *et al.*, 2005, 2011; McKee *et al.*, 2009, 2013; Goldstein *et al.*, 2014; Montenigro *et al.*, 2017). Recent research has shown that contact sport athletes with repetitive head injuries and military veterans with blast exposure demonstrate similar patterns of post-mortem CTE neuropathology (Omalu *et al.*, 2005, 2011; McKee *et al.*, 2009, 2010, 2013; Goldstein *et al.*, 2012; Shively *et al.*, 2016). These observations support the hypothesis that neurotrauma induced by different injuries triggers common pathogenic mechanisms that induce convergent CTE neuropathology. This hypothesis is further supported by research showing that laboratory mice exposed to experimental blast develop progressive brain pathologies and functional sequelae that resemble CTE in humans (Goldstein *et al.*, 2012; Huber *et al.*, 2013; Kondo *et al.*, 2015). This experimental work implicates traumatic head motion as a plausible mechanism underpinning the observed similarities in human CTE brain pathology despite differences in the mechanisms of injury. Based on this evidence, we hypothesized that biomechanical and pathophysiological determinants underpinning blast neurotrauma would also drive early CTE neuropathology after closed-head impact injury (Goldstein *et al.*, 2012; Ghajari *et al.*, 2017). Furthermore, emerging clinical evidence (Guskiewicz *et al.*, 2007*b*; Bazarian *et al.*, 2014; Davenport *et al.*, 2014; Talavage *et al.*, 2014) and clinicopathological correlation analysis (McKee *et al.*, 2013, 2014, 2015; Stein *et al.*, 2015*a*; Mez *et al.*, 2017) suggest that TBI and CTE pathobiology may be independent of the mechanisms that trigger concussion. These observations suggest that repeat head injuries, even in the absence of concussion, may induce TBI and CTE brain pathologies.

Despite growing awareness of links between head injury and CTE, the substrates and mechanisms underpinning this association, and relationships to concussion and TBI, remain largely unknown and matters of significant controversy. Most notably, there is insufficient knowledge regarding changes in brain structure and function during the acute-subacute period after head injury that may represent the earliest antecedent pathologies of CTE.

Here we developed a novel mouse model of lateral closed-head concussive impact injury that produces head kinematics matched to a companion blast neurotrauma mouse model (Goldstein *et al.*, 2012; Kondo *et al.*, 2015). We deployed both animal models to test the hypothesis that neurotrauma induced by different injury mechanisms triggers common pathogenic mechanisms and convergent CTE neuropathology. We used non-anaesthetized mice to facilitate comparative investigation of acute neurobehavioural responses to different types of neurotrauma. We conducted biomechanical modelling, computational simulations, and human clinicopathological correlation analysis to investigate mechanisms leading to observed differences in acute neurobehavioural responses and similarities in chronic brain pathologies induced by neurotrauma.

Materials and methods

Human subjects

The brain and spinal cord from a total of eight teenage and young adult athletes (Supplementary Table 1), four males with recent sports-related closed-head impact injuries sustained 1 day to 4 months prior to death ($n = 4$; ages 17 to 18 years; mean, 17.5 years) and four males without history of symptomatic impact head injury or neurological disease ($n = 4$; ages 17 to 22 years; mean, 19.2 years). Impact exposure, trauma history, and neurological status at the time of death were determined through review of medical records and interviews with next of kin. This study was approved by the Institutional Review Board at Boston University School of Medicine and conforms to principles of human subject protection in the Declaration of Helsinki.

Animal subjects

Adult male C57BL/6 mice (Charles River Laboratories) and male CCR2^{RFP}/CX3CR1^{GFP} mice (The Jackson Laboratory), 10–12 weeks of age, were group-housed at the Laboratory Animal Science Center, Boston University School of Medicine. B6.129(Cg)-Ccr2$^{tm2.1Ifc}$/J mice and B6.129P-Cx3cr1^{tm1Litt}/J were transferred, bred, and utilized for experiments in accordance with the Material Transfer Agreement between The Jackson Laboratory, Bar Harbor, ME, USA and Boston University School of Medicine, Boston, MA, USA. Cohort size was 8–10 per group or as noted. Mice were provided with standard mouse chow and water *ad*

libitum. Ambient temperature was controlled at 20–22°C with 12-h light-dark cycles. Animal experiments were conducted in accordance with guidelines from the Association for Assessment and Accreditation of Laboratory Animal Care, National Research Council Guide for the Care and Use of Laboratory Animals, and the Laboratory Animal Welfare Act. Animal experiments were approved by Institutional Animal Care and Use Committees at Boston University School of Medicine and New York Medical College. See Supplementary material for additional details.

Human and murine neuropathology

Post-mortem human brain and spinal cord were received as fresh tissue and as fixed tissue in formalin after processing by medical examiners. Neuropathological analysis followed established protocols at the Boston University Alzheimer's Disease Center and Chronic Traumatic Encephalopathy Center and included comprehensive examination for all neurodegenerative conditions (McKee *et al.*, 2013, 2016). Sections of fixed, paraffin-embedded human brain were stained with Luxol fast blue, haematoxylin and eosin, or processed for immunohistochemistry or immunohistofluorescence. Mice were euthanized by CO_2 asphyxiation followed by open thoracotomy and transcardial perfusion with phosphate-buffered saline. Mouse brains were prefixed in 10% neutral buffered formalin, block-sectioned into coronal slabs, post-fixed in 4% paraformaldehyde, paraffin-embedded, and serially sectioned at 10 µm. Primary detection antibodies for human and murine brains neuropathology (Goldstein *et al.*, 2012; McKee *et al.*, 2013; Kondo *et al.*, 2015): glial fibrillary acidic protein (GFAP) mouse monoclonal antibody GA5 (Millipore), rabbit polyclonal antibody Z0334 (Dako); phosphorylated tau protein (pS202, pT205) mouse monoclonal antibody AT8 (Pierce Endogen); phosphorylated tau protein (pS202) mouse monoclonal antibody CP13 (Peter Davies, Albert Einstein College of Medicine); *cis*-phosphorylated tau protein (*cis*-pT231) mouse monoclonal antibody (Kun Ping Lu, Harvard Medical School); amyloid precursor protein (human APP, aa66-81) mouse monoclonal antibody 22C11 (Millipore); phosphorylated neurofilament mouse monoclonal antibody SMI-34 (Abcam); HLA-DR II (MHC) mouse monoclonal antibody LN3 (Invitrogen); ionized calcium-binding adaptor molecule 1 (human Iba1, aa135-147) rabbit polyclonal antibody Iba1 (Wako); serum albumin (human SALB) chicken polyclonal antibody ab106582 (Abcam); phosphorylated Smad2/3 (human Smad2, pS465, pS467) rabbit polyclonal antibody 3101 (Cell Signaling); transforming growth factor-β complex (TGF-β, human C-terminal peptide) rabbit polyclonal antibody ab66043 (Abcam). Ultrastructural studies were conducted on fixed mouse brain specimens embedded in Epon™, sectioned at 60 nm, stained with uranyl acetate or lead citrate, and examined with a Tecnai-G2 Spirit BioTWIN electron microscope with an AMT 2K CCD camera. See Supplementary material for additional details.

Experimental closed-head concussive impact injury

A compressed gas-driven closed-head impact injury system (Supplementary Fig. 1A) was custom designed and fabricated at the Boston University Neurotrauma Laboratory, Boston University School of Medicine, for use in awake, unanaesthetized (anaesthesia-naïve) young adult male C57BL/6 mice. The instrument uses a momentum transfer mechanism to deliver a scalable closed-head impact that results in traumatic head acceleration without gross skull deformation. As implemented in this study, left-lateral impact produced right-lateral flexion of the cervical spine and rightward translation of the head in the horizontal plane of motion (Fig. 2A and B). Mouse positioning and instrument parameters were set such that head kinematics produced by experimental impact were comparable to our blast neurotrauma mouse model (Supplementary Table 2) (Goldstein *et al.*, 2012; Kondo *et al.*, 2015). Instrument data were acquired and processed in MATLAB (MathWorks, Natick, MA). Animal experiments were conducted without anaesthesia to: maximize clinical relevance and animal model fidelity with respect to human head injuries and facilitate accurate assessment of acute neurobehavioural responses post-injury (Huang *et al.*, 2016); maintain physiological responsivity of central receptors, channels, and neurotransmitter systems; and prevent anaesthetic modulation of neuroinflammation and tau protein phosphorylation (Planel *et al.*, 2007; Luh *et al.*, 2011; Wojnarowicz *et al.*, 2017). Unanaesthetized mice were pretreated with a non-sedating dose of the analgesic buprenorphine (0.2 mg/kg, i.p.), placed in a modified DecapiCone (Braintree Scientific, Inc.), and secured in the instrument in the prone position. The head and cervical spine were not restrained during experimental exposure. The single-repeat design incorporated two impacts separated by 15 min to mimic a minimal repeat head injury as commonly occurs during a single session of contact sport play or practice (Crisco *et al.*, 2010). Experimental head injury was compatible with 100% survival without evidence of skull fracture, spinal trauma, persistent gross neurological impairment, or post-traumatic apnoea. See Supplementary material for additional details.

High-speed videography kinematic analysis

High-speed videography was conducted with a FASTCAM SA5 camera (Photron USA, Inc., Tech Imaging) operated at 10 µs frame capture rate (100 000 fps; 100 kHz). Videographic records were reassembled and processed in MATLAB (MathWorks). A 2 kHz second-order, zero-phase Butterworth filter was applied to position-time data. First, second, and third derivatives (velocity, acceleration, jerk) were calculated from the filtered position versus time vectors using discrete differentiation.

Acute neurobehavioural response test battery

The test battery is a quantitative multidimensional evaluation protocol for objective assessment of transient neurobehavioural responses to experimental neurotrauma in awake, unanaesthetized (anaesthesia-naïve) mice (Supplementary Fig. 1B). A composite score (0–15) was derived by summing component scores on each of three subtests: open-field, inverted wire mesh, beam walk. Each subtest was conducted over 30 s and scored on a six-point scale (0–5) based on standardized metrics that capture graded neurobehavioural deficits specific for each test (Supplementary Fig. 1B). A composite score of 15 indicated unimpaired performance in all three subtests. Lower scores

indicate increasing impairment (mild: 14–10; moderate: 9–5; severe: 4–0). Testing was conducted before exposure (pre-injury baseline), 2 min after exposure (post-injury), and after 3 h rest period (recovery). See Supplementary material for additional details.

Tau protein immunoblot analysis

Quantitative phosphorylated and total tau protein immunoblot analyses were conducted on homogenates of left and right hemisected brains from perfused mice sacrificed 2 weeks after impact injury or sham (no injury) control exposure. Snap-frozen hemisected brains were thawed, resuspended in 0.7 ml of protease-phosphatase inhibitor buffer, and homogenized. Protein concentrations were normalized and equal sample volumes analysed by polyacrylamide gel electrophoresis (Goldstein *et al.*, 2012). Immunoblot detection was conducted with monoclonal antibody CP-13 (courtesy of Peter Davies, Albert Einstein College of Medicine) directed against phosphorylated tau protein (pS^{202}) and rabbit polyclonal antibody Tau 5 (Cell Signaling) directed against total tau protein (bovine tau, aa210-241). Triplicate measurements were analysed with ImageJ software.

Blood–brain barrier functional analysis

Mice were injected with Evans blue dye (4 ml/kg, i.p.) 1 h before impact injury or sham (no-injury) control exposure. Following sacrifice, mice were transcardially perfused with saline. Gross pathology was documented by photomacroscopy with a Nikon D5200 digital camera under cross-polarized white light illumination. Brains were sectioned (2 mm) coronally and imaged with an IVIS Spectrum *In Vivo* Imaging System (PerkinElmer). Fluorescence images were acquired at 0.5 s exposure with a 535 nm excitation filter and the following emission filters: 580, 600, 620, 640, 660, 680, 700, 720, 740, 760, 780, 800, 820, 840 nm. Non-specific autofluorescence was removed by spectral unmixing (Living Image software, PerkinElmer). Calibrated images were masked in Adobe Photoshop and analysed with a custom MATLAB script (MathWorks, Natick, MA) was used to process pixel data. Evans blue-specific fluorescence signal intensity was normalized to pixel area for each masked region. Percentage of pixels demonstrating Evans blue-specific fluorescence was calculated by thresholding to the mean 95th percentile of all counts in control sections. Total percentage of Evans blue extravasation pixels for each mouse brain was calculated by summation across all slices. Grouping by Evans blue extravasation was performed using a Gaussian mixture model.

Dynamic contrast-enhanced MRI

In vivo T_1-weighted and dynamic contrast-enhanced MRI were performed using a 11.7 T MRI (Bruker) at the Boston University High-Field NMR Imaging Core Facility. Mice were anaesthetized with 0.5–2.5% isoflurane during imaging with respiration rate monitoring. For the dynamic sequence, 0.1 ml gadofosveset trisodium (0.25 mmol/ml; Lantheus Medical Imaging) was administered by tail vein catheter. Five baseline scans were obtained before injection. After injection, 145 scans were acquired over 31 min. Post-acquisition image analysis was performed using customized MATLAB scripts (MathWorks). See Supplementary material for additional details.

Metallomic imaging mass spectrometry brain mapping

Ultra-trace elemental and isotopic analytical brain mapping for gadolinium (Gd) was performed by laser ablation-assisted metallomic imaging mass spectrometry (Gd-MIMS) at the Boston University Center for Biometallomics. A quadrupole inductively-coupled plasma mass spectrometer (iCAP-Q, Thermo Scientific) was custom hyphenated to a Nd-YAG laser with frequency quadrupling to attain 213 nm output. Laser pulse duration was 5 ns with a pulse repetition rate of 20 Hz. Spot size was 20 µm and scan speed was 40 µm/s. Laser-generated aerosol was transported from a custom-designed laminar flow laser ablation cell to the mass spectrometer by carrier gas mixture at constant flow rates. Generated ions were transported by mass flow into the mass spectrometer and separated according to mass-to-charge ratio. Analytical calibration was performed with a reference standard (SRM 612, NIST). Datasets were exported to a customized MATLAB program (Mathworks) for analytical processing, quantitation, and 2D analytical mapping.

Flow cytometry immunophenotyping

Flow cytometry was performed on single-cell suspensions prepared from homogenized brains (Jay *et al.*, 2015). Briefly, cells were separated on a 30–70% Percoll® gradient (GE Healthcare). Single-cell suspensions were stained with a master mix composed of anti-CD45-APC (1:100; BioLegend), anti-CD11b-Efluo450 (1:200; eBioscience), anti-Ly-6G-FITC (1:1000; BioLegend), anti-Ly-6C-PE/Cy7 (1:200; BioLegend), TREM2-PE (1:100; R&D Systems). Cell populations were defined as inflammatory cells, $CD45^+$; microglia, $CD45^{low}CD11b^+$; and monocytes, $CD45^{high}CD11b^+Ly\text{-}6G^-$. Ly-6 C was used to phenotype distinct monocyte subpopulations ($Ly\text{-}6C^{high}$, $Ly\text{-}6C^{middle}$, $Ly\text{-}6C^{low}$). Events were gated on single cells and CD11b-positive events. Samples with >5000 CD11b-positive events were used for analysis. Fluorescence Minus One (FMO) was used to assess cells expressing triggering receptor expressed on myeloid cells 2 protein ($TREM2^+$). The percentage of cells from each population was determined by flow cytometry at the Boston University School of Medicine Flow Cytometry Core on a LSR-II (BD Biosciences). Analyses were performed using FlowJo software (FlowJo, LLC, Ashland, OR). The absolute number of each cell population was calculated as the percentage multiplied by isolated cells per brain. Significant differences between groups were determined by one-way ANOVA with *post hoc* Student's *t*-tests using the Bonferroni correction. See Supplementary material for additional details.

Hippocampus and medial prefrontal cortex electrophysiology

Mice were decapitated under deep isoflurane anaesthesia and brains quickly harvested by manual dissection. The forebrain

was mounted on a cutting stage and immediately submerged in ice-cold cutting solution (200 mM sucrose, 10 mM NaCl, 2.5 mM KCl, 1.25 mM NaH_2PO_4, 25 mM $NaHCO_3$, 0.5 mM $CaCl_2$, 4 mM $MgCl_2$, saturated with 95% O_2 and 5% CO_2). Slices containing the hippocampus or medial prefrontal cortex (Supplementary Figs. 5A–C) were cut by vibratome at 350 µm thickness. Slices were transferred to an incubation chamber, warmed to 32°C for 30 min, and equilibrated in a slice recording chamber at 32°C with continuous perfusion (2 ml/min) of artificial CSF (10 mM glucose, 126 mM NaCl, 2.5 mM KCl, 1.25 mM NaH_2PO_4, 1.3 mM $MgCl_2$, 2.5 mM $CaCl_2$, 26 mM $NaHCO_3$ saturated with 95% O_2 and 5% CO_2). Axonal conduction velocity was assessed with two recording electrodes placed in CA1 stratum alveus spaced ~200 µm (Supplementary Fig. 5A). Long-term potentiation (LTP) of synaptic neurotransmission in the medial prefrontal cortex was assessed with a stimulating electrode placed in mixed inputs in layer VI and extracellular recording electrode placed as indicated in Supplementary Fig. 5C. See Supplementary material for additional details.

Mouse headform pressure measurements

Pressure film measurements were conducted with a mouse headform consisting of a 15 ml polypropylene vial filled with 10% gelatin. Fuji Prescale® pressure sensitive film (Sensor Products, Inc.) was fixed flush to the outer surface of the vial and exposed to a single blast or impact under conditions identical to the *in vivo* experiments. Control films were fixed to identical headforms and placed in the experimental instruments without impact or blast exposure. Exposed films were digitally scanned, imported into MATLAB (MathWorks), and converted to monochrome luminescence images (NTSC standard, RGB colour: Y = 0.2989*R + 0.5870*G + 0.1140*B, equivalent to rgb2gray MatLab). A 1000 × 500 pixel boundary was applied to all images. Histogram analysis was used to identify the lower threshold of pixel values attributable to noise and subtracted from all images. The sum of noise-corrected pixels in the bounded region was measured and recorded.

Computational simulations

Computational simulations were conducted using ALE3D (Noble *et al.*, 2017) in explicit dynamics mode with the solid regions held Lagrangian and the gas regions allowed to advect and relax to prevent mesh entanglement. All elements for the impact simulations were 3D linear reduced integration elements, whereas the blast simulations used 2D axisymmetric reduced integration elements. In all simulations, materials were initialized to 295 K, and 1 bar ambient pressure, except gas pressure in the blast tube driver chamber. All materials were initially at rest, except for the impact rod. Gases were described by gamma-law gas equations of state ($\gamma = 1.4$, air; 1.67, He). Predicted blast pressure histories were validated against analytic solutions for shock tube dynamics (Liepmann and Roshko, 1957). The skull was modelled as an isotropic linear elastic hollow sphere with 1.08 cm outer diameter, 0.02 cm thickness, four radial zones and 2.5° zoning. CSF was modelled as a water layer 0.02 cm thick with four radial zones. The brain was modelled as a 0.5-cm radius viscoelastic sphere, with 30 radial zones. Material properties for the skull and brain were incorporated as previously described (Moss *et al.*, 2009). The gas zones surrounding the skull were ratio-zoned, increasing from 0.03 cm thickness at the skull, to a fixed value of 0.2 cm thickness 4 cm from the skull centre. The calculated Reynolds number for non-steady airflow in the blast simulation was $\sim 10^5$, indicating a turbulent flow field, that was accounted for in the simulation. The sled and impact rod were modelled as linear elastic solids. See Supplementary material for additional details.

Statistical analyses

Linear mixed-effects regression analyses were used to evaluate group differences and test for correlation with composite and subtest scores on the acute neurobehavioural response test battery. Linear mixed-effects regression analyses were also used to determine group differences of Evans blue extravasation (dye-specific fluorescence signal intensity) in post-mortem brains. For each linear mixed-effects regression analysis, we allowed for outcome-specific fixed effects and subject-specific random effects. Outcomes were correlated using an unstructured covariance matrix for within-subject correlation. Mixed effect analyses represent more realistic outcome models than using independent regression models for each outcome while removing multiple comparisons and providing greater power (Goldstein, 2011; Gelman *et al.*, 2012). Immunoblot densitometry and biochemical data were evaluated by two-tailed Student's *t*-test. Flow cytometry data were evaluated by one-way ANOVA followed by *post hoc* Student's *t*-tests using the Bonferroni correction. Comparisons of axonal conduction velocity and LTP magnitude were made using three-way ANOVA. Spearman's rank-order coefficient was computed between lost points on the test battery and end-point metrics (Supplementary Table 3). Levels of significance: $^*P < 0.05$; $^{**}P < 0.01$; $^{***}P < 0.001$; NS = no significant difference. Statistical significance was set at an alpha-level of $P < 0.05$. Exact *P*-values are reported for statistical significance except when $P < 0.0001$.

Results

CTE pathologies in brains from teenage athletes in the acute-subacute period after mild closed-head impact injury

We conducted neuropathological examinations of rare post-mortem brains obtained from teenage athletes (four males, aged 17–18 years; mean, 17.5 years; Supplementary Table 1, Cases 1–4) who sustained sports-related closed-head impact injuries and died in the acute-subacute period 1 day to 4 months post-injury (Fig. 1A, C–J, L, M and O–R). We compared these brains to post-mortem control brains from comparably-aged athletes (four males; aged 17–22 years; mean, 19.2 years; Supplementary Table 1, Cases 5–8) without recent head injury (Fig. 1B, K and N). None of the cases showed

evidence of skull fracture, subdural haematoma, subarachnoid haemorrhage, or other evidence of moderate-to-severe TBI.

We included four cases in the acute-subacute post-TBI cohort. Case 1, an 18-year-old male high school athlete (American football, baseball, basketball, weight-lifting) who died by suicide from hanging 4.2 months after sustaining a mild closed-head injury while snowboarding. The decedent's head injury exposure history was notable for amateur participation in American football (9 years total). He played fullback and middle linebacker, positions associated with frequent high-magnitude head impacts (Crisco *et al.*, 2011). He sustained 10 concussions, none other than the last with loss of consciousness. Four months before death, he sustained a concussion while snowboarding and briefly lost consciousness (~2 min). He was evaluated at a local hospital and released without follow-up. After the injury, he complained of frequent headaches and mental fogginess. His parents noted increased frustration, emotional lability, verbal hostility, physical aggression, and school absences. He was clinically evaluated and diagnosed with post-concussive syndrome. Due to school absences, school officials did not allow him to participate in his high school graduation ceremony. The next day, 4.2 months after the snowboarding injury, he hanged himself in his bedroom. His past medical history was notable for attention deficit hyperactivity disorder that was diagnosed in the third grade and treated for 1 year with methyphenidate. He had no history of depression, anxiety, or prior episodes of suicidal ideation or suicide attempts. The intact brain (1460 g) was obtained as a fresh specimen with a post-mortem interval of 1 day. Grossly, the brain did not show evidence of atrophy, asymmetry, swelling, cavum septum pellucidum, or contusions.

Case 2, an 18-year-old male high school athlete (American football, rugby, soccer, in-line hockey) who died suddenly 10 days after the second of two sports-related head injuries. The decedent's head injury exposure history was notable for four sports-related concussions. He played American football at the amateur level starting at age 11 and continued intermittently through high school (3 years total). In his junior and senior year of high school, he played rugby (amateur then semi-professional level). One month before death, he sustained a severe concussion during a rugby match that resulted in post-traumatic somnolence. Two weeks later he sustained a second rugby-related head injury that resulted in sideline collapse and a 2-day hospitalization for clinical observation and recuperation. Seven days after hospital discharge, he engaged in light weightlifting after which he collapsed suddenly while eating dinner with his family. He was taken to the hospital where he died from acute cerebral oedema, the recorded cause of death. Selected brain regions were obtained as fixed sectioned specimens on microscope slides. The brain weight was 1680 g. The post-mortem interval is not known.

Case 3, a 17-year-old male high school American football and lacrosse player who died by suicide from hanging. The decedent was diagnosed with two sports-related concussions during life, the last sustained 2 days before death. He was evaluated in an emergency room after his last head injury (no reported loss of consciousness) where he was noted to be confused, could not recall events and circumstances surrounding the injury, and was unable to recite the days of the week in reverse order. He had no history of depression, anxiety, mood disorder, impulsivity, suicidal ideation, or prior suicide attempts. The intact whole brain (1600 g) was obtained as a fresh specimen with a post-mortem interval of 3 days. Grossly, the brain was diffusely swollen without evidence of atrophy, asymmetry, or contusions. A small anterior cavum septum pellucidum was noted.

Case 4, a 17-year-old male high school American football player who sustained three sports-related concussions (26 days, 6 days, 1 day) before death from second impact syndrome. During the football game in which he sustained a terminal head injury, he received a hard tackle, landed on his helmet, and was rendered immobile and unresponsive. A tonic-clonic seizure ensued. He was intubated and ventilated on the field, then transferred to a hospital emergency ward. A CT head scan showed global cerebral oedema without evidence of haemorrhage. Despite surgical decompression, cerebral swelling progressed to fatal brain herniation. He died 1 day after the proximate head injury. The recorded cause of death was second impact syndrome. The brain (1450 g) was obtained as coronal tissue sections on glass slides. The post-mortem interval is not known.

We included four cases in the control athlete cohort. Case 5, a 19-year-old male high school American football player who died of multiple organ failure and cardiac arrest. The intact brain (1430 g) was obtained as a formalin-fixed tissue specimen with an unknown post-mortem interval. Grossly, the brain did not show evidence of atrophy, asymmetry, herniation, or contusions. Case 6, a 19-year-old male college hockey player with a history of six concussions who died of a cardiac arrhythmia. The intact brain (1500 g) was obtained as a formalin-fixed tissue specimen with an unknown post-mortem interval. Grossly, the brain did not show evidence of atrophy, asymmetry, or contusions. Case 7, a 17-year-old male high school American football player who died from oxycodone overdose. The brain was obtained as formalin-fixed coronal slabs of available tissue with an unknown post-mortem interval. A 0.3-cm cavum septum pellucidum was noted. Case 8, a 22-year-old male former high school American football player who died by suicide (unknown mechanism). The decedent's head injury exposure history was notable for three remote concussions, one with loss of consciousness of indeterminate duration, all sustained more than 7 years before death. He was diagnosed with bipolar disorder and had two suicide attempts prior to the completed suicide. The intact whole brain (1630 g) was obtained as a fresh tissue specimen with a 2-day post-mortem interval. Grossly, the brain did not show evidence of atrophy, asymmetry, or contusions.

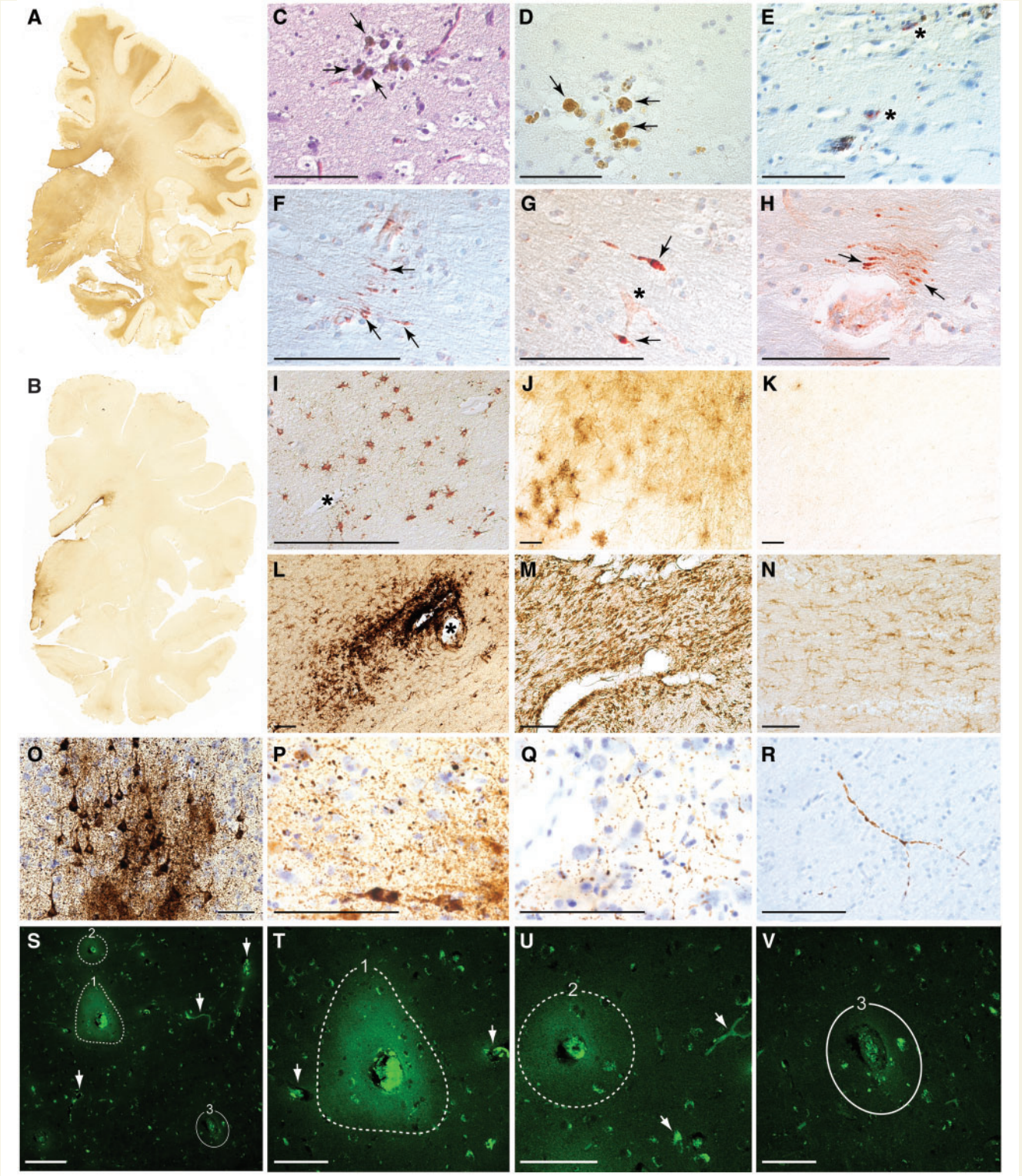

Figure 1 Post-mortem pathologies in brains from teenage athletes in the acute-subacute period after mild closed-head impact injury. (**A**) Coronal brain section immunostained for the astrocytic marker glial fibrillary acid protein (GFAP) in Case 3, a 17-year-old male high school American football player who died by suicide 2 days after a closed-head impact injury. Widespread GFAP immunoreactivity (brown staining) indicative of reactive astrocytosis was diffusely present in white matter fibre tracts throughout the brain. Representative whole-mount brain section, 50 μm thickness. (**B**) Coronal brain section immunostained for GFAP in control Case 8, a 22-year-old male former high school American football player without history of recent head injury who died by suicide. GFAP immunoreactivity is restricted to the periventricular area and diencephalon. Representative whole-mount brain section, 50 μm thickness. (**C** and **D**) Haemosiderin-laden macrophages (arrows) surrounding a small blood vessel consistent with prior microhaemorrhage in Case 1, an 18-year-old male high school American football player who died by suicide 4 months after a closed-head impact injury. Representative Luxol fast blue haematoxylin and eosin (**C**) and haematoxylin

(continued)

Microscopic examination of post-mortem brains from young athletes in the acute-subacute period after sports-related head injury revealed diffuse astrocytosis with increased glial fibrillary acidic protein immunoreactivity in white matter (Fig. 1A) and surrounding small blood vessels in the cerebral cortex (Fig. 1I and J); perivascular foci of hemosiderin-laden macrophages indicative of resolved microhaemorrhage (Fig. 1C and D); dystrophic axons with swellings immunoreactive for amyloid precursor protein (Fig. 1F–H); perivascular clusters of activated microglia (Fig. 1L and M) in all four cases. Multifocal axonal injury was observed diffusely in frontal, temporal, and subcortical white matter. Axonal spheroids and retraction balls with digestion chambers were noted in the dorsolateral midbrain and cerebellar white matter (Case 1) (McKee *et al.*, 2014). We detected focal phosphorylated tau protein in two of the four cases, and early-stage CTE in one case. These cases were notable for perivascular pretangles, neurofibrillary tangles, dot neurites, and dystrophic axons immunoreactive for phosphorylated tau protein (Fig. 1E and O–R). Focal cortical lesions demonstrating perivascular accumulation of serum immunoglobulin G (Fig. 1S–U) were detected in proximity to neighbouring blood vessels of similar calibre that did not show microvascular pathology (Fig. 1V). These results are consistent with extravasation and intraparenchymal accumulation of serum proteins secondary to localized traumatic microvascular injury and focal blood–brain barrier disruption. By contrast, none of the post-mortem brains from the control group demonstrated evidence of microvascular or axonal injury, astrocytosis, microgliosis, or phosphorylated tauopathy indicative of CTE or other neurodegenerative disease (Fig. 1B, K and N). None of the cases, including those with early CTE pathology, showed evidence of neuropathology associated with Alzheimer's disease or other neurodegenerative diseases.

Mechanistic links between experimental closed-head impact injury, early CTE pathologies, and functional sequelae

A novel mouse model of closed-head impact injury

Clinicopathological correlation suggested that impact injury may, in some cases, trigger early pathologies associated with CTE. However, causal mechanisms underpinning this association cannot be established with certainty based solely on post-mortem neuropathological examination. We hypothesized that closed-head impact injury is mechanistically linked to, causally determinative of, and temporally associated with early CTE brain pathologies.

Figure 1 Continued

(**D**) staining, 10 μm paraffin sections. Scale bars = 100 μm. (**E**) Case 1, microhaemorrhage surrounded by neurites immunoreactive for phosphorylated tau protein (asterisks) detected by monoclonal antibody AT8 directed against hyperphosphorylated tau protein (pSer202, pThr205) with haematoxylin counterstain, 10 μm paraffin section. Scale bar = 100 μm. (**F–H**) Perivascular anti-amyloid precursor protein (APP)-immunoreactive axonal swellings (arrows) in the corpus callosum from Case 3. Representative APP immunostaining with haematoxylin counterstain, 10 μm paraffin sections. Asterisk in **G** marks a small blood vessel. Scale bars = 100 μm. (**I** and **J**) Perivascular astrocytosis in white matter from Case 3. Representative GFAP immunostaining with haematoxylin counterstain, 10 μm paraffin section (**I**) and 50 μm free-floating section (**J**). Asterisk in **I** marks a small blood vessel. Scale bars = 100 μm. (**K**) Minimal GFAP-immunoreactive astrocytosis in the white matter from control Case 8. Representative GFAP immunostaining, 50 μm free-floating section. Scale bar = 100 μm. (**L**) Perivascular clusters of activated microglia around a small blood vessel in the subcortical white matter from Case 4, a 17-year-old male high school American football player who sustained three closed-head impact injuries 26 days, 6 days, and 1 day before death. Representative LN3 immunostaining directed against human leukocyte antigen DR-II (HLA-DR II), 50 μm free-floating section. Asterisk indicates small blood vessel. Scale bar = 100 μm. (**M**) Microgliosis in brainstem white matter in Case 1. Representative LN3 immunostaining, 50 μm free-floating section. Scale bar = 100 μm. (**N**) Few activated microglia in brainstem white matter in control Case 8. Representative LN3 immunostaining, 50 μm free-floating section. Scale bar = 100 μm. (**O**) Phosphorylated tau protein-containing neurofibrillary tangles, pretangles, and neurites in the sulcal depths of the cerebral cortex consistent with neuropathological diagnosis of early-stage CTE in Case 4. Representative CP13 immunostaining directed against hyperphosphorylated tau protein (pSer202), 50 μm free-floating section. Scale bar = 100 μm. (**P** and **Q**) Perivascular dot-like neurites immunoreactive for CP13-immunoreactive phosphorylated tau protein in frontal cortex sulcal depths consistent with early-stage CTE in Case 4. Representative CP13 immunostaining, 50 μm free-floating section. Scale bar = 100 μm. (**R**) Dystrophic axons immunoreactive for CP13-immunoreactive phosphorylated tau protein in frontal cortex white matter in Case 4. Representative CP13 immunostaining, 50 μm free-floating section. Scale bar = 100 μm. (**S**) Persistent vascular leakage in Case 1 demonstrated by anti-IgG immohistofluorescence in the brain parenchyma surrounding two blood vessels (dashed lines, 1 and 2) in the dorsolateral frontal cortex. These findings are consistent with focal blood–brain barrier disruption. Another blood vessel of similar calibre in the same field (denoted by solid line, number 3) does not exhibit evidence of blood–brain barrier disruption, consistent with the high degree of focality. Other smaller blood vessels (white arrows) are also devoid of perivascular IgG immunoreactivity, thereby confirming specificity of the microvascular pathology. Scale bar = 200 μm. (**T**) High magnification photomicrograph of the same field in Case 1 showing perivascular IgG immunoreactivity in the brain parenchyma surrounding blood vessel 1 (dashed line, 1). The intensely immunoreactive material in the centre of the lesion is residual blood in the vessel lumen. Two nearby blood vessels (arrows) do not show evidence of blood–brain barrier disruption. Scale bar = 100 μm. (**U**) High magnification photomicrograph of the same field in Case 1 showing perivascular IgG immunoreactivity in the brain parenchyma surrounding blood vessel 2 (dashed line, 2). Scale bar = 100 μm. (**V**) High magnification photomicrograph of the same field in Case 1 showing the absence of perivascular IgG immunoreactivity in the brain parenchyma surrounding blood vessel 3 (solid line, 3). Scale bar = 100 μm.

To test this hypothesis, we developed an experimental instrument that uses momentum transfer to produce traumatic head acceleration without gross skull deformation in awake (anaesthesia-naïve) mice. Experimental parameters were optimized to match head kinematics in our companion blast neurotrauma mouse model (Goldstein *et al.*, 2012; Kondo *et al.*, 2015). The developed instrument (Supplementary Fig. 1A) was designed for use in unanaesthetized young adult male mice to model subject variables, injury conditions, and brain pathology as in the human cases (Goldstein *et al.*, 2014; Wojnarowicz *et al.*, 2017). The instrument incorporates a gas-driven momentum transfer mechanism to deliver a lateral closed-head impact that induces traumatic head acceleration without gross skull deformation (Fig. 2A and B). The rationale for this design was to enable evaluation of acute neurobehavioural responses and cellular-molecular effects without confounding interference of systemic anaesthetics (Statler *et al.*, 2006; Planel *et al.*, 2007, 2008; Fish *et al.*, 2011; Luh *et al.*, 2011; Whittington *et al.*, 2013; Gao *et al.*, 2016). Unanaesthetized mice were restrained across the thorax in the prone position such that the inner pad of the sled contacted the left temporal-zygomatic region of the head. Linear translation of the sled resulted in left-lateral closed-head impact, right lateral flexion at the cervical spine, and traumatic acceleration of the head in the horizontal plane of motion (Fig. 2A and B). Head motion was assessed by high-speed videography (100 000 fps, 100 kHz).

Sled velocity of 5.1 ± 0.2 m/s [mean ± standard deviation (SD)] produced the following head kinematics (mean ± SD, $n = 18$): swing radius, 30.0 ± 2.3 mm; peak X-acceleration, $12.6 \times 10^3 \pm 3.4 \times 10^3$ m/s^2; peak angular acceleration, 398.8 ± 111.0 krad/s^2; peak X-jerk, $5.3 \times 10^7 \pm 2.5 \times 10^7$ m/s^3 (Fig. 2C). Impact-induced head kinematics ($n = 18$) were statistically indistinguishable (Bonferroni-corrected two-tailed Student's *t*-tests, $P > 0.05$) from head motion produced by experimental blast exposure ($n = 8$) at a peak pressure of 72.3 ± 2.8 kPag (Goldstein *et al.*, 2012; Kondo *et al.*, 2015). These results justified setting the impact instrument sled velocity at 5.0 m/s and holding operating parameters constant (Supplementary Table 2). Experimental impact head injury at this intensity was compatible with 100% survival without evidence of skull fracture or deformation; subdural, epidural, or subarachnoid haemorrhage; cervical trauma or spinal cord injury; post-traumatic apnoea; or persistent gross neurological impairment.

Closed-head impact injury induces acute neurobehavioural deficits in unanaesthetized mice

Unanaesthetized mice subjected to unilateral closed-head impact injury exhibited variable degrees of transient neurobehavioural dysfunction with abrupt onset, transient course, and spontaneous recovery (Supplementary Video 1). To objectively assess this transient concussion-like syndrome, we developed an acute neurobehavioural response test battery and standardized scoring criteria (Supplementary Fig. 1B). The test battery consists of three subtests: open-field, inverted wire mesh, and beam walk. Each 30-s subtest is scored on a six-point scale (0–5) according to graded criteria that capture neurobehavioural deficits specific to each subtest (Supplementary Fig. 1B). A composite score of 15 reflects unimpaired performance in all three subtests. Lower composite scores indicate increasing impairment (mild, 14–10; moderate, 9–5; severe, 4–0). The test battery was used to assess neurocognitive function before exposure (pre-injury baseline), after exposure (post-injury), and following a 3-h rest period (recovery).

Awake, unanaesthetized (anaesthesia-naïve) adult male mice, 10 weeks of age, were exposed to single-repeat impact injury or sham (no injury) control condition. This experimental protocol was designed to model a common head injury scenario in contact sports (Crisco *et al.*, 2010). A total of 320 adult male mice were subjected to experimental closed-head impact injury ($n = 203$) or sham (no-injury) control condition ($n = 117$). Impact-exposed mice demonstrated significant post-injury decrements in composite and subtest scores on the acute neurobehavioural response test battery (Fig. 2D). Sled velocity (between 3.75 m/s and 6.25 m/s) did not significantly correlate with test battery composite scores (Spearman $r = -0.16$, $P = 0.025$, $n = 203$). However, the significant decrement in composite scores detected after second impact (Fig. 2D) showed significant positive correlation with composite scores after first impact (Spearman $r = 0.52$, $P < 0.0001$, $n = 203$). Post-traumatic deficits were noted only in impact-injured mice, spanned multiple functional domains, and followed a transient course with spontaneous recovery (Fig. 2D). Mean composite test battery scores showed a highly significant difference between impact and control groups (linear mixed-effects regression analysis, $P < 0.0001$). Comparisons within the impact group revealed a significant decrement in mean composite score from baseline (pre-injury) to first post-injury tests [mean ± standard error of the mean (SEM): 14.9 ± 0.0, 11.6 ± 0.2; $P < 0.0001$] and further significant decrement after second impact (mean ± SEM: 10.1 ± 0.2; $P < 0.0001$). There were no significant differences in composite or subtest scores in the control group at any time point. Impact-injured mice demonstrated spontaneous recovery with complete resolution of deficits and return to baseline (pre-injury) performance by 3 h post-injury (mean ± SEM: 14.8 ± 0.0).

Despite tight control of the experimental injury parameters, the spectrum of acute neurobehavioural responses showed wide variation with skewing towards the milder end of the spectrum (Fig. 2E and F). 81.8% ($n = 166/203$) of all impact-injured mice exhibited minimal or no acute neurological impairment (composite test battery score $\geqslant 10$) post-injury (Supplementary Video 1, Mouse P-238). Nearly two-thirds of these mice (66.5%; $n = 135$) showed minimal or no acute neurological impairment after a second head injury. 15.8% ($n = 32/203$) of all impact-injured mice demonstrated transient unilateral acute neurological impairment (composite score 9–5) post-injury

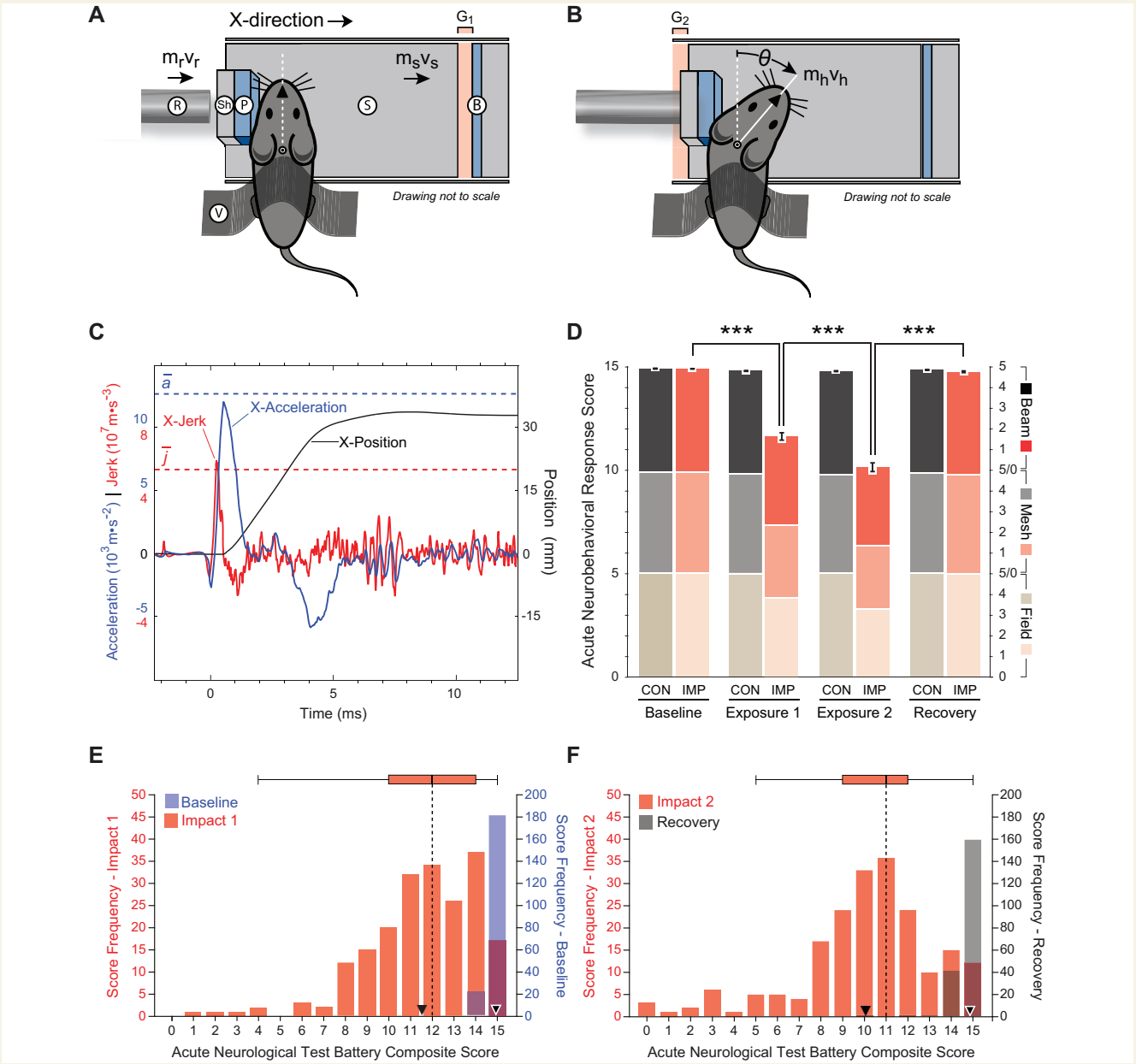

Figure 2 Experimental closed-head impact injury in awake, unanaesthetized (anaesthesia-naïve) mice induces abrupt onset, transient course, and rapid resolution of neurobehavioural impairments that resemble human concussion. (**A** and **B**) Schematic of momentum transfer instrument before (**A**) and after (**B**) experimental closed-head impact injury. The developed instrument was designed for use with unanaesthetized C57BL/6 mice and is compatible with 100% survival without evidence of skull fracture; subdural, epidural, or subarachnoid haemorrhage; cervical trauma or spinal cord injury; commotio cordis or retinae; or post-traumatic apnoea. Animal subjects are secured across the thorax and positioned prone such that the head is in physical contact with a helmet analogue composed of an inner foam pad (P) and an outer hard shell (Sh) fixed to a mobile sled (S). Sled movement is constrained to linear translation by a low-friction monorail track (not shown). Sled motion is initiated by an operator-triggered computer program that actuates a solenoid valve, releases a bolus of pressurized gas, and accelerates a stainless-steel slug within the instrument barrel. Vent holes in the barrel convert slug motion to constant velocity. Sequential momentum transfer from the slug to a captive stainless-steel rod (R; known mass, m_r, empirically-determined velocity, v_r) and finally to the sled (S; known mass, m_s, empirically-determined velocity, v_s). Sled motion results in closure of the distal gap (G1), opening of the proximal gap (G2), and termination by the backstop (**B**). A detailed schematic of the developed instrument is shown in Supplementary Fig. 1A. (**C**) Head motion analysis (time-history plot) during experimental closed-head impact injury reconstructed from high-speed videographic records (100 000 fps; 100 kHz). Head position, acceleration, and jerk are plotted as a function of time after initiation of head motion ($t = 0$). Maximal head acceleration and jerk are observed within the first millisecond after impact. Experimental parameters were selected to kinematically match head motion in our blast neurotrauma mouse model (Supplementary Table 2). Blue dashed line, mean peak X-acceleration ($n = 18$ mice). Red dashed line, mean peak X-jerk ($n = 18$ mice). (**D**) Composite and subtest scores on the acute neurobehavioural response test battery (Supplementary Fig. 1B) assessed in awake unanaesthetized (anaesthesia-naïve) mice: (i) at pre-injury (baseline test); (ii) at 2 min after experimental closed-head impact injury (IMP) or

(continued)

(Supplementary Video 1, Mouse L-070). The observed motor deficits in this group were exclusively ipsilateral with respect to impact (i.e. left-lateral impact induced right-sided neurological deficits). Only rarely (2.5%, $n = 5/203$) did we observe mice that demonstrated global neurological impairment (sustained immobility or frank seizure; composite test battery score $\leqslant 4$) after the first impact (Supplementary Video 1, Mouse P-199). Severe global responses were rare ($n = 13$, 6.4%) after the second impact. Head-injured mice recovered to neurological baseline, typically within minutes and always by the end of the 3-h recovery period (Fig. 2E, F and Supplementary Video 1).

Closed-head impact injury induces early CTE brain pathologies in unanaesthetized mice

Previous research in our laboratory and others pointed to the intensity of traumatic head motion, rather than the type of insult, as the causally determinative mechanism that triggers CTE brain pathologies (Goldstein *et al.*, 2012; Huber *et al.*, 2013; Kondo *et al.*, 2015). To test this hypothesis, we set experimental parameters in our impact injury mouse model such that head motion was kinematically comparable to our blast model (Supplementary Table 2). We hypothesized that impact injury would initiate shearing forces in the brain, thereby causing microvascular injury, reactive neuroinflammation, and accumulation of pathogenic species of phosphorylated tau protein similar to the cascade triggered by blast exposure (Goldstein *et al.*, 2012; Huber *et al.*, 2013; Kondo *et al.*, 2015). To investigate this hypothesis, we examined brains from mice sacrificed 24 h, 3 days, and 2 weeks after single-repeat left-lateral impact injury (24 h post-injury: impact-injured mice, $n = 7$; uninjured sham control mice, $n = 3$; 3 days post-injury: impact, $n = 6$; sham, $n = 2$; 2 weeks post-injury: impact, $n = 7$; sham, $n = 3$; 5.5 months post-injury, *cis*-p-tau only: impact, $n = 3$; sham, $n = 1$). In contrast to the diffuse brain pathology noted after blast exposure (Goldstein *et al.*, 2012), the brain lesions observed after lateral impact injury localized predominantly to ipsilateral cerebral cortex subjacent to the impact contact zone (Fig. 3). Affected brain regions included left perirhinal, insular, entorhinal, and piriform cortices, as well as adjacent regions of the left basolateral amygdala. Histopathological examination of brains 24 h post-injury revealed shrunken acidophilic neurons with eosinophilic cytoplasm and pyknotic basophilic nuclei at various stages of degeneration (Fig. 3A). Dystrophic axons (Fig. 3D) containing hyperphosphorylated neurofilaments were observed in proximity to activated astrocytes (Fig. 3G) and reactive microglia (Fig. 3J). By 3 days post-injury, we observed decreased neuronal density indicative of neuronal demise, brisk astrocytosis and reactive microgliosis in the ipsilateral perirhinal cortex (Fig. 3B, E, H and K). By 2 weeks post-injury, we noted regions of markedly decreased neuronal density, resolving astrocytosis and microgliosis, and clusters of perivascular hemosiderin-laden macrophages (Fig. 3C, F, I and L). The contralateral perirhinal cortex was histopathologically normal at all three time points. We did not detect trauma-related brain pathology in uninjured control mice (Supplementary Fig. 2A–O). Neuropathological analysis of post-mortem brains from mice subjected to a single exposure closed-head impact (24 h post-injury: impact, $n = 6$; sham, $n = 3$; 3 days post-injury: impact, $n = 6$; sham, $n = 3$; 2 weeks post-injury: impact, $n = 5$; sham, $n = 3$) under identical experimental conditions revealed a similar pattern and time course of TBI-related brain pathologies (Supplementary Fig. 3) as that observed in brains of mice exposed to two impacts.

Analysis of phosphorylated tauopathy revealed a more complex pattern. Post-mortem brains at 24 h, 3 days, and 2 weeks post-injury did not reveal evidence of neuronal or astroglial phosphorylated tauopathy when probed with a monoclonal antibody directed against a mature tau proteoform phosphorylated at serine residue 202 (CP13; pSer202; Fig. 3M–O). However, we detected robust immunostaining with the monoclonal antibody *cis*-p-tau directed against a highly pathogenic phosphorylated tau proteoform with the *cis*-Thr231-Pro motif, an early driver of tau-mediated neurotoxicity in Alzheimer's disease and TBI (Nakamura *et al.*, 2012; Kondo *et al.*, 2015; Lu *et al.*, 2016). *Cis*-p-tau immunostaining (Fig. 3P–W) revealed pronounced axonal pathology in ipsilateral perirhinal cortex as early as 24 h post-injury. Importantly, *cis*-p-tau was not detected elsewhere in the brain at this early time point nor in brains from control mice at any time point (Supplementary Fig.

Figure 2 Continued

exposure to the sham (no injury) control condition (CON) (post-injury test); and (iii) after a 3-h rest period (recovery test). Mice subjected to experimental impact injury showed significant decrements in composite scores and all three sub-test scores (open-field, inverted wire mesh, beam walk). IMP, $n = 203$ mice. CON; $n = 117$. Values represent means ± SEM. $^{***}P < 0.001$. Transient neurobehavioural impairments spanned multiple functional domains (including arousal, responsivity to environmental stimuli, locomotion, exploration, motor performance, habituation) that recapitulate features of concussion in humans (Supplementary Video 1). (**E**) Histogram and box-and-whiskers plot for population frequency distribution of composite scores on the acute neurobehavioural response test battery at baseline (pre-impact) and after first impact in awake (anaesthesia-naïve) mice exposed to experimental closed-head injury ($n = 203$). Baseline test: median score, 15; mean ± SEM, 14.9 ± 0.0 (white-bordered black inverted triangle). Impact 1 test: median score, 12; mean ± SEM, 11.6 ± 0.2 (black inverted triangle). (**F**) Histogram and box-and-whiskers plot for population ($n = 203$) frequency distribution of composite scores on the acute neurobehavioural response test battery after second impact and 3-h recovery. Impact 2 test: median score, 11; mean, 10.1 ± 0.2 (black inverted triangle). Recovery test: median score, 15; mean, 14.8 ± 0.0 (white-bordered black inverted triangle).

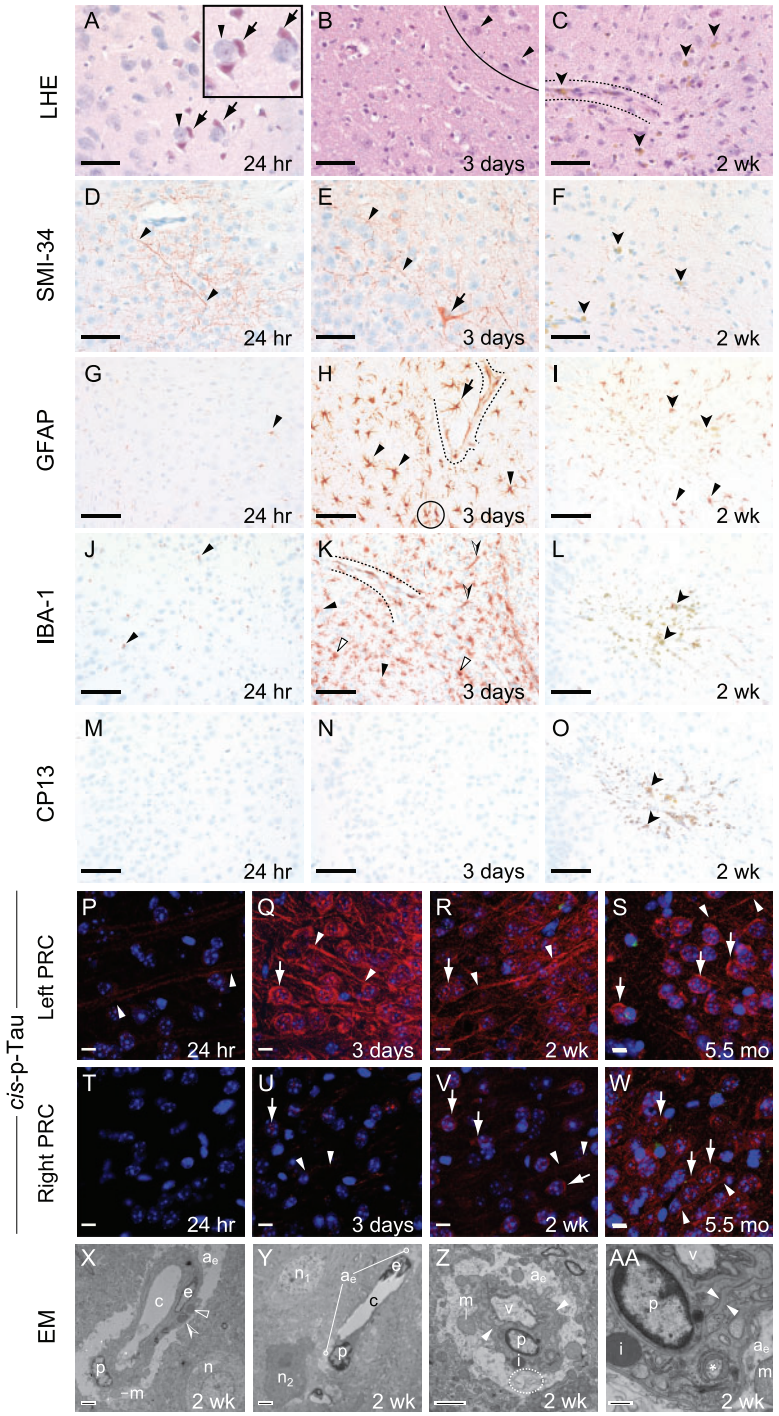

Figure 3 Experimental closed-head injury induces early and progressive brain pathologies associated with CTE in cerebral cortex ipsilateral and subjacent to impact. (**A–C**) Luxol fast blue haematoxylin and eosin (LHE) staining in ipsilateral (left) perirhinal cortex 24 h (**A**), 3 days (**B**), 2 weeks (**C**) post-injury. (**A**) LHE staining at 24 h post-injury revealed dying neurons (arrows) with pyknotic basophilic nuclei and intensely eosinophilic cytoplasm interspersed with normal-appearing neurons (arrowheads). Black box, magnified view showing neuronal necrosis. Scale bar = 100 μm. (**B**) Decreased neuronal density (below line) indicative of neuronal demise, ipsilateral (left) perirhinal cortex 3 days post-injury. Normal-appearing neurons (arrowheads, above line). Scale bar = 100 μm. (**C**) Decreased neuronal density (below line) indicative of neuronal demise and gliosis near a small blood vessel (between dashed lines). Clusters of haemosiderin-laden macrophage (darts) represent microhaemorrhage residua. Scale bar = 100 μm. Contralateral (right) perirhinal cortex was histopathologically normal by LHE staining (Supplementary Fig. 2A–C). (**D–F**) Immunostaining with monoclonal antibody SMI-34 (phosphorylated neurofilament) in ipsilateral (left) perirhinal cortex 24 h (**D**), 3 days (**E**), 2 weeks (**F**) post-injury. (**D** and **E**) SMI-34 immunostaining revealed neurons with swollen, beaded neuronal processes (arrowheads) and cytoplasmic immunoreactivity (arrow, **E**). Scale bars = 100 μm. (**F**) Haemosiderin-laden macrophages (darts), but not SMI-34 immunoreactivity, were observed in the ipsilateral (left) perirhinal cortex 2 weeks post-injury. Scale bar = 100 μm. Contralateral (right) perirhinal

(continued)

2P–W). By 3 days and 2 weeks post-injury, *cis*-p-tau immunoreactivity was present not only in axons but also as dot-like puncta that were miscompartmentalized in the soma and dendrites of neurons in the ipsilateral (left) perirhinal cortex, and to a lesser degree, contralateral (right) perirhinal cortex. Surprisingly, *cis*-p-tau immunoreactivity was robustly present in perirhinal and primary motor cortices of both hemispheres 5.5 months post-injury (Fig. 3S and W). The presence of bilateral *cis*-p-tau immunoreactivity at this remote post-injury time point, and in brain regions distant from the primary locus of brain injury, suggests either extreme persistence of incipient tauopathy, or alternatively, progressive tauopathy involving spread beyond the originating injury (see 'Discussion' section). Neuropathological analysis of post-mortem brains from mice subjected to a single closed-head impact (Supplementary Fig. 3Y–HH) revealed a similar pattern and time course of tau protein pathologies as that observed in brains of mice exposed to two impacts.

Perivascular accumulation of phosphorylated tau protein in the depths of cortical sulci represents the defining pathological hallmark of CTE (McKee *et al.*, 2016) and points to traumatic microvascular injury (Kenney *et al.*, 2016) as a likely contributor to CTE pathogenesis. To test the hypothesis that experimental impact injury induces traumatic microvascular injury, we conducted electron microscopic analysis of brains from mice 2 weeks post-injury. Ultrastructural examination of these brains revealed evidence of persistent, focal microvascular injury notable for dysmorphic capillaries; abnormal endothelial cells with

Figure 3 Continued

cortex was histopathologically normal by SMI-34 immunostaining (Supplementary Fig. 2D–F). (**G–I**) Immunostaining for astrocytic glial fibrillary acidic protein (GFAP) in ipsilateral (*left*) perirhinal cortex 24 h (**D**), 3 days (**E**), 2 weeks (**F**) post-injury. (**G**) Sparse GFAP-immunoreactivity (arrowhead) was present 24 h post-injury. Scale bar = 50 μm. (**H**) Brisk reactive astrocytosis at 3 days post-injury. Clusters of hypertrophied GFAP-immunopositive reactive astrocytes (arrowheads) with ramified processes and perivascular astrocytes (arrow) with hydropic end-feet terminating on small blood vessels (dashed lines) were present 3 days post-injury. Overlapping astrocytic processes (black circle) indicate disruption of domain restriction. Scale bars = 50 μm. (**I**) Reactive astrocytes (arrowheads) were present 2 weeks post-injury. Haemosiderin-laden macrophages (darts), representing microhaemorrhage residua, were scattered throughout the affected region. Scale bar = 50 μm. Contralateral (right) perirhinal cortex was histopathologically normal by GFAP immunostaining (Supplementary Fig. 2G–I). (**J–L**) Immunostaining for the myeloid cell marker Iba1 (arrowheads) in ipsilateral (left) perirhinal cortex revealed minimal microgliosis at 24 h (**J**), brisk microgliosis at 3 days (**K**), resolved microgliosis at 2 weeks (**L**) post-injury. Scale bars = 50 μm. (**K**) Peak microgliosis at 3 days post-injury revealed clusters of intensely Iba1-immunoreactive, ramified myeloid cells (arrowheads) and less abundant amoeboid and rodlike Iba1-immunoreactive microglia (open and half-filled arrowheads, respectively). Iba1-immunoreactive perivascular myeloid cells were associated with the parenchymal (abluminal) surface of a small blood vessel (between dashed lines). Scale bar = 50 μm. (**L**) Microgliosis was largely resolved by 2 weeks post-injury. Haemosiderin-laden macrophage (darts) were observed throughout the affected region. Scale bar = 50 μm. Contralateral (*right*) perirhinal cortex was histopathologically normal by Iba1 immunostaining (Supplementary Fig. 2J–L). (**M–O**) Phosphorylated tau protein immunostaining with monoclonal antibody CP13 (pS202) was negative throughout the brain at 24 h (**M**), 3 days (**N**), and 2 weeks (**O**) post-injury. Haemosiderin-laden macrophage (darts) were observed throughout the affected region by 2 weeks post-injury (**O**). Scale bars = 50 μm. The contralateral (*right*) perirhinal cortex did not demonstrate CP13 immunostaining (Supplementary Fig. 2M–O). (**P–W**) Immunohistofluorescence staining for *cis*-p-tau (*cis*-motif, pThr231-Pro), a highly pathogenic early phosphorylated tau proteoform, was present at 24 h (**P**), 3 days (**Q**), 2 weeks (**R**), and 5.5 months (**S**) post-injury in ipsilateral (left) perirhinal cortex. Faint *cis*-p-tau immunoreactivity was observed in axons (arrowheads) in the ipsilateral (left, **P**) but not contralateral (right, **T**) perirhinal cortex 24 h post-injury. By 3 days post-injury, *cis*-p-tau immunoreactivity in the ipsilateral perirhinal cortex (**Q**) was intense, not only in axons (arrowheads), but also as dot-like inclusions in neuronal soma and dendrites (arrow). *Cis*-p-tau immunoreactivity in the contralateral perirhinal cortex (**U**) was present but faint at this time point. By 2 weeks post-injury, *cis*-p-tau immunoreactivity was observed in axons (arrowheads) and as dot-like inclusions in neuronal soma and dendrites (arrow) in both hemispheres. *Cis*-p-tau immunoreactivity was more pronounced in the ipsilateral (left, **R**) than contralateral (right, **V**) perirhinal cortex. Surprisingly, we detected *cis*-p-tau immunoreactivity 5.5 months post-injury (the longest time point measured) in axons (arrowheads) and as dot-like inclusions in neuronal soma and dendrites (arrow) in perirhinal cortex of both hemispheres (left, **S**; right, **W**). Scale bars = 20 μm. Sham (no-injury) control mice did not show evidence of *cis*-p-tau immunoreactivity in either hemisphere at any of the analysed time points (Supplementary Fig. 2P–W). (**X–AA**) Ultrastructural evidence of persistent traumatic microvascular injury revealed by electron microscopy 2 weeks post-injury. (**X**) Low-power electron micrograph of CA1 region of the left hippocampus shows abnormal capillary (c) and nearby neuron (n). A capillary endothelial cell (e) and adjacent pericyte (p) are encircled by hydropic astrocytic end-feet (ae). Perivascular astrocyte processes exhibit pale oedematous cytoplasm with few mitochondria (m), subcellular organelles, or cytoskeletal elements. The capillary basal lamina is thickened, highly branched, and tortuous. Electron-dense inclusion bodies (open arrowheads) and lipofuscin granules with lipid droplets (partially-filled arrowhead) are evident. These ultrastructural pathologies are inconsistent with processing artefact. Magnification × 1500. Scale bar = 2 μm. (**Y**) Low-power electron micrograph of left medial prefrontal cortex 2 weeks after injury shows an abnormal capillary (c) and two nearby neurons, one with normal ultrastructure (n1) and the other undergoing cellular involution (n2). Endothelial cell (e), perivascular pericyte (p), and hydropic astrocytic end-feet (ae) are present. Magnification × 1200. Scale bar = 2 μm. (**Z**) Electron micrograph of the CA1 region of the left hippocampus shows a hydropic astrocytic end-foot (ae) and pericyte (p) of an involuting capillary. The basal laminae are thickened and tortuous (arrowheads). Electron-dense inclusion body (i), swollen mitochondria (m), and autophagosomic vacuoles (v, dashed ellipse) are present. Magnification × 3000. Scale bar = 2 μm. (**AA**) High magnification electron micrograph of the same CA1 region of the left hippocampus showing ultrastructural details of the hydropic astrocytic end-foot (ae) and pericyte (p). Thickened, tortuous basal lamina (arrowheads), inclusion body (i), swollen mitochondrion (m), and degenerating mitochondrion (asterisk) are present. Magnification × 10 000. Scale bar = 500 nm. *n* = 4 mice per group.

irregularly shaped nuclei and thickened, tortuous basal laminae; and perivascular astrocytes with grossly enlarged, highly-vacuolated, hydropic end-feet (Fig. 3X–AA). Perivascular astrocytes and pericytes in the perirhinal cortex, hippocampus, and frontal cortex were also notable for electron-dense inclusion bodies, lipofuscin granules, myelin figures, and autophagosomic vesicles. Pericytes, microglial cells, dystrophic nerve fibres, and dark neurons were observed in proximity to small blood vessels in brains from impact-injured mice but not uninjured controls. These findings provide direct evidence that experimental closed-head impact injury damages small blood vessels and induces persistent focal traumatic microvascular injury (Goldstein *et al.*, 2012; Huber *et al.*, 2013; Hay *et al.*, 2015; Doherty *et al.*, 2016; Kenney *et al.*, 2016).

Closed-head impact injury triggers differential expression of phosphorylated tau proteoforms

Given the effects of closed-head impact on the microvasculature and induction of *cis*-p-tauopathy, we were surprised by the absence of mature tau protein neuropathology in impact-injured mice (Fig. 3M–O). We hypothesized that epitopes detected by *cis*-p-tau (*cis*-pThr231) and CP13 (pSer202) antibodies represent earlier and later stage tauopathy, respectively. To investigate the possible presence of CP13-immunoreactive molecular pathology, we performed quantitative tau protein immunoblot analysis of brains from impact-injured mice ($n = 16$) compared to sham (uninjured) control mice ($n = 14$) (Fig. 4). We detected a significant increase in both the intensity and mobility range of CP13-immunoreactive phosphorylated tau protein in brains from impact-injured mice compared to controls (Bonferroni-corrected two-tailed Student's *t*-test, $P = 0.006$). This effect was accompanied by a significant increase in total tau protein (Tau5) ($P = 0.001$), indicating accumulation of both phosphorylated and non-phosphorylated tau protein species. Increased brain levels of tau protein were detected bilaterally. Also notable was the increase in higher apparent molecular weight tau protein species in the contralateral compared to ipsilateral hemispheres of impact-injured mice. This finding may indicate differences in tau protein phosphorylation or proteoform composition at sites of traumatic injury compared to brain regions affected by latent tau propagation or spread.

Relationship of traumatic microvascular injury to early CTE tau pathology

Neuropathological examination of teenage athlete brains in the acute-subacute period after closed-head impact injuries (Fig. 1) and histopathological and ultrastructural analyses of brains from impact-injured mice (Fig. 3) suggested traumatic microvascular injury and blood–brain barrier disruption as candidate mechanisms linking closed-head impact to acute brain injury and chronic post-traumatic sequelae (Martland, 1928; Hay *et al.*, 2015; Doherty *et al.*, 2016; Kenney *et al.*, 2016), including CTE (Goldstein *et al.*, 2012; McKee *et al.*, 2013, 2016). To investigate this hypothesis, we injected mice with Evans blue, an albumin-binding sulphonated diazo dye (960 Da) that is normally excluded from the brain by an intact blood–brain barrier (Rawson, 1943; Povlishock, 1998). Examination of post-mortem brains from Evans blue-injected mice sacrificed 24 h after left-lateral impact injury ($n = 12$) or the uninjured sham control condition ($n = 7$) revealed a spectrum of macroscopic pathologies (Fig. 5A). Brains from ~50% of impact-injured mice were grossly normal and showed no evidence of Evans blue extravasation, contusion, necrosis, haematoma, haemorrhage, or other gross brain pathologies (Grade 0; Fig. 5A). Brains from ~40% of impact-injured mice demonstrated faint Evans blue extravasation without evidence of frank haemorrhage, haematoma, or contusion (Grade I; Fig. 5A). These focal lesions localized exclusively to the lateral surface of the ipsilateral perirhinal cortex subjacent to the impact contact zone. Together, these two classes of normal or minor brain pathology (Grades 0 and I, respectively) constituted ~90% of the experimentally head-injured mice. By contrast, brains from ~10% of impact-injured mice exhibited focal contusions with petechial haemorrhages surrounded by a penumbra of extravasated Evans blue dye (Grade II; Fig. 5A). These complex lesions localized exclusively to surface cortex ipsilateral to impact. Evidence of gross neuropathology (Grades I, II) in ~50% of impact-injured mice contrasts with the absence of gross pathology in all mice exposed to experimental blast under conditions of comparable head kinematics (Goldstein *et al.*, 2012).

We confirmed blood–brain barrier disruption by quantitative Evans blue fluorescence brain imaging (Fig. 5B–D). Evans blue-specific fluorescence signal intensity was determined after spectral unmixing to remove background autofluorescence. Cluster analysis using a Gaussian mixture model (Fig. 5D) identified three distinct injury classes based on fluorescence signal intensity: Grade 0, intact blood–brain barrier (411.4 ± 83.3 counts/pixel, $2.9 \pm 1.7\%$ suprathreshold pixels); Grade I, minor blood–brain barrier disruption (707.5 ± 191.2 counts/pixel, $18.8 \pm 6.2\%$ suprathreshold pixels); Grade II, severe blood–brain barrier disruption (1203.6 ± 210.5 counts/pixel, $58.4 \pm 8.2\%$ suprathreshold pixels). In the control group ($n = 7$), six mice (86%) were classified as Grade 0, one mouse (14%) as Grade I, and none (0%) as Grade II. In the impact group ($n = 12$), five mice were classified as Grade 0 (42%), five mice (42%) as Grade I, and two mice (17%) as Grade II. The three injury classes mirrored the groups identified by gross pathology (Fig. 5A). Inclusion of all groups revealed a statistically significant effect of impact on ipsilateral blood–brain barrier disruption when compared to control (linear mixed-effects regression analysis, $P = 0.0004$; Fig. 5C). Consistent with the post-injury neuropathology (Fig. 3), blood–brain barrier disruption was not detected in the contralateral hemisphere of brains from impact-injured mice.

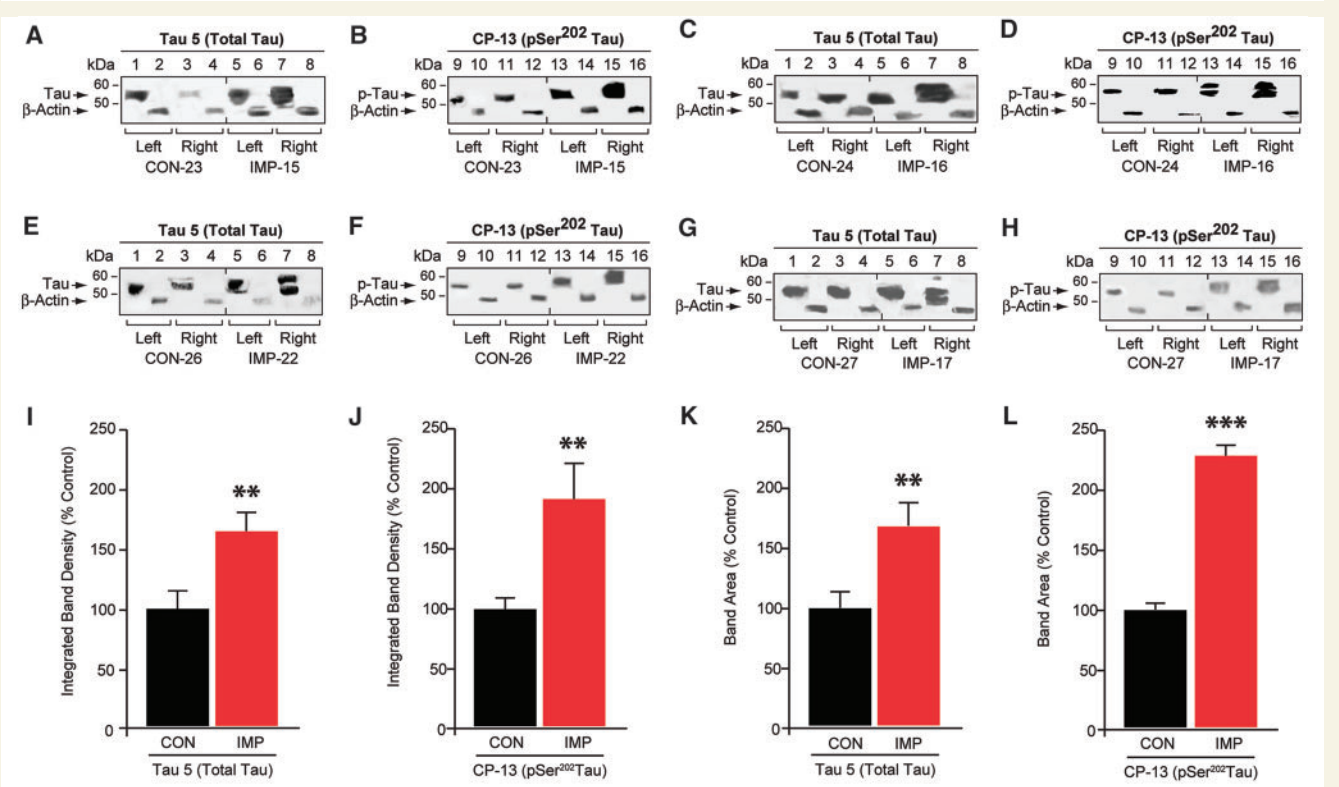

Figure 4 Unilateral closed-head impact injury induces persistent bilateral phosphorylated tau proteinopathy in awake, anaesthesia-naïve mice. (**A–H**) Phosphorylated tau protein immunoblot analysis of brain homogenates from left and right hemispheres from mice exposed to experimental left-lateral closed-head impact injury (IMP) or sham (no injury) control exposure (CON) probed for total tau protein (Tau 5; **A**, **C**, **E** and **G**), phosphorylated tau protein (CP-13, pSer202; **B**, **D**, **F** and **H**), and β-actin (**A–H**) 2 weeks after CON (lanes 1–4, 9–12) or IMP (lanes 5–8, 13–16) exposure. Immunoblot analysis revealed a broad band of CP-13-immunoreactive phosphorylated tau protein that migrated with an apparent molecular mass of 53 kD (arrows). (**I–L**) Densitometric quantitation of total tau protein (**I** and **K**) and CP-13 phosphorylated tau protein (**J** and **L**) in brain homogenates from mice 2 weeks after IMP or CON exposure. $n = 8$ mice per group, mean values ± SEM in arbitrary densitometric units (a.u.) normalized to control values. $^{***}P < 0.001$, $^{**}P < 0.01$ (unpaired two-tailed Student's *t*-test).

These results suggested mechanistic links between impact-induced traumatic microvascular injury and pathological and functional sequelae associated with closed-head impact injury. Since impact injury was associated with ipsilateral blood–brain barrier disruption, we investigated the possibility that mild TBI may promote non-haemorrhagic accumulation of extravasated serum albumin in the brain. Mice subjected to unilateral impact demonstrated robust evidence of ipsilateral serum albumin extravasation and co-localizing reactive astrocytosis (Fig. 5H–P; *cf.* 5E–G). Focal albumin deposition and co-localizing reactive astrocytosis were detected exclusively in ipsilateral (left) perirhinal cortex in impact-injured mice (Fig. 5H–J) but not in any brain region in control mice (Fig. 5E–G and Supplementary Fig. 2). Peak signals for extravasated serum albumin and astrocytosis co-localized at 3 days post-injury in impact-injured mice. Extravasated albumin also co-localized with TGF-β1-associated astrocytosis and downstream markers of transforming growth factor beta signalling, in ipsilateral (Fig. 5K–P; Supplementary Fig. 4A and D) but not in contralateral perirhinal cortex of impact-injured mice (Supplementary Fig. 4B and E) or in any brain region of uninjured control mice (Supplementary Fig. 4C and F).

In vivo detection of traumatic microvascular injury by dynamic brain imaging

We reasoned that the blood–brain barrier disruption we detected *ex vivo* (Fig. 5A–P) would be detectable *in vivo* using a modified dynamic contrast-enhanced MRI strategy (Weissberg *et al.*, 2014) combined with systemically administered gadofosveset trisodium, a gadolinium-based contrast agent that binds albumin (Lauffer *et al.*, 1998). We performed a proof-of-concept feasibility study to validate this strategy for *in vivo* diagnostic evaluation of traumatic microvascular injury. *In vivo* dynamic neuroimaging combined with systemic administration of gadofosveset trisodium confirmed acute and persistent blood–brain barrier disruption in left but not right perirhinal cortex (ipsilateral and contralateral to impact, respectively) in impact-injured mice but not control mice (Fig. 5S–T). The ipsilateral blood–brain barrier permeability defect in impact-injured mice co-localized with T_1-weighted hyperintensities in the affected cortical field (Fig. 5Q–R). Blood–brain barrier

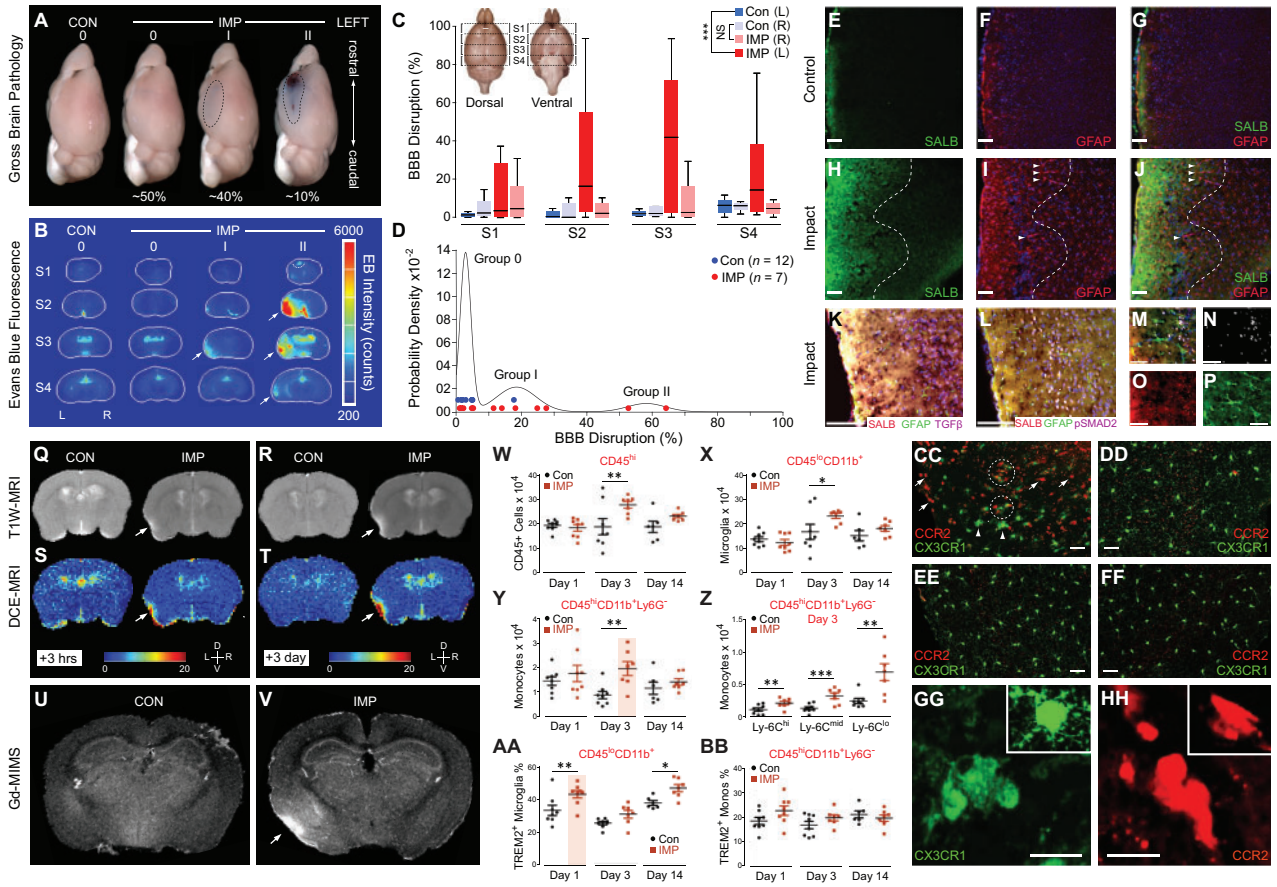

Figure 5 Unilateral, closed-head impact injury induces focal blood–brain barrier disruption, serum albumin extravasation, astrocytosis, myeloid inflammatory cell infiltration, and TREM2+ microglial activation in cerebral cortex ipsilateral and subjacent to impact. (**A**) Gross pathology in representative brains from a control mouse (CON) exposed to sham (no injury) control condition compared to brains from mice subjected to experimental closed-head impact injury (IMP) with varying degrees of gross brain pathology (Grade 0, I, II, respectively) 24 h post-injury. Grade 0: absence of gross brain pathology with no evidence of macroscopic tissue damage (contusion, necrosis, hematoma, haemorrhage, or extravasated Evans blue) was observed in 100% of brains from CON mice and ~50% of brains from IMP mice. Grade I: minimal brain pathology marked only by focal Evans blue extravasation (indicative of disruption of the blood–brain barrier, BBB) was observed in ~40% of IMP mice but none (0%) of the CON mice. Grade II: relatively rare brains marked by complex lesions that included Evans blue extravasation and contusion observed in ~10% of IMP mice but none (0%) in CON mice. (**B**) Evans blue-specific fluorescence imaging of representative mouse brain sections showing blood–brain barrier disruption 24 h post-injury. Arrows, left-lateral fluorescence signal indicating area of blood–brain barrier disruption (in Evans blue-specific fluorescence intensity counts) in cerebral cortex ipsilateral and subjacent to experimental impact injury (IMP) but not sham (no-injury) control condition (CON). Serial brain sections (anterior to caudal, S1–S4, respectively) and gross pathology injury grade (0, I, II) as indicated. (**C**) Quantitative analysis of blood–brain barrier disruption by coronal section Evans blue-specific fluorescence brain imaging 24 h after IMP or CON exposure. Blood–brain barrier disruption localized to the perirhinal, insular, entorhinal, and piriform cortices and basolateral amygdala of the left hemisphere ipsilateral and subjacent to the impact contact zone. *Inset*: rostral-to-caudal brain sections, S1–S4. ***$P < 0.001$; NS = not statistically different. (**D**) Gaussian mixed model analysis of Evans blue fluorescence brain imaging yielded three groups that corresponded to gross pathology classification (Grades 0, I, II). (**E–J**) Anatomical localization of extravasated serum albumin (SALB; **E**, **G**, **H** and **J**) and co-localizing reactive astrocytosis (GFAP; **F**, **G**, **I** and **J**) in left perirhinal cortex ipsilateral to impact 3 days post-injury (**H–J**) but not in corresponding cortex from CON mice (**E–G**). DAPI (blue channel: **F**, **G**, **I** and **J**), cell nuclei. Hashed lines (**H–J**) demarcate cortical region with maximal post-injury serum albumin extravasation (**H** and **J**) and co-localization with reactive astrocytosis (**I** and **J**). Arrowheads, GFAP-immunopositive processes of activated astrocytes. Scale bars = 100 μm. (**K–P**) Left perirhinal cortex at peak of reactive astrocytosis 3 days post-injury. Composite fluorescence microscopic images showing co-localization of extravasated serum albumin (SALB, red: **K**, **L**, **M** and **O**) with reactive astrocytosis (GFAP, green: **K**, **L**, **M** and **P**); TGFβ expression (TGFβ, violet: **K**) and phosphorylated-SMAD2, a marker downstream of TGF-β signalling (pSMAD2, violet: **L**, **M** and **N**). Cell nuclei (DAPI, blue: **K**, **L** and **M**). Yellow-white areas indicate overlapping SALB and GFAP immunoreactivity (**K**, **L** and **M**). High magnification (×40) composite fluorescence image (**M**) and fluorescence channels (**N**, pSMAD2; **O**, SALB; **P**, GFAP). Magnification: **K** and **L** = ×20; **M–P** = ×40. Scale bars in **K** and **L** = 100 μm; **M–P** = 50 μm. Serum albumin extravasation, GFAP-immunoreactive astrocytosis, and pSMAD2-TGFβ upregulation were not observed in the contralateral perirhinal cortex of IMP mice nor in perirhinal cortex of either hemisphere in CON mice (Supplementary Fig. 4A–F). (**Q–V**) Focal blood–brain barrier disruption and co-localizing serum albumin extravasation detected in the brains of living mice by dynamic contrast-enhanced MRI (DCE-MRI) neuroimaging with

(continued)

permeability defects were not detected by neuroimaging in the contralateral cortex of impact-injured mice or either hemisphere in uninjured control mice. Post-mortem neuropathological examination did not reveal evidence of haemorrhagic contusion, suggesting that the permeability defect resulted from blood–brain barrier dysfunction rather than intraparenchymal haemorrhage.

To confirm that the detected neuroimaging abnormalities represented true blood–brain barrier permeability disruption, we used laser ablation-assisted metallomic imaging mass spectrometry to map tissue concentrations and spatial distribution of gadolinium in coronal sections of brains harvested from impact-injured and control mice. Mice in both groups received intravenous gadofosveset trisodium during dynamic neuroimaging (Fig. 5Q–V). Metallomic imaging mass spectrometry maps of brains obtained from impact-injured mice revealed enhanced gadolinium accumulation in left perirhinal cortex (Fig. 5V) that co-localized with the neuroimaging abnormalities (Fig. 5Q–T). Enhanced gadolinium accumulation was not detected in contralateral perirhinal cortex of impact-injured mice or control mice. These results confirm that impact injury was associated with ipsilateral traumatic microvascular injury and focal blood–brain barrier disruption in mice exposed to unilateral closed-head impact injury. Our results provide 'proof of concept' validation of dynamic brain imaging with gadofosveset trisodium for diagnostic evaluation of blood–brain barrier dysfunction in the acute-subacute period after closed-head impact injury.

Relationship of neuroinflammation to traumatic microvascular injury and early CTE tau pathology

Given the co-localization of three CTE-associated brain pathologies—phosphorylated tauopathy, traumatic microvascular injury, and blood–brain barrier disruption—after impact neurotrauma and the known involvement of myeloid-derived cells in tau processing (Asai *et al.*, 2015) and association with CTE (Cherry *et al.*, 2016), we hypothesized that focal neuroinflammatory responses would be triggered by impact injury. To test this hypothesis, we used flow cytometry to characterize inflammatory cell phenotypes and time course of neuroinflammatory responses triggered by experimental closed-head impact injury (Fig. 5W–BB; Supplementary Fig. 4G–I). We observed a significant increase in the number of infiltrating peripheral myeloid cells 3 days post-injury in brains from impact-injured mice ($n = 7$) compared to controls ($n = 8$) [one-way ANOVA, $F(5,38) = 3.74$, $P = 0.0076$; Bonferroni-corrected two-tailed Student's t-test, $P = 0.0054$] (Fig. 5W). The Day 3 leucocyte peak coincided with peak astrocytosis and microgliosis detected by histopathology (Fig. 3H and K). Immunophenotyping analysis revealed co-expression of molecular markers that identify these cells as presumptive inflammatory monocytes and brain macrophage derived from inflammatory monocytes (Fig. 5Y) (Murray and Wynn, 2011). Sub-phenotyping based on monocyte surface antigen expression in impact-injured mouse brains at Day 3 post-injury revealed a significant increase in all three functional classes (Fig. 5Z):

Figure 5 Continued

gadofosveset trisodium, an FDA-approved gadolinium-based contrast agent that binds serum albumin. High-field (11.7 T) T_1-weighted MRI (**Q** and **R**) and DCE-MRI (**S** and **T**) with systemically administered gadofosveset trisodium. T_1-weighted MRI and DCE-MRI were conducted 3 h (**Q**, T_1-weighted MRI (T1W-MRI); **S**, DCE-MRI) and 3 days (**R**, T_1-weighted MRI; **T**, DCE-MRI) after IMP or CON exposure. T_1-weighted hyperintensity (**Q** and **R**) co-localized with blood–brain barrier permeability defect detected by DCE-MRI (**S** and **T**) in the left perirhinal cortex (arrows) 3 h and 3 days after IMP but not CON exposure. Non-specific signal was observed in the ventricles and sagittal sinus. D = dorsal, V = ventral; L = left, R = right. (**U** and **V**) Confirmation of serum albumin extravasation indicating blood–brain barrier disruption by gadolinium metallomic imaging mass spectrometry (Gd-MIMS) in perfused post-mortem brains from the same mice imaged by T_1-weighted MRI (**Q** and **R**) and DCE-MRI (**S** and **T**). Enhanced gadolinium accumulation was observed in the left lateral perirhinal and piriform cortices (arrow) 2 weeks after IMP (**V**) but not CON (**U**) exposure. Gadolinium accumulation detected by Gd-MIMS co-localized with T_1-weighted hyperintensity and blood–brain barrier permeability defect detected by DCE-MRI, thus confirming intracerebral blood–brain barrier disruption. (**W–BB**) Flow cytometry analysis showed that IMP triggers increased number of CD45 + inflammatory cells and activation of TREM2 + microglia in the brain post-injury. CD45 + inflammatory cells (**W**) and $CD45^{lo}CD11b^{+}$ microglia (**X**) were significantly increased 3 days after IMP compared to CON exposure. (**Y**) $CD45^{hi}CD11b^{+}Ly^{-}6G^{-}$ inflammatory cells accumulated in the brain 3 days after IMP compared to CON exposure. (**Z**) All three major subpopulations (Ly-$6C^{hi}$, Ly-$6C^{mid}$, Ly-$6C^{lo}$) were represented in $CD45^{hi}CD11b^{+}Ly^{-}6G^{-}$ inflammatory cells detected 3 days post-injury. (**AA** and **BB**) Upregulation of TREM2 expression in microglia (**AA**) but not CD45 + inflammatory cells (**BB**) at 1 and 14 days after IMP compared to CON exposure. For flow cytometry experiments, $n = 6$–8 mice per group per time point. ***$P < 0.001$; **$P < 0.01$; *$P < 0.05$. See Supplementary Fig. 4G–I for flow cytometry population dot plots. (**CC–HH**) Brain accumulation of $Ccr2^{RFP}$-expressing inflammatory cells (red-labelled cells) and activation of brain-resident $Cx3cr1^{GFP}$-expressing microglia (green-labelled cells) were confirmed by fluorescence microscopy in perirhinal cortex ipsilateral and subjacent to experimental impact injury in $Ccr2^{RFP}/Cx3cr1^{GFP}$ mice at 3 days post-injury (IMP: **CC**, **DD**, **GG** and **HH**) or control (CON: **EE** and **FF**). Representative fluorescence microscopy images show red-labelled $Ccr2^{RFP}$-expressing inflammatory cells (arrows, **CC**) throughout the ipsilateral (left) perirhinal and adjacent cortex, basolateral amygdala, and overlying dura and leptomeninges (**CC** and **HH**) 3 days post-injury. The affected cortex was also notable for large numbers of ameboid $Cx3cr1^{GFP}$-expressing microglia (arrowheads; **CC** and **GG**) that were also present, but to a lesser degree, in the contralateral (right) hemisphere (DD). Note clustering of $Ccr2^{RFP}$-expressing inflammatory cells and $Cx3cr1^{GFP}$-expressing microglia in the left perirhinal cortex (dashed circles, **CC**), the primary locus of post-traumatic brain pathology ipsilateral and subjacent to the impact. By contrast, $Ccr2^{RFP}$-expressing inflammatory cells were minimally present and amoeboid $Cx3cr1^{GFP}$-expressing microglia were absent in brains from $Ccr2^{RFP}/Cx3cr1^{GFP}$ mice 3 days after CON exposure (**EE** and **FF**). Bars (**CC**–**FF**), 40 microns; (**GG**, **HH**), 20 microns.

short-lived inflammatory monocytes [one-way ANOVA, $F(1,13) = 17.15$, $P = 0.0012$] (Geissmann *et al.*, 2003); immature monocytes [one-way ANOVA, $F(1,12) = 17.73$, $P = 0.0005$] (Sunderkötter *et al.*, 2004); and patrolling monocytes [one-way ANOVA, $F(1,13) = 16.29$, $P = 0.0014$] (Auffray *et al.*, 2007). Flow cytometry also revealed an apparent expansion of microglia on Day 3 post-injury in brains from impact-injured mice but not control mice [one-way ANOVA, $F(5,38) = 4.207$, $P = 0.0039$; Bonferroni-corrected two-tailed Student's *t*-test, $P = 0.043$] (Fig. 5X).

We hypothesized that neuroinflammatory reactions to closed-head impact injury would be accompanied by trauma-stimulated microglial phenotype transformation. To evaluate this hypothesis, we investigated microglial expression of TREM2 (triggering receptor expressed on myeloid cells 2 protein), an immunoglobulin superfamily cell surface receptor and homeostatic regulator of cytokine production, phagocytic clearance, innate immunity responses, and tissue repair (Bhaskar *et al.*, 2010; Kokiko-Cochran *et al.*, 2016; Ulrich and Holtzman, 2016). TREM2 expression is upregulated in activated microglia (Schmid *et al.*, 2002; Kawabori *et al.*, 2015; Wang *et al.*, 2015). Moreover, *TREM2* gene variants in human populations are associated with increased risk of age-related neurodegenerative diseases, including Alzheimer's disease (Guerreiro *et al.*, 2013; Jonsson *et al.*, 2013; Phimister and Tanzi, 2015; Ulrich and Holtzman, 2016). Flow cytometry immunophenotyping revealed a significant increase in the percentage of microglia expressing TREM2 [one-way ANOVA, $F(5,38) = 13.14$, $P < 0.0001$; Bonferroni-corrected two-tailed Student's *t*-tests: 24 h, $P = 0.0072$, Impact $n = 8$, Control $n = 8$; 2 weeks, $P = 0.0348$, Impact $n = 7$, Control $n = 6$] compared to controls (Fig. 5AA). Notably, activation of microglial TREM2 expression temporally preceded peripheral monocyte infiltration in brains of impact-injured mice. By contrast, we did not detect a significant change in TREM2-expressing infiltrating myeloid cells in brains from impact-injured mice compared to controls at any of the three time points (Fig. 5BB).

To confirm cellular phenotype localization and transformation of brain-resident microglia and presumptive brain-infiltrating monocytes, we crossed genetically-modified mice that produce red fluorescent protein-labelled inflammatory monocytes ($Ccr2^{RFP}$ mice) with genetically-modified mice that produce green fluorescent protein-labelled brain-resident microglia and perivascular macrophages ($Cx3cr1^{GFP}$ mice). F1 progeny expressed red fluorescent protein-labelled monocytes (red cells) and green fluorescent protein-labelled brain-resident microglia and perivascular macrophages (green cells). We subjected crossed mice to impact injury under the same experimental conditions used in the preceding experiments. Fluorescence microscopic analysis of brain sections obtained from these mice at Day 3 post-injury revealed large numbers of red-labelled monocytes throughout the ipsilateral perirhinal, insular, and piriform cortices and overlying leptomeninges subjacent to impact (Fig. 5CC and HH). Presumptive infiltrating monocytes co-localized with large ameboid-shaped microglia and perivascular macrophages (Nayak *et al.*, 2014) (Fig. 5CC and GG). Presumptive red-labelled infiltrating monocytes and green-labelled ameboid-shaped microglia and macrophages were also present but far more scarce in the contralateral (right) hemisphere at Day 3 post-injury (Fig. 5DD). By contrast, presumptive infiltrating monocytes were minimally present and co-localizing ameboid-shaped microglia and macrophages were absent in brains from uninjured control mice (Fig. 5EE–FF).

Unilateral impact injury induces bilateral electrophysiological deficits in hippocampus and prefrontal cortex

Given the known clinical association of mild TBI with cognitive impairment and executive dysfunction (Evans, 2006; Ropper and Gorson, 2007; Alosco *et al.*, 2017), and recent recognition of concordant abnormalities in early-stage CTE (i.e. traumatic encephalopathy syndrome; Montenigro *et al.*, 2014, 2017), we hypothesized that experimental head injury could disrupt neurophysiological function in two critical brain regions subserving these functions, namely, the hippocampus and medial prefrontal cortex (McDonald *et al.*, 2002; Sigurdsson and Duvarci, 2015; Place *et al.*, 2016). To test this hypothesis, we evaluated axonal conduction velocity of hippocampal pyramidal cell compound action potentials in the stratum alveus (Fig. 6A–D and Supplementary Fig. 5A) and activity-dependent LTP of synaptic transmission at excitatory inputs to pyramidal neurons in the medial prefrontal cortex (Fig. 6E–J and Supplementary Fig. 5B–D). Analysis of hippocampal pyramidal cell compound action potentials (Fig. 6A) revealed significant and persistent decrements in axonal conduction velocity in the ipsilateral (left) hippocampus at 24 h, 3 days, and 2 weeks post-injury (Fig. 6B–D). Three-way ANOVA [main factors: injury (levels: TBI and control), post-injury interval (levels: 24 h, 3 days, and 2 weeks), and side (levels: ipsilateral and contralateral to impact)] revealed a significant effect for injury [$F(1,119) = 71.431$; $P < 0.0001$] on axonal conductance, with comparable decrements in hippocampus ipsilateral and contralateral to impact 24 h, 3 days, and 2 weeks post-injury (Fig. 6B and C). There was no significant effect for either post-TBI interval [$F(2,119) = 0.212$; $P = 0.8094$] or brain hemisphere [$F(1,119) = 0.033$; $P = 0.8554$]. While axonal conduction velocity in the right (contralateral) hippocampus returned to baseline levels by 2 weeks post-injury, axonal conduction velocity in the left (ipsilateral) hippocampus remained impaired at this time point (Fig. 6D).

Given the impact-induced functional impairments in hippocampal axonal conduction velocity, we examined the effect of impact injury on synaptic transmission and stimulus-evoked LTP of synaptic strength at excitatory inputs to pyramidal neurons in the medial prefrontal cortex (Supplementary Fig. 5B and C). The rationale for this investigation is based on neuroanatomical and functional

connections between the hippocampus and medial prefrontal cortex, and additionally, the prominence of executive dysfunction (mediated, in part, by the medial prefrontal cortex) that commonly accompanies closed-head impact injuries in humans (see 'Discussion' section). Analysis of white matter-evoked postsynaptic field potential input-output relations indicated that impact injury did not alter baseline synaptic transmission (Supplementary Fig. 5D). However, left-lateral impact induced significant and persistent bilateral decrements in stimulus-evoked LTP in the medial prefrontal cortex at 24 h, 3 days, and 2 weeks post-injury (Figs. 6E–J). Three-way ANOVA (main factors and levels as above) determined that only injury had a significant effect on LTP in the medial prefrontal cortex [$F(1,60) = 60.227$; $P < 0.0001$], with no effect of either post-TBI interval [$F(2,60) = 0.029$; $P = 0.9761$] or recording side [$F(1,60) = 0.949$; $P = 0.3340$], and no interaction of main factors. Moreover, the magnitude of post-tetanic potentiation immediately after application of theta-burst stimulation was also reduced at all three time points. Together, these results indicate that exposure to unilateral closed-head impact injury induces acute, persistent, and bilateral impairments in hippocampal axonal conduction velocity and disruption of short- and long-term activity-dependent synaptic plasticity in the medial prefrontal cortex.

Acute neurobehavioural responses to closed-head impact injury do not correlate with TBI and CTE endpoints

Recent clinical findings suggest that cumulative concussion exposure correlates poorly with post-traumatic brain pathologies and functional sequelae (Breedlove *et al.*, 2012; Davenport *et al.*, 2014; Talavage *et al.*, 2014; Abbas *et al.*, 2015; Montenigro *et al.*, 2017). Moreover, post-mortem studies have confirmed that a subset (~20%) of former athletes with neuropathologically-verified CTE did not have a history of concussion (Bieniek *et al.*, 2015; Stein *et al.*, 2015*a*). Our experimental results allowed us to evaluate the putative relationship between concussion and CTE brain pathology by testing for possible correlations between composite scores on the acute neurobehavioural response test battery and quantitative endpoints associated with TBI and early CTE (Supplementary Table 3). Target metrics included blood–brain barrier disruption by Evans blue-specific fluorescence, neuroinflammation assessed by myeloid cell flow cytometry, phosphorylated tau proteinopathy by quantitative immunoblot analysis, impaired hippocampal axonal conduction velocity, and defective LTP in the medial prefrontal cortex. Time point selection was based on peak post-injury responses for each TBI and CTE metric. Consistent with clinical (Breedlove *et al.*, 2012; Davenport *et al.*, 2014; Talavage *et al.*, 2014; Abbas *et al.*, 2015; Montenigro *et al.*, 2017) and pathological findings in humans (Bieniek *et al.*, 2015; Stein *et al.*, 2015*a*), we did not detect any statistically significant correlation between test battery composite scores and quantitative endpoints associated with TBI and early CTE (Supplementary Table 3).

Based on these results, we hypothesized that the mechanisms underpinning concussion-like deficits after experimental impact injury may be independent of the mechanisms that drive TBI and CTE brain pathologies. We investigated the mechanistic underpinnings of this hypothesis in the following section.

Head impact and blast exposure induce different force loading, shear stress, and concussion-like deficits

The brain pathologies and functional sequelae observed after experimental impact injury are generally consistent with corresponding responses following blast exposure (Goldstein *et al.*, 2012; Huber *et al.*, 2013; Kondo *et al.*, 2015). While the manner in which kinetic energy is transferred to the head is different in the two types of insult, the brain pathologies associated with each are similar in laboratory animals and humans (Omalu *et al.*, 2011; Goldstein *et al.*, 2012; Huber *et al.*, 2013; McKee *et al.*, 2013; Kondo *et al.*, 2015; Shively *et al.*, 2016; Mez *et al.*, 2017). Concordance of head motion in our impact and blast mouse models enabled comparative evaluation of acute neurobehavioural responses, structural brain pathologies, and functional sequelae produced by these two biomechanically different neurotrauma mechanisms under exposure conditions matched for head kinematics (Supplementary Table 2).

We subjected awake, anaesthesia-naïve C57BL/6 male mice to experimental closed-head impact injury ($n = 203$) or blast exposure ($n = 24$) under conditions that produce comparable head kinematics and evaluated mice after exposure using the acute neurobehavioural responses test battery (Fig. 7A). Baseline (pre-injury) testing showed that mice in both groups exhibited indistinguishable mean composite test battery scores (mean ± SEM: impact, 14.9 ± 0.0; blast, 14.8 ± 0.1; linear mixed-effects regression analysis, $P > 0.05$). While impact-injured mice demonstrated the expected significant decrement in post-injury composite scores (mean ± SEM: 11.6 ± 0.2; linear mixed-effects regression analysis, $P < 0.0001$; Supplementary Video 1), blast-exposed mice did not (mean ± SEM: 14.5 ± 0.1; linear mixed-effects regression analysis, $P > 0.05$; Supplementary Video 1). This result was robust, reliable, and entirely unexpected, especially given comparable head kinematics in the two models. It is worth noting that the absence of acute neurobehavioural deficits following blast exposure comports with the low incidence of concussion after pure blast exposure in the absence of concomitant contact injury (Barrow and Rhoads, 1944; Luethcke *et al.*, 2011). After 3-h recovery, both experimental groups again demonstrated

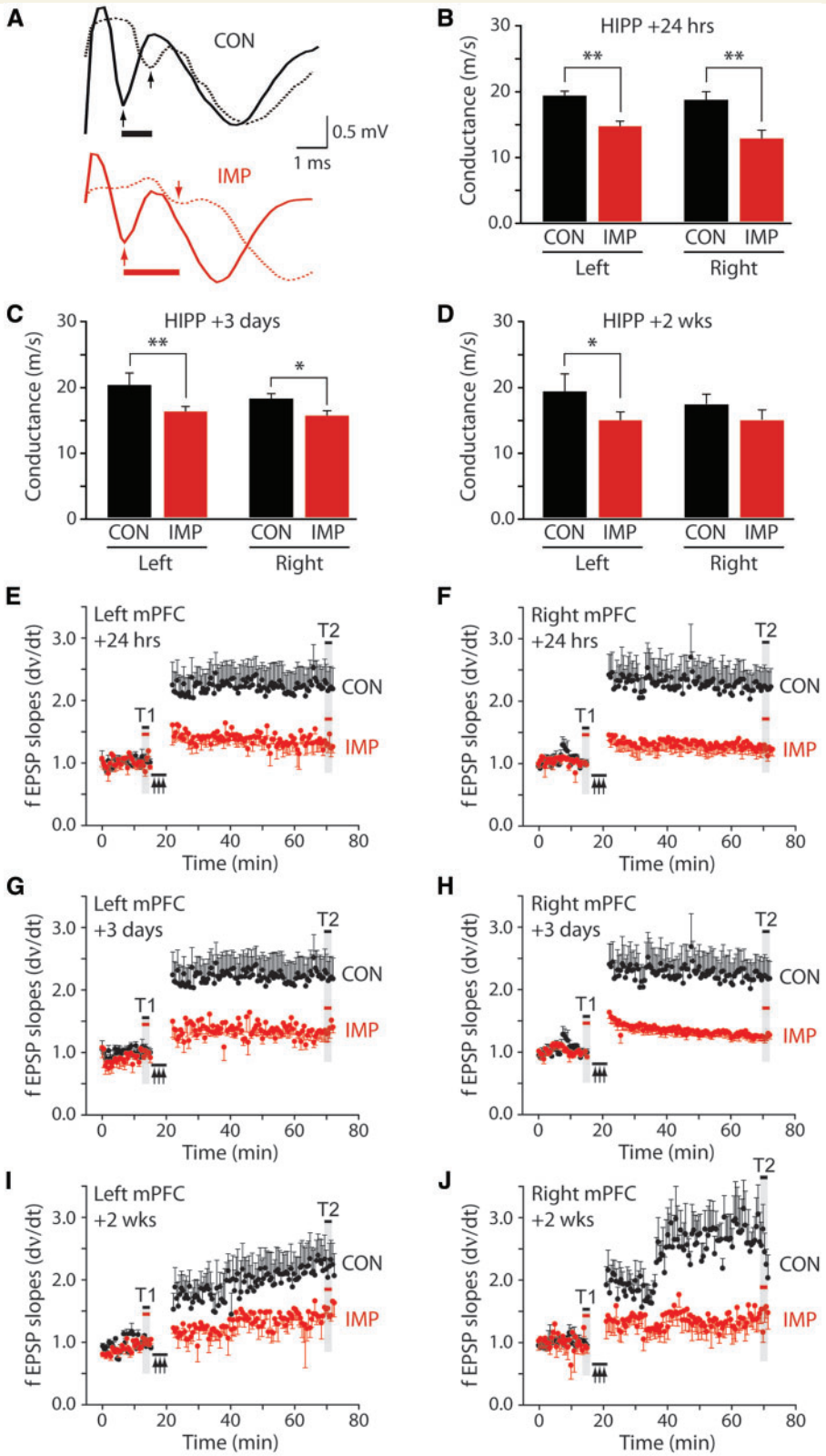

Figure 6 Unilateral closed-head impact injury induces early, persistent, bilateral impairments in hippocampal axonal conduction velocity and medial prefrontal cortical long-term potentiation of synaptic neurotransmission. (**A–D**) Time course of impaired axonal conduction velocity in the hippocampus (HIPP) CA1 subregion of mice exposed to unilateral (left-sided) closed-head impact injury (IMP, red) or sham (no injury) control (CON, black). Time points: 24 h, 3 days, 2 weeks post-exposure. Experimental testing arrangement in relation to neuroanatomy and circuitry is shown in Supplementary Fig. 5A. (**A**) Representative stimulus-evoked compound action potentials at proximal (solid lines) and distal (dashed lines) recording sites in the CA1 subregion of hippocampus slices obtained from mice exposed to

(continued)

indistinguishable mean composite test battery scores that were also indistinguishable from baseline scores (mean ± SEM: impact, 14.7 ± 0.0; blast, 14.5 ± 0.1; linear mixed-effects regression analysis, $P > 0.05$). Given that head motion in the two experimental models was kinematically comparable, our observation of decrements in test battery composite scores after impact injury but not after blast exposure argues against head motion *per se* as a primary causative mechanism that differentiates concussion-like neurobehavioural responses after these insults.

To investigate the origins of this unexpected difference, we constructed mouse headforms to which we attached pressure-sensitive film on the lateral surface. Impact and blast exposures were conducted as above. Force loading was assessed by determining total pixel intensity registered by the pressure-sensitive film (Fig. 7B). Total pixel intensity on film exposed to impact was significantly greater than for blast (mean ± SEM, $n = 5$: impact, $6.49 \pm 0.43 \times 10^6$ a.u.; blast, $0.28 \pm 0.04 \times 10^6$ a.u.; Bonferroni-corrected one-tailed Student's *t*-test, $P = 0.0002$) while both impact and blast generated significantly greater pixel intensities than respective controls (mean ± SEM, $n = 5$: impact control, $1.58 \pm 0.66 \times 10^4$ a.u.; blast control, $2.67 \pm 0.51 \times 10^4$ a.u.; Bonferroni-corrected one-tailed Student's *t*-tests: impact versus impact control, $P = 0.0002$; blast versus blast control, $P = 0.0089$). Moreover, impact produced high pressure loading that was restricted to the contact zone, whereas blast generated far lower pressure that was evenly distributed within the measurement area (Fig. 7B). These results point to fundamentally different energy loading regimes at the moment of traumatic contact.

Experimental methods are not currently available to measure stresses in discrete regions of the living mouse brain at microsecond time resolution. Thus, we investigated how these results relate to the observed differences in acute neurobehavioural responses to impact injury and blast exposure by using dynamic computational simulations of our two experimental mouse models. We used the Arbitrary-Lagrangian-Eulerian hydrostructural finite element code ALE3D (Noble *et al.*, 2017) developed at the Lawrence Livermore National Laboratory to simulate the experimental impact instrument described above and blast tube used here and in previous studies (Goldstein *et al.*, 2012; Kondo *et al.*, 2015). We simplified the computational analysis by assuming a spherical mouse head consisting of a 0.2 mm thick skull, 0.2 mm subdural layer (with CSF), and a 10 mm diameter brain (Fig. 7C). Initial conditions were set such that the resulting centre-of-geometry motions were similar to each other and representative of empirically-derived experimental data in both animal models. Since the spherical mouse head model excluded mass external to the skull, it was necessary to proportionally scale the impact rod velocity to produce head motion that matched peak head acceleration calculated for blast. Skull deflection during impact was 19.8 µm (< 0.2% of the skull diameter) consistent with an absence of skull fracture or significant skull deformation in our closed-head impact injury mouse model. The close agreement of the simulation results with empirically-derived head kinematic data obtained in living mice provided validation for the computational methods used in the computational comparisons below. Peak accelerations and calculated head injury criterion (HIC) provided further confirmation of the kinematic similarity of the impact and blast simulations (Fig. 7C and D).

While head accelerations were closely approximated in the two simulations (Fig. 7D), calculated overpressures in the brain were larger at each of three intracerebral Lagrangian tracer locations during blast exposure than during impact injury (Supplementary Fig. 6A and B). If increased pressure were the dominant factor responsible

Figure 6 Continued

unilateral impact (IMP, red) versus sham (no-injury) control mice (CON, black). Arrows indicate peak negativities used to calculate conduction velocity. (**B**) Conduction velocity measurements from first peak compound action potential delay as a function of distance between recording electrodes in CA1 pyramidal cell axons in the stratum alveus of hippocampus slices from mice subjected to unilateral left-sided IMP (red bars: left, $n = 9$, right $n = 10$) compared to CON (black bars: left, $n = 10$; right, $n = 7$) 24 h post-exposure. Each bar is mean axonal conduction velocity ± SEM of *n* slices. $^{**}P < 0.01$. (**C**) Conduction velocity measurements in CA1 pyramidal cell axons in stratum alveus of hippocampus slices from mice subjected to unilateral left-sided IMP (red bars: left, $n = 14$; right, $n = 16$) compared to CON (black bars: left $n = 7$; right, $n = 9$) 3 days post-exposure. $^{**}P < 0.01$; $^{*}P < 0.05$. (**D**) Axonal conduction velocity measurements in CA1 pyramidal cell axons in the stratum alveus of hippocampus slices from mice subjected to unilateral IMP (red bars: left, $n = 16$; right, $n = 12$) compared to CON (black bars; left, $n = 7$; right, $n = 8$) 2 weeks post-exposure. $^{*}P < 0.05$. (**E–J**) Impaired theta burst-evoked long-term potentiation (LTP) of mixed excitatory inputs to the medial prefrontal cortex (mPFC) in slices from mice after unilateral (left-sided) closed-head impact injury (IMP, filled red circle) compared to sham (no injury) control condition (CON, filled black circle). LTP calculated as ratio of field excitatory postsynaptic potential (fEPSP) slope at time points T1/T2 (vertical grey bands). Theta burst high-frequency stimulation, arrows. Each point is mean ± SEM of fEPSP slope in *N* slices. (**E**) Time course of LTP in left (ipsilateral) mPFC from mice 24 h after exposure to left-lateral IMP (filled red circle, $n = 7$) or CON (filled black circle, $n = 7$). (**F**) Time course of LTP in right (contralateral) mPFC from mice 24 h after exposure to left-lateral IMP (filled red circle, $n = 8$) or CON (filled black circles, $n = 6$). (**G**) Time course of LTP in left (ipsilateral) mPFC from mice 3 days after exposure to left-lateral IMP (filled red circles, $n = 11$) or CON (filled black circles, $n = 8$). (**H**) Time course of LTP in right (contralateral) mPFC from mice 3 day after exposure to left-lateral IMP (filled red circles, $n = 10$) or CON (filled black circles, $n = 8$). (**I**) Time course of LTP in left (ipsilateral) mPFC from mice 2 weeks day after exposure to left-lateral IMP (filled red circles, $n = 9$) or CON (filled black circles, $n = 6$). (**J**) Time course of LTP in right (contralateral) mPFC from mice 2 weeks day after exposure to left-lateral IMP (filled red circles, $n = 10$) or CON (filled black circles, $n = 6$). White matter-evoked synaptic field potential input-output relations were not affected by experimental impact injury (Supplementary Fig. 5D).

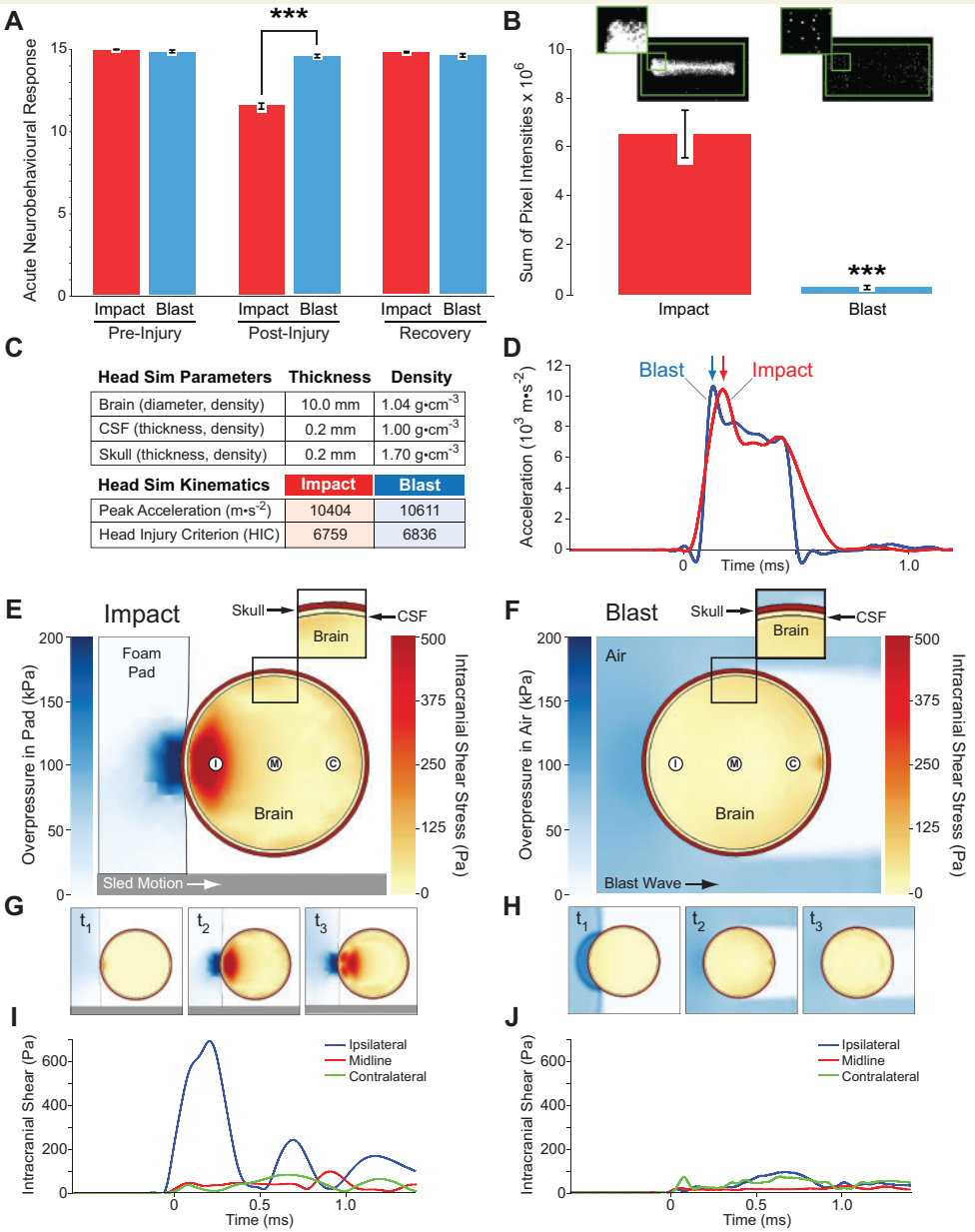

Figure 7 Differential force loading on the head and ipsilateral shear stress in the brain differentiate the presence or absence of acute concussion-like neurobehavioural deficits after unilateral closed-head impact injury or blast exposure. (**A**) Mean composite scores on the acute neurobehavioural response test battery in awake, unanaesthetized (anaesthesia-naïve) mice 2 min after unilateral closed-head impact injury (red bars; $n = 203$) or blast exposure (blue bars; $n = 24$) under experimental conditions matched for comparable head kinematics (Supplementary Table 2). Unilateral closed-head impact triggered abrupt onset of transient neurobehavioural deficits (Supplementary Video 1). Impact-induced decrements in mean test battery composite scores recovered to baseline when tested after 3-h recovery period. By contrast, blast exposure under conditions that produce comparable head motion did not induce decrements in mean composite scores on the post-exposure test battery. Mean composite scores ± SEM. ***$P < 0.001$, linear mixed-effects regression analysis. (**B**) Evaluation of force loading regimes during impact injury (red bar) compared to blast exposure (blue bar) at the surface of a mouse headform. Experimental conditions were identical to those utilized in the live animal experiments. Representative images of pressure-sensitive film strips (black boxes, above) after exposure to impact (*left*) or blast (*right*) with corresponding pixel intensity histograms (below). Large green boxes indicate pressure signal summation areas. Inset boxes show magnified view of the summation area and reveal differences in the spatial distribution of the pressure signals. Mean sum of pixel values ± SEM in arbitrary units (a.u.). ***$P < 0.001$, one-tailed Student's *t*-test. (**C**) Material densities and head geometry used in the computational simulation analyses and resulting kinematics. (**D**) Computational simulations showing comparable head kinematics and peak acceleration at the centre of the brain in the impact and blast simulation models. Arrows, corresponding peak head x-acceleration for impact (red) and blast (blue) models. Kinematic results for the models were statistically indistinguishable. The small initial negative deflection on the blast simulation is a filtering artefact. (**E** and **F**) Simulation results showing intracranial shear (von Mises) stress and extracranial overpressure during impact (**E**, slice of three-dimensional simulation) and blast (**F**, slice of two-dimensional simulation) exposure at peak head x-acceleration time

(continued)

for the observed differences in acute neurobehavioural responses to impact injury compared to blast exposure, then we would expect blast-exposed mice to preferentially exhibit greater impairment than impact-injured mice. Our experimental results indicated the opposite effect (Fig. 7A). This result indicates that intracranial pressure is not likely to be a primary physical driver of differential concussion-like responses that occur after impact injury but not after blast exposure. As an alternative hypothesis, we postulated that intraparenchymal shear stress could differentiate impact and blast with respect to the observed differences in acute neurobehavioural responses. Selected computational solutions at peak head acceleration are shown as spatially-mapped numerical values of the von Mises stress (a measure of shear stress) in the skull, CSF, and brain along with coincident overpressure in the padding for impact and overpressure in the air surrounding the head for blast (Fig. 7E and F). The magnitude and temporal evolution of shear stress in the head (skull, CSF, brain) is shown at time of contact, at peak head acceleration, and 150 μs after peak head acceleration in both simulations (Fig. 7G and H) and as time histories at each of the three selected intracerebral Lagrangian tracer locations (Fig. 7I and J). The temporal history of stress dynamics in the impact and blast simulation models are shown in Supplementary Video 2.

The impact simulation model revealed a large area of relatively sustained high peak shear stress that localized within a discrete brain region ipsilateral and subjacent to the impact contact zone (Fig. 7E). By contrast, the blast simulation demonstrated modest and relatively brief peak shear stress that was limited to a small area in the contralateral region of the brain on the leeward side of head (Fig. 7F). The relatively minor shear stress resulting from blast coalesced ~25 μs after the blast reached the skull and dissipated ~85 μs later (total duration, ~60 μs). Representative time histories of the von Mises stress at selected tracer points in the model head showed that impact produced 7-fold greater peak shear stress compared to blast (Figs. 7I–J). Moreover, impact-induced shear stress exhibited strong spatial dependence with peak magnitude in the ipsilateral brain subjacent to the impact contact zone. Importantly, peak shear stress triggered by impact occurred ~0.25 ms after contact (centre of mass motion $\leqslant$ 300 μm) and before onset of gross head motion. These simulations (Fig. 7E–J) show that spatially and temporally localized shear stress in impact and absence in blast result from differences in focal loading and the low shear modulus of the brain.

These computational results are consistent with our observation of acute onset of transient neurobehavioural deficits across multiple functional domains in mice subjected to experimental impact injury but not after blast exposure under conditions matched for head kinematics (Fig. 7A). The impact simulation results are also consistent with experimental observations of abrupt onset of right-sided motor weakness and incoordination after left-sided impact injury. These results are also concordant with neuropathological evidence demonstrating that unilateral closed-head impact injury in our mouse model produces acute-subacute brain pathology that localizes predominantly in cerebral cortex and neighbouring brain regions (e.g. basolateral amygdala) ipsilateral and subjacent to the head impact contact zone.

Discussion

We examined post-mortem brains obtained from teenage contact sport athletes who died in the acute-subacute period (1 day–4 months) after closed-head impact injuries and compared results to control brains from an age-matched control cohort of contact sport athletes without recent head injuries. Neuropathological analysis revealed a spectrum of post-traumatic pathologies, including astrocytosis, axonopathy, microvasculopathy, neuroinflammation, and phosphorylated tauopathy. The presence of haemosiderin-laden macrophage, reactive astrogliosis, and perivascular microgliosis is consistent with traumatic microvascular injury, blood–brain barrier disruption, and secondary neuroinflammation (Cherry *et al.*, 2016; Jullienne *et al.*, 2016; Kenney *et al.*,

Figure 7 Continued

points indicated by arrows in **D**. Computed extracranial overpressure measurements at peak head acceleration are shown calibrated to scale (light-dark blue scale; kPa) for the foam padding (impact model) and ambient air (blast model). Computed shear (von Mises) stresses in the skull, CSF, and brain parenchyma at peak head x-acceleration are shown calibrated to scale (yellow–red scale; Pa) for both simulation models. Intracranial Lagrangian tracers: C = contralateral with respect to impact or blast contact surface on the head; I = ipsilateral; M = midline. *Insets*: relationship of intracranial compartments in the mouse head simulation models. (**G** and **H**) Representative time sequence frames (t_1: contact, t_2: peak head x-acceleration, t_3: 150 μs after peak head x-acceleration) for intracranial shear (von Mises) stress and extracranial overpressure (padding, ambient air) in the impact (**G**) and blast (**H**) simulations. Impact induces focal point loading on the head and 7-fold greater magnitude shear stress in the brain that localizes to (and persists in) a discrete region of brain ipsilateral and subjacent to the impact contact zone. Sustained asymmetric shear stress in the simulation recapitulates the ipsilateral locus of post-traumatic brain pathology observed in the animal experiments. Note that impact produces peak shear stress in the brain before onset of gross motion of the head. By contrast, blast exposure under conditions that induces comparable head kinematics results in distributed loading on the head and lower magnitude shear stress in the brain. (**I** and **J**) Time dependence of the intracranial shear stress for impact (**I**) and blast (**J**) simulation models at the ipsilateral, midline, and contralateral Lagrangian tracer locations. Full-sequence computational simulation time histories for impact and blast are available for viewing (Supplementary Video 2).

2016; McKee *et al.*, 2016). Notably, two of four brains showed evidence of phosphorylated tauopathy and one case qualified for neuropathological diagnosis of early stage CTE (McKee *et al.*, 2016). Clinicopathological correlation suggested mechanistically causal linkage between early CTE brain pathologies, including phosphorylated tauopathy, and antecedent closed-head impact injury (Goldstein *et al.*, 2012; McKee *et al.*, 2013; Kondo *et al.*, 2015; Kenney *et al.*, 2016).

Few published case series have investigated brain pathology in individuals who have sustained mild forms of closed-head impact injury and died in the acute-subacute period post-injury (Oppenheimer, 1968; Blumbergs *et al.*, 1994; McKee *et al.*, 2014). Limitations pertinent to these studies and ours include: (i) small number of cases; (ii) variation in mechanics, severity, and timing of head injury; (iii) potential confounds associated with comorbidities, history of prior neurotrauma, and genetic and medical risk factors; (iv) duration and circumstances of the agonal period and post-mortem interval; (v) incomplete case information; (vi) adequacy of control brains; (vii) methodological and technical issues; (viii) exclusive male sex bias (this study); and (ix) inherent limitations of clinicopathological correlation to establish mechanistic causality (Goldstein *et al.*, 2014; Wojnarowicz *et al.*, 2017).

Caveats notwithstanding, these case reports are highly informative. Oppenheimer (1968) observed perivascular microglia and astrocytes in proximity to petechial and capillary haemorrhages as early as 15 h post-injury (Oppenheimer, 1968). Blumbergs *et al.* (1994) reported post-traumatic axonopathy 2–99 days after mild concussive head injury. The neuropathologies that we observed in young athletes in the acute-subacute period after closed-head impact injury included axonopathy, microvascular disruption, and perivascular neuroinflammation are consistent with the earlier reports. To this triad we highlight a fourth element, phosphorylated tauopathy (Goldstein *et al.*, 2012; McKee *et al.*, 2014). In the cases reported here, we detected pathogenic accumulation of phosphorylated tau protein accumulation in brains of two of four acute-subacute head injury cases, one of which met diagnostic criteria for early-stage CTE.

Clearly, not every individual who sustains a head injury, even if repeated, will develop CTE brain pathology. While clinicopathological correlation in our case series suggests that closed-head impact injury can trigger early brain pathologies associated with CTE, the causal mechanisms, temporal relationships, and contextual circumstances that link specific brain pathology to a particular antemortem insult are impossible to ascertain with certainty based solely on post-mortem neuropathology. This point is germane to the findings reported here given the documented head injury exposure histories of the decedents. Rather, the critical question addressed in this study is whether or not antecedent head injury *per se* is sufficient to causally induce (mechanistically determine) early CTE brain pathologies. To investigate hypothesized causal connections between impact injury and early CTE pathology, we developed a mouse model of closed-head impact injury that uses momentum transfer to produce traumatic head acceleration without gross skull deformation. The developed impact mouse model is notable for matching head kinematics in our previously published blast neurotrauma mouse model (Goldstein *et al.*, 2012; Kondo *et al.*, 2015). Unanaesthetized (anaesthesia-naïve) mice subjected to unilateral closed-head impact, but not experimental blast exposure, exhibited abrupt onset of transient neurobehavioural deficits with rapid and complete spontaneous resolution. The observed deficits, temporal course, and rapid recovery constitute an experimental concussion-like syndrome with phenomenological resemblance to human concussion (Supplementary Video 1). We used the acute neurobehavioural response test battery to objectively evaluate these transient neurobehavioural deficits. It is important to note that test battery composite and subtest scores capture integrated neurobehavioural performance that includes neuromotor function (strength and coordination of proximal, distal, and axial muscle groups), gait and balance, locomotion, exploratory drive, arousal level, responsivity to environmental stimuli, orientation behaviour, thigmotaxis, anxiety-neophobia, and habituation, amongst others (Walsh and Cummins, 1976; Brooks and Dunnett, 2009; Sukoff Rizzo and Crawley, 2017). Interestingly, we noted variation in the sensitivity of the subtests to discriminate neurobehavioural impairment post-injury (i.e. open field $\approx$ inverted mesh $>$ beam walk). This finding may prove useful in teasing out specific substrates, mechanisms, and pathways underpinning particular concussive signs. We also noted that left-lateral impact invariably produced transient right-sided (contralateral) neuromotor deficits, a finding consistent with hemispheric cross-lateralization of cortical motor control. Furthermore, abrupt onset of deficits was invariably followed by rapid and complete neurological recovery that began within minutes after injury. We did not observe persistent gross neurological impairment, post-traumatic apnoea, skull fracture, status epilepticus, cervical trauma, or spinal cord injury in any of the more than 200 impact-injured mice used in this study.

Given the absence of correlation between composite scores on the test battery and TBI and CTE endpoints, our results point to a disturbance of brain function (as opposed to structural lesions) as the aetiological origin of the concussion-like neurobehavioural deficits that we observed after impact injury. Our findings indicate that, while impact injury and blast exposure elicit similar long-term neuropathology and sequelae, these insults starkly differentiate the concussion-like syndrome produced by the former (impact), but not the latter (blast).

Several points deserve emphasis. First, the test battery provides gross assessment of integrated neurobehavioural performance across functional domains, including arousal, anxiety-neophobia, stimulus responsivity, exploratory drive, locomotion, gait and balance, muscle strength, and neuromotor coordination (Walsh and Cummins, 1976;

Suarez and Gallup, 1981; Crawley, 1999; Brooks and Dunnett, 2009). When deployed with repeated testing as here, the test battery reliably elicits habituation, a simple learning response that relies on recent memory (Walsh and Cummins, 1976; Crawley, 1999). Second, the neurological deficits that we observed post-injury model clinical features of concussion in humans (Supplementary Video 1). This similarity was underscored by phenomenological similarities with respect to the abrupt onset, temporal progression, transient course, and rapid resolution of acute deficits following impact. Third, despite tight control of the experimental injury (Supplementary Table 2), we observed wide individual variation in test battery scores. Moreover, variation in the severity of acute responses did not correlate with impact intensity. Thus, sled velocity (between 3.75 m/s and 6.25 m/s) did not significantly correlate with test battery composite scores (Spearman $r = -0.16$, $P = 0.025$, $n = 203$). This finding supports findings in human athletes that show wide variation in acute neurological responses following sports-related head injuries (McCaffrey *et al.*, 2007; Broglio *et al.*, 2010; Guskiewicz and Mihalik, 2011; Post and Hoshizaki, 2012). Fourth, we observed further significant decrement in composite scores after second impact (Fig. 2D) that showed significant positive correlation with composite scores after first impact (Spearman $r = 0.52$, $P < 0.0001$, $n = 203$). These results are consistent with reports in human athletes that show increased injury susceptibility, severity, and sequelae after an index head injury (Laurer *et al.*, 2001; Prins *et al.*, 2013; Terwilliger *et al.*, 2016).

Microscopic examination of brains from impact-injured mice revealed evidence of focal microvasculopathy, blood–brain barrier disruption, serum albumin extravasation, astrocytosis, and reactive microgliosis. Flow cytometry showed that post-traumatic neuroinflammation featured activation of TREM2 + expression in brain-resident microglia and presumptive infiltration of monocytes consistent with recent experimental evidence of similar TREM2 activation after open-skull cavitating TBI (Saber *et al.*, 2016). That we detected a similar pattern of neuroinflammation stimulated by far milder closed-head impact injury suggests that common and persistent response pathways may be triggered across the brain injury spectrum. This point is underscored by a recent case study of repetitive head injuries on the mild end of the spectrum (Cherry *et al.*, 2016) and comparison to more severe brain injury cases reported by Strich (1956, 1961, 1970) and others (Gentleman *et al.*, 2004; Johnson *et al.*, 2013*a*; Smith *et al.*, 2013*a*; Cherry *et al.*, 2016).

Our results point to possible involvement of TREM2-mediated microglial activation. TREM2 binds apolipoprotein E (Atagi *et al.*, 2015) and also membrane lipids (Wang *et al.*, 2015), suggesting that this microglial receptor may act as a surface sensor of damaged cell membranes (Kleinberger *et al.*, 2014; Phimister and Tanzi, 2015; Ulrich and Holtzman, 2016). Significantly, the R47H mutant TREM2 protein shows reduced binding to both ligands (Atagi *et al.*, 2015; Wang *et al.*, 2015) and is associated with elevated risk of Alzheimer's disease (Guerreiro *et al.*, 2013; Jonsson *et al.*, 2013). In our study, mice subjected to experimental impact showed dramatic microglia phenotypic transformation and co-localizing accumulation of inflammatory cells in the ipsilateral perirhinal cortex and adjacent brain regions subjacent to the impact contact zone (*cf.* Russo and McGavern, 2016). Recent evidence indicates that microglial activation and exosomal processing are critical for spreading tauopathy (Asai *et al.*, 2015). Moreover, activated microglia induce a subset of reactive astrocytes that promote neurodegeneration (Liddelow *et al.*, 2017). Consistent with these findings, we observed early, persistent, and progressive *cis*-p-tauopathy that was initially detectable only in axons of the ipsilateral perirhinal cortex and later in axons, soma, and dendrites in cerebral cortex in both hemispheres, including sites distant from the primary injury.

Our results comport with recent experiments that point to somatodendritic miscompartmentalization as a driver of extracellular tau release and transynaptic propagation (Wu *et al.*, 2016). Remarkably, we detected *cis*-p-tauopathy bilaterally in cerebral cortex 5.5 months after unilateral impact. Moreover, tau proteinopathy detected at this remote time point was present not only at the primary locus of acute brain injury, but also at distant sites in both hemispheres of the brain. The origin and evolution of this tau pathology and relationship to the inciting injury are as yet undetermined, but may include nucleation-dependent aggregation, seed-dependent aggregation, and prion-like transcellular spread (Clavaguera *et al.*, 2009; Jucker and Walker, 2013; Goedert, 2015; Woerman *et al.*, 2016; Goedert *et al.*, 2017).

It is notable that we did not observe mature neurofibrillary tangles in brains from impact-injured mice at any time point post-injury. This finding is consistent with other studies conducted in non-transgenic mice that express murine tau protein (Goldstein *et al.*, 2012; Huber *et al.*, 2013; Mannix *et al.*, 2013; Petraglia *et al.*, 2014; Kondo *et al.*, 2015). This discordance may reflect incomplete phenotypic expression (*forme fruste*) resulting from the high solubility and aggregation resistance of native murine tau protein, or alternatively, protracted time dependencies beyond the experimental design of the present studies. Nevertheless, phosphorylated tau proteoforms, especially *cis*-p-tau as reported here, are potent drivers of microtubule disruption, mitochondrial dysfunction, spreading tauopathy, and neurodegeneration in laboratory animals and humans (Nakamura *et al.*, 2012; Kondo *et al.*, 2015; Lu *et al.*, 2016). Early accumulation, somatodendritic miscompartmentalization, and persistence of *cis*-p-tau suggest that aberrant accumulation of this (and likely other) pathogenic phosphorylated tau species may represent the earliest antecedent pathology of CTE.

CTE neuropathology is defined by perivascular accumulation of phosphorylated tau protein in the depths of

cortical sulci (McKee *et al.*, 2016). The perivascular localization of these pathognomonic lesions suggests microvascular dysfunction as a likely contributor to CTE pathogenesis (Fig. 8). Extravasated serum albumin in the brain is a known activator of inflammatory TGFβ signalling, reactive astrocytosis, and neuronal dysfunction (Heinemann *et al.*, 2012; Weissberg *et al.*, 2015). Traumatic microvasculopathy in this study was accompanied by blood–brain barrier dysfunction and serum albumin extravasation (Fig. 8B). Serum albumin potently stimulates astrocytic uptake and phosphorylation of Smad2/3, a transcriptional co-regulator of inflammatory TGFβ signalling (Bar-Klein *et al.*, 2014; Cheslow and Alvarez, 2016), aberrant neuroglial communication (David *et al.*, 2009), abnormal dendritic branching (Tomkins *et al.*, 2007), reduced GABAergic inhibition, and impaired neuronal plasticity (Lippmann *et al.*, 2017). That extravasated serum albumin co-localized with reactive astrocytosis is consistent with activation of this injury response pathway and suggests plausible targets for therapeutic intervention that are now under investigation.

This same pathway affords potential as a diagnostic neuroimaging marker for traumatic microvascular injury, an understudied TBI endophenotype. We combined dynamic contrast-enhanced brain imaging (Veksler *et al.*, 2014; Weissberg *et al.*, 2014) with systemic administration of gadofosveset trisodium, a gadolinium-containing contrast agent that binds serum albumin (Richardson *et al.*, 2015), to detect blood–brain barrier disruption in living mice. TBI-induced gadofosveset accumulated in ipsilateral perirhinal cortex and co-localized with T_1-weighted hyperintensities and blood–brain barrier permeability defects that we confirmed by metallomic imaging mass spectrometry brain mapping.

Collectively, our neuropathological and ultrastructural findings are consistent with impact-induced microvascular dysfunction rather than traumatic intraparenchymal haemorrhage. Blood–brain barrier disruption is associated with neuronal glutamate release (Vazana *et al.*, 2016), pericyte degeneration (Bell *et al.*, 2010), astrocytic end-feet swelling and capillary retraction (Ito *et al.*, 2011; Goldstein *et al.*, 2012). These factors promote blood–brain barrier compromise, local hypoxia, perivascular neuroinflammation, synaptic dysfunction, and neurodegeneration (Barkhoudarian *et al.*, 2016) (Fig. 8B). Our results not only provide supportive evidence for blood–brain barrier disruption as a clinically-relevant post-traumatic endophenotype (Hay *et al.*, 2015; Doherty *et al.*, 2016; Kenney *et al.*, 2016), but also serve as justification for clinical evaluation of dynamic neuroimaging with gadofosveset as a novel diagnostic test for traumatic microvascular injury and presumptive risk factor test for CTE.

We were surprised that unilateral impact was accompanied by persistent bilateral impairments in hippocampal axonal conduction and medial prefrontal cortical synaptic plasticity. These findings represent post-traumatic functional sequelae that comport with experimental and clinical evidence indicating neurophysiological abnormalities in athletes and laboratory animals in the acute-subacute period after closed-head impact injuries (Goldstein *et al.*, 2012; De Beaumont *et al.*, 2013; Namjoshi *et al.*, 2014; Kondo *et al.*, 2015; Major *et al.*, 2015). Loss of white matter structural and functional integrity has been reported in patients following closed-head impact injury (Blennow *et al.*, 2012; Shenton *et al.*, 2012; Johnson *et al.*, 2013*a*). These effects may be mediated by direct axonal injury (Strich, 1961; Adams *et al.*, 1982; Gennarelli *et al.*, 1982; Povlishock and Christman, 1995), Wallerian degeneration, axonal transport dysfunction, post-traumatic demyelination, microvascular injury, pathogenic phosphorylated tau protein aggregation, or a combination of these and other factors (Fig. 8B and C).

Our observation that closed-head impact injury also disrupts prefrontal cortical projection neuron synaptic plasticity suggests that acute neurotrauma may interfere with *N*-methyl D-aspartate glutamate receptor activation, intracellular second messengers, gene expression, protein synthesis, and/or post-translational modifications that are required for LTP-dependent memory mechanisms (Sweatt *et al.*, 2016). Aberrant neurophysiological responses in the hippocampal-prefrontal cortex network (Xu and Südhof, 2013; Sigurdsson and Duvarci, 2015; Place *et al.*, 2016) are plausible substrates for cognitive, affective, attentional, and executive disturbances associated with post-concussive syndrome (Evans, 2006), traumatic encephalopathy syndrome (Montenigro *et al.*, 2014), and post-traumatic stress disorder (Mahan and Ressler, 2012). Bilateral electrophysiological deficits detected in our study are notable for the anatomical distance of the hippocampus and medial prefrontal cortex from the primary locus of injury pathology. In our previous blast TBI study (Goldstein *et al.*, 2012) we observed similar impairments in hippocampal axonal conduction velocity and hippocampal LTP. Intriguingly, we detected ultrastructural evidence of persistent microvascular injury in both the hippocampus and medial prefrontal cortex. Recent evidence also indicates that neurophysiological deficits, including impaired LTP *in vitro* and memory dysfunction *in vivo*, may be precipitated by pathogenic accumulation of phosphorylated tau protein (Sydow *et al.*, 2011; Kondo *et al.*, 2015; Fá *et al.*, 2016). The relationship of tau proteinopathy to post-traumatic neurophysiological sequelae awaits further investigation.

Experimental closed-head impact injury in this study involved contact with the temporomandibular region of the head and force loading across the zygomatic arch of the skull. In the mouse, the zygomatic process and squamosal converge over the lateral perirhinal cortex. Gross pathology observed in impact-injured mice comports with classical coup injury biomechanics as documented in analogous brain pathology after impact injuries in humans (Graham *et al.*, 2002; Blennow *et al.*, 2012; Johnson *et al.*, 2013*b*; Jordan, 2013; Leestma and Thibault, 2014; Kenney *et al.*, 2016; Sharp *et al.*, 2016; Ghajari *et al.*,

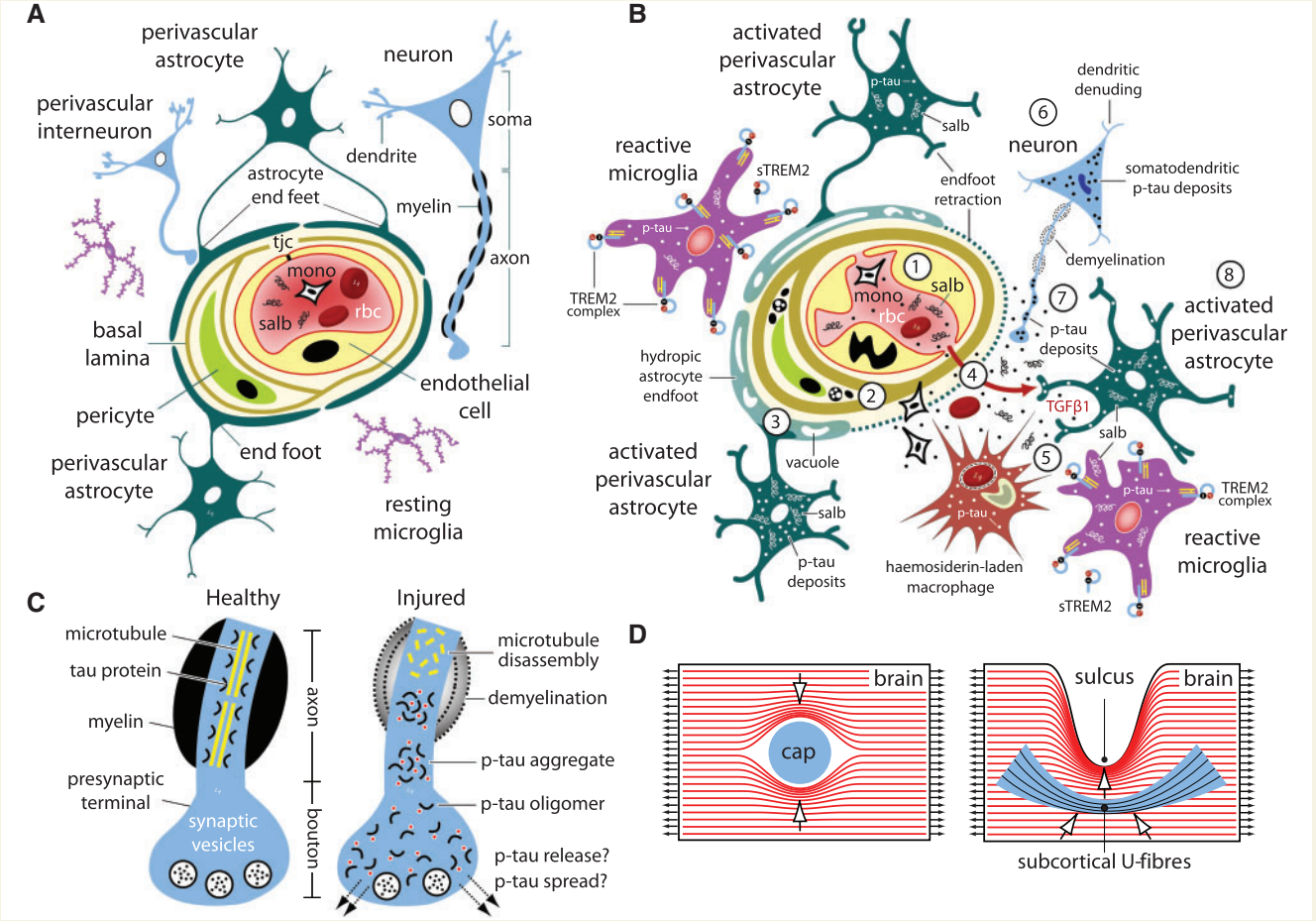

Figure 8 Model of traumatic microvascular injury, blood–brain barrier disruption, microglial activation, perivascular neuroinflammation, myelinated axonopathy, and phosphorylated tauopathy after closed-head impact injury. (**A**) Brain capillary with intact blood–brain barrier and neurovascular unit. The contents within the capillary lumen include blood plasma, blood proteins (including serum albumin, salb) and formed elements (red blood cells, rbc; circulating monocytes, mono; other white blood cells and platelets, not shown). The capillary luminal wall is a structurally continuous sheath formed by endothelial cell membranes that are joined at intercellular clefts by tight junction complexes (tjc). The basal lamina separates endothelial cells from pericytes, multifunctional mural cells that support microvascular and neurovascular unit function. Astrocyte endfeet ensheath the abluminal capillary wall. The neurovascular unit comprises endothelial cells, astrocytes, pericytes, neurons, and extracellular matrix components that regulate blood–brain barrier function, gas exchange, and bidirectional transit of fluid, metabolites, nutrients, and signalling molecules between the blood and brain. (**B**) Injured brain capillary after neurotrauma. (1) Intraparenchymal shearing forces initiated by focal mechanical injury disrupt local microvascular structure and blood–brain barrier functional integrity. (2) Compensatory changes in the extracellular matrix, elaboration and expansion of the basal lamina, formation of stress granules, inclusion bodies, and autophagosomic vacuoles are indicative of traumatic microvascular injury and post-traumatic repair and remodelling. (3) Astrocytic endfoot engorgement (astrocytic hydrops), organelle degradation (autophagy, mitophagy), and vacuolization are prominent ultrastructural features of capillaries damaged by neurotrauma. Perivascular astrocytes assume a reactive phenotype with concomitant loss of endfoot organellar integrity and secondary fluid accumulation (presumably from vascular fluid transit and pump failure or endfoot membrane loss). Together these processes lead to loss of cellular polarity and astrocyte endfoot retraction (involution) along the abluminal capillary wall. (4) Post-traumatic alterations in microvascular structure further compromise blood–brain barrier integrity and promote extravasation of pro-inflammatory plasma proteins (e.g. serum albumin, salb) into the brain parenchyma. Damaged capillaries may also facilitate inflammatory cell diapedesis and red blood cell transit (microhaemorrhage) into the brain parenchymal. (5) Serum albumin and other blood proteins (e.g. fibrinogen) are highly stimulatory to astrocytes, microglia, and CNS-resident macrophage and drive cellular transformation from resting to reactive phenotypes. These and other molecular triggers induce local activation and phenotypic transformation of brain-resident microglia, including increased expression of the triggering receptor expressed on myeloid cells 2 (TREM2), an innate immune receptor expressed on the surface of activated microglia. Microglial TREM2 expression may be accompanied by endoproteolytic cleavage of the TREM2 ectodomain and shedding of the resulting cleavage product (sTREM2). Our results indicate that post-traumatic microglial activation and phenotypic transformation precede infiltration and accumulation of peripheral inflammatory cells at sites of focal brain injury. Localized clusters of hemosiderin-laden macrophage represent chronic residua of prior microhaemorrhage. (6) Secondary changes in neurons triggered by neurotrauma lead to axonopathy (e.g. demyelination, blebbing, axonal transport dysfunction, phosphorylated tau protein aggregation), dendritic denuding, hyperexcitability, synaptic dysfunction, and neurodegeneration. (7) Tau protein dissociates from microtubules, undergoes pathogenic phosphorylation (p-tau), aggregates abnormally within axons, and stimulates pathogenic transport to and miscompartmentalization within the soma and dendrites of

(continued)

2017). Virtually all mice subjected to experimental impact in this study demonstrated transient neurobehavioural deficits that bear striking resemblance to the spectrum of concussion-related responses in humans. By contrast, and to our surprise, mice exposed to blast under conditions matched for head kinematics did not exhibit acute neurobehavioural deficits post-injury (Goldstein *et al.*, 2012). This unexpected observation argues against the concept that kinematic variables are primary determinants of concussive phenomena (Denny-Brown and Russell, 1941; Shaw, 2002). Rather, our experimental and computational results suggest that the observed acute neurobehavioural responses to closed-head impact injury are triggered by force point loading and intraparenchymal shear stress foci in the cerebral cortex that occur before onset of gross head motion.

These observations are consistent with the following postulated mechanistic sequence based on reported experimental findings. Cortical shear stresses triggered by impact elicit rapid neuronal membrane depolarization, massive glutamate release, and metabolic dyshomeostasis (Faden *et al.*, 1989; Katayama *et al.*, 1990; Yoshino *et al.*, 1991) in cerebral cortex ipsilateral to injury. Released glutamate activates excitatory amino acids receptors that elicit further depolarization by altering Na^+ and Ca^{2+} gating properties and opening voltage-sensitive ion channels that amplify transmembrane cation fluxes (Hemphill *et al.*, 2015). These responses interfere with synaptic neurotransmission, thereby inducing transient loss of contralateral motor strength, tone, and coordination as well as impairing vegetative brain functions controlling attention, arousal, and affect. Neurophysiological function is restored following neurotransmitter reuptake and synaptic recovery, consistent with our observations of abrupt onset and rapid recovery of neurobehavioural deficits post-injury. Mechanical membrane deformation can directly open stretch-sensitive channels that produce aberrant ion fluxes (Hemphill *et al.*, 2015) and intracellular Ca^{2+} dyshomeostasis (Gurkoff *et al.*, 2012; Barkhoudarian *et al.*, 2016). Sudden changes in local ion concentrations can trigger spreading depolarization (Dreier, 2011; Lippmann *et al.*, 2017) and post-traumatic seizure (Annegers *et al.*, 1998). While post-traumatic seizure was rare in our animal experiments (<1% of impact-injured mice), when present these events invariably evolved as a classical Jacksonian march noted first on the right side contralateral to left-sided impact with progression to generalized tonic-clonic seizure followed by post-ictal immobility. This pattern is consistent with a left-sided motor cortex seizure focus. Taken together, our results indicate that the transient neurobehavioural impairments triggered by impact result from disruption of cortical function rather than damage to cortical structures, and as such, agree with neuronal excitation theories of concussion (Denny-Brown and Russell, 1941; Walker *et al.*, 1944; Shaw, 2002).

Interactions between the functional and structural effects of neurotrauma are complex, dynamic, bidirectional, and dependent on a variety of injury-related factors, including type, rate, intensity, geometry, location, and biomechanics of the inciting insult. Specifically, we found that different types of neurotrauma produce varying levels of concussive functional effects. Furthermore, we observed wide variation in acute neurological responses within a single mode of head injury (i.e. impact) (Fig. 2E and F). Moreover, we found that variation in acute functional responses in our experimental animal model did not correlate with any of the measured quantitative indices that we used to assess brain injury and CTE-related sequelae (Supplementary Table 3). We interpret these findings as evidence supporting interactive linkage rather than dissociation between functional and structural consequences of neurotrauma. This point is underscored by the fact that functional effects of head injury, including neurophysiological responses underpinning concussion, are capable of potentiating structural changes and secondary alterations that lead to further brain injury and neurological sequelae. For example, sudden release of glutamate in the brain, intracellular calcium dysregulation, and spreading depolarization triggered by neurotrauma are all known precipitants of metabolic dyshomeostasis, neurotoxicity, neuronal dysfunction, and neurodegeneration (Dreier *et al.*, 2006; Lau and Tymianski, 2010; Dreier, 2011; Hartings *et al.*, 2011; Prins *et al.*, 2013; Giza and Hovda, 2014; Pietrobon and Moskowitz, 2014; Lewerenz and Maher, 2015; Østergaard *et al.*, 2015; Barkhoudarian *et al.*, 2016; Rogers *et al.*, 2017). From this perspective, concussion can be viewed as an observable clinical manifestation that reflects a spectrum of altered neurological functional states that may or may not be associated with antecedent structural brain injury. Moreover, the neurobiological conditions underpinning these concussive

Figure 8 Continued

traumatized neurons. (8) P-tau also accumulates in activated microglia, reactive astrocytes, and possibly other brain cells. P-tau propagation and spread may proceed via extracellular, paracellular, transcellular, and/or glympathic mechanisms. (**C**) Schematic representation of the axonal compartment of a healthy neuron (*left*) and traumatized neuron (*right*). In healthy neurons, tau protein associates with and stabilizes microtubules in axons and dendrites. In traumatized neurons, tau protein dissociates from microtubules and undergoes aberrant phosphorylation. P-tau is prone to pathogenic oligomerization, aggregation, and accumulation within axons, terminals, dendrites, spines, and soma of affected neurons. Miscompartmentalization of abnormally processed phosphorylated tau promotes release and transmission of p-tau species that contribute to progressive neurotoxicity and neurodegeneration. (**D**) Internal force lines (red) show increased stress concentration at structural dishomogeneities in the brain. Anatomical features such as capillaries (cap), depths of cortical sulci, and grey-white matter interfaces are subject to shear stress amplification (stress concentration) and focal mechanical trauma (arrows). See text for details and discussion.

states may, *ipso facto*, alter ongoing metabolic, homeostatic, cellular, and electrophysiological responses, thereby modulating post-traumatic brain function and neurological sequelae.

We note several unexpected findings pertinent to the origins of concussion and relationships to TBI and CTE. First, we did not detect a correlation between impact intensity (sled velocity) and acute neurobehavioural responses to mild closed-head impact injury. Second, acute responses to experimental impact injury did not correlate with TBI and CTE endpoints. Specifically, composite scores on the test battery did not correlate with quantitative endpoints of blood–brain barrier disruption, neuroinflammation, neurophysiological defects, or phosphorylated tauopathy. Finally, we observed dissociation between the mechanism of experimental neurotrauma (impact versus blast) and induction of acute neurobehavioural deficits. Mice subjected to impact injury reliably demonstrated transient concussion-like impairments, whereas mice exposed to blast with comparable head motion did not.

Computational simulations revealed dramatic differences in the evolution of shear stress in the head and brain during impact compared to blast. Specifically, our results point to differences in shear (von Mises) stress as the primary driver of acute neurobehavioural impairments triggered by impact injury. Indeed, we found 7-fold larger intracerebral shear (von Mises) stress during impact compared to blast under conditions matched for head kinematics. The differences in intracerebral shear stress (and differential propensity for acute impairments) derived from distinct loading conditions in the two types of neurotrauma. For blast, airflow around the skull produces relatively uniform pressure on the head (Fig. 7F) that does not generate significant shear stress in the brain. By contrast, impact produces focally-concentrated point loading at the impact site. Non-uniform point loading on the head creates significant shear stress in the brain that persists in a focal region of the brain ipsilateral and subjacent to the impact contact zone. Focal shear persistence results from extremely low shear wave velocity in the brain (Fig. 7G). Intracerebral shear stresses predicted by impact simulation is in the order of hundreds of Pascals, a value well above reported thresholds for disruption of brain cell homeostasis (Ravin *et al.*, 2012; Maneshi *et al.*, 2015). Our results suggest that trauma-induced disturbances in brain function may occur in the absence of overt structural brain pathology. While focal shear stresses in the brain may be important for production of concussion-like neurobehavioural responses in an animal model of closed-head impact injury, the neurological consequences of this biomechanical perturbation may not be limited to acute brain dysfunction. Rather, our data suggest that exposure to focal shear stress may also be associated with structural brain injury and its aftermath.

The differential biomechanical effects of impact and blast suggest possible substrates and mechanisms that underpin and link concussion, TBI, and sequelae. While experimental impact injury and blast exposure both trigger TBI and early CTE brain pathologies, only impact induced acute concussion-like neurobehavioural deficits. Computational simulations showed that impact induced point loading on the head and asymmetric shear stress in the brain, whereas blast exposure, under conditions matched for head kinematics, led to diffuse loading with 7-fold lower intracerebral shear stress. Our results indicate that the primary biomechanical determinant driving impact-induced acute neurological deficits is focally-concentrated shear stress that arises in the cerebral cortex before onset of gross head motion. By contrast, structural brain injury, focal pathologies, and functional sequelae correlate with slower-acting inertial forces associated with head motion (Holbourn, 1943; Goldstein *et al.*, 2012; Ghajari *et al.*, 2017).

Shear stress within the brain is subject to localized amplification (stress concentration) due to structural anisotropy and inhomogeneities (Ommaya and Gennarelli, 1974; Gennarelli *et al.*, 1993; Cloots *et al.*, 2008; Ghajari *et al.*, 2017). Specific anatomical features that contribute to stress concentration (e.g. depths of cortical sulci, grey–white matter interfaces, microvascular-brain parenchyma junctures; Fig. 8D) also represent brain structures that exhibit the greatest burden of TBI- and CTE-related neuropathology (McKee *et al.*, 2016; Ghajari *et al.*, 2017; Holleran *et al.*, 2017). These same structures are also vulnerable to repeated injury, especially if subsequent neurotrauma is sustained during brain recovery (Laurer *et al.*, 2001; Prins *et al.*, 2013). Prior brain injury is well known to increase risk of subsequent injury, slower recovery, poorer outcomes, and in rare cases, second impact syndrome (Cantu, 1998; Guskiewicz *et al.*, 2003; Evans, 2006; Mannix *et al.*, 2013; Terwilliger *et al.*, 2016).

Limitations of the animal experiments include use of young adult male C57BL/6 mice subjected to a single-repeat unilateral impact at one injury intensity and evaluated exclusively in the acute-subacute period post-injury (with exception of *cis*-p-tauopathy that was evaluated 5.5 months post-injury). While comparing murine and human ages is fraught with complications (Spear, 2004; Flurkey *et al.*, 2007), the selected age range represents an informed choice that balances age as a function of longevity (Hedrich, 2012), maturational comparability to the human cases and previous studies (Goldstein *et al.*, 2012; Kondo *et al.*, 2015), cervical and facial muscle development, skull thickness, and brain development (Kobayashi *et al.*, 1963; Flurkey *et al.*, 2007; Counotte *et al.*, 2010; Hedrich, 2012; Smith *et al.*, 2017). Importantly, white matter microglia reached adult distribution and phenotype at the selected mouse age, a factor of particular significance for the neuroinflammation analyses. The selected murine age range is consistent with sexual maturity, attainment of adult body weight and skull thickness, and completion of major brain development milestones. By these metrics, mice in this study were roughly comparable in age to the

human cases. Interpretation and generalizability of our animal experiments are constrained by animal subject homogeneity (strain, genotype, age, and sex) as well as species differences in physiology, metabolism, and anatomy (skull deformability, spine stability, cervical range of motion).

Another limitation of the animal model centres on the definition of concussion (Angoa-Pérez *et al.*, 2014; Semple *et al.*, 2015; Giza *et al.*, 2017; McCrory *et al.*, 2017; Wojnarowicz *et al.*, 2017). Our working definition of concussion is based on observable neurobehavioural signs that are primarily, but not exclusively, related to neuromotor function. Impaired balance and gait are considered part of the constellation of signs associated with sports-related concussion (McCrory *et al.*, 2017), and accordingly, were rigorously evaluated in this study. However, other prominent clinical features of concussion—cognitive impairment, amnestic deficits, disorientation, slowed reaction time, headache, emotional lability, alterations in consciousness, somnolence and sleep disturbances—were not amenable to experimental evaluation using the current version of the acute neurobehavioural response test battery. These limitations warrant caution with respect to generalizing experimental findings in laboratory animals to clinical conditions in humans. Future studies will benefit from inclusion of test battery components that are sensitive to specific alterations in cognitive, affective, and behavioural domains that are affected by concussion in humans.

Additional limitations apply to the computational simulations. We considered effects on and within a computationally simplified headform, while neglecting contributions of neck and torso tethering to the body. However, with respect to the calculated timescales of interest, we observed pronounced shear stresses prior to onset of gross head motion when tethering effects would not be significant. We also assumed a simplified spherical head with concentric material layers of skull and CSF without dura or soft tissues, as well as isotropic brain composition without internal structure. We note that a more complex anatomical description would not have changed the conclusions deduced from the simulations. In addition, we only considered a single set of initial conditions for the impact and blast simulations. Future studies in which the magnitude of shear forces within a single model is systematically varied may yield additional information germane to establishing causal links between loading conditions during injury and its aftermath. Moreover, the temporal relationships between initiation and propagation of shear stress foci in the brain and onset of acute neurological responses remain to be empirically validated *in vivo*. Despite these caveats, the computational simulations closely agreed with experimental head kinematics and support mechanistic explanations that comport with simple biomechanical principles and clinical observations.

Based on this evidence, we conclude that the mechanisms underpinning the transient concussion-like deficits observed in mice after experimental closed-head impact are triggered by fast-acting, high-amplitude shear stress fields that arise in the cerebral cortex before onset of gross head motion. Our results also suggest that concussion, TBI, and CTE represent distinct nosological entities subserved by different pathobiological mechanisms. Specifically, our findings indicate that closed-head impact injury, independent of concussion, represents a potent insult with potential to induce enduring neurophysiological dysfunction and persistent (and possibly progressive) sequelae, including CTE brain pathology. Furthermore, our findings from blast and impact support the concept that disparate types of neurotrauma with distinct injury mechanisms and differing potential for concussion can trigger convergent brain pathologies and functional sequelae.

Collectively, these results raise concern that repetitive neurotrauma, independent of concussion, may induce early CTE brain pathologies, even in teenagers and young adults. Cumulative exposure to such injuries may also increase risk for other tau protein neurodegenerative diseases, including Alzheimer's disease (Stein *et al.*, 2015*b*). These considerations are important not only for understanding and differentiating concussion, TBI, and CTE, but also to inform clinical practice, return-to-play protocols, and public health policy.

This study also raises many questions. How much tau pathology is clinically significant? What is the relationship of specific tau species and other molecular and cellular pathologies to latent brain disease and chronic sequelae triggered by brain injury? How do pathogenic tau proteoforms propagate through the brain and can this process be prevented or reversed? Which clinical biomarkers are best suited for diagnostic detection, endophenotype differentiation, prognostic stratification, and longitudinal monitoring of TBI and CTE? Animal models that recapitulate clinical features of concussion, TBI, and CTE provide a powerful platform to address these issues. We anticipate that answers to these questions will facilitate development of new diagnostics, therapeutics, protective equipment, and preventive measures for acute and chronic effects of impact neurotrauma.

Acknowledgements

The authors gratefully acknowledge the use of resources and facilities at and support from the Edith Nourse Rogers Memorial Veterans Hospital (Bedford, MA, USA), Boston VA Healthcare System (Jamaica Plain, MA, USA), Boston University School of Medicine (Boston, MA, USA), and Boston University Alzheimer's Disease Center, CTE Program (Boston, MA, USA). We thank Tom Balon, Ph.D., Director, Boston University Metabolic Phenotyping and *In Vivo* Imaging Core, for assistance with the IVIS imaging system (NIH-NCRR, S10RR024523). The authors gratefully acknowledge resource support from Thermo Scientific (Waltham, MA), Tech Imaging (Saugus, MA), Teledyne CETAC Technologies (Omaha, NE), and Office

of the Dean, Boston University School of Medicine. Work by W.C.M. and A.T.A. was performed under the auspices of the U.S. Department of Energy by Lawrence Livermore National Laboratory under Contract DE-AC52-07NA27344. Work by W.C.M. was performed, in part, while a Consulting Professor in the Department of Structural Biology, Stanford University School of Medicine. The authors also gratefully acknowledge the individuals and families whose participation and contributions made this work possible.

Funding

NIH F31NS077796 (C.A.T.), NIH 5T32EB006359 (C.A.T.), NIH 1F31NS080564 (A.G.B.), University of California, Berkeley Bakar Fellowship (D.K.). NIH R01AG029385 (K.P.L.), NIH R01NS32151 (R.M.R.), NIH R01NS044421 (P.K.S.), NIH-NIA Boston University Alzheimer's Disease Center P30AG13846 and supplement 0572063345 (N.W.K.), NIH-NIA Boston University Framingham Heart Study R01AG1649, NIH-NINDS 1UO1NS086659 (A.C.M.); U.S. Department of Veterans Affairs Veterans Affairs Biorepository CSP 501 (A.C.M.), Veterans Health Administration Clinical Sciences Research and Development Merit Award I01-CX001038 (T.D.S.); U.S. Department of Defense W81XWH-13-2-0064 and VA I01 RX 002170 (A.C.M.); Peer Reviewed Alzheimer's Research Program (DoD-PRARP) 13267017 (A.C.M.), DoD-PRARP W81XWH1310263 (L.E.G.); U.S. Department of Energy contract to Lawrence Livermore National Laboratory DE-AC52-07NA27344 (A.T.A., W.C.M.). Alzheimer's Association NIRG-305779 (T.D.S.), European Union Seventh Framework Program EPITARGET 602102 (A.F.), Israel Science Foundation (A.F.), Canadian Institute of Health Research (A.F.), National Operating Committee on Standards for Athletic Equipment (A.C.M.), The Linden Fund (P.K.S.) Concussion Legacy Foundation (A.C.M., L.E.G.), WWE (A.C.M., L.E.G.); unrestricted gifts from the Andlinger Foundation (A.C.M.), WWE (A.C.M.), National Football League (A.C.M.); Crown Family for support of the US-Israel TBI Collaborative Research Program (A.F., L.E.G.).

The views and opinions of authors V.E.A., B.R.H., N.W.K., T.D.S., and A.C.M. expressed herein should not to be construed as official positions of the Department of Veterans Affairs or the U.S. government.

Conflict of interest

K.P.L. and X.Z.Z. are inventors of Pin1 technology, which is licensed by Beth Israel Deaconess Medical Center (BIDMC) to Pinteon Therapeutics, Inc. (Concord, MA). K.P.L. and X.Z.Z. are equity holders and consult for Pinteon. Their interests were reviewed and managed by BIDMC in accordance with its conflict of interest policy. R.M.R. is an employee of Biogen and holds company stock. R.C.C. receives consulting remuneration from National Football League (NFL), National Operating Committee on Standards for Athletic Equipment (NOCSAE), and the Concussion Legacy Foundation. R.C.C. also receives book royalties. C.J.N. is a salaried employee of the Concussion Legacy Foundation, a tax-exempt nonprofit organization. C.J.N. has received travel reimbursement while serving on advisory boards for the NFL Players Association, Major League Lacrosse, WWE, and The Ivy League, is eligible for book royalties, and receives speaking fees and travel reimbursement for educational lectures. L.E.G. is a consultant for Rebiscan, Inc.

Supplementary material

Supplementary material is available at *Brain* online.

References

Abbas K, Shenk TE, Poole VN, Breedlove EL, Leverenz LJ, Nauman EA, et al. Alteration of default mode network in high school football athletes due to repetitive subconcussive mild traumatic brain injury: a resting-state functional magnetic resonance imaging study. Brain Connect 2015; 5: 91–101.

Adams JH, Graham DI, Murray LS, Scott G. Diffuse axonal injury due to nonmissile head injury in humans: an analysis of 45 cases. Ann Neurol 1982; 12: 557–63.

Alosco M, Kasimis A, Stamm J, Chua A, Baugh C, Daneshvar D, et al. Age of first exposure to American football and long-term neuropsychiatric and cognitive outcomes. Transl Psychiatry 2017; 7: e1236.

Angoa PM, Kane MJ, Briggs DI, Herrera MN, Viano DC, Kuhn DM. Animal models of sports-related head injury: bridging the gap between preclinical research and clinical reality. J Neurochem 2014; 129: 916–31.

Annegers JF, Hauser WA, Coan SP, Rocca WA. A population-based study of seizures after traumatic brain injuries. N Eng J Med 1998; 338: 20–4.

Asai H, Ikezu S, Tsunoda S, Medalla M, Luebke J, Haydar T, et al. Depletion of microglia and inhibition of exosome synthesis halt tau propagation. Nat Neurosci 2015; 18: 1584–93.

Atagi Y, Liu C-C, Painter MM, Chen X-F, Verbeeck C, Zheng H, et al. Apolipoprotein E is a ligand for triggering receptor expressed on myeloid cells 2 (TREM2). J Biol Chem 2015; 290: 26043–50.

Auffray C, Fogg D, Garfa M, Elain G, Join-Lambert O, Kayal S, et al. Monitoring of blood vessels and tissues by a population of monocytes with patrolling behavior. Science 2007; 317: 666–70.

Bar-Klein G, Cacheaux LP, Kamintsky L, Prager O, Weissberg I, Schoknecht K, et al. Losartan prevents acquired epilepsy via TGF-beta signaling suppression. Ann Neurol 2014; 75: 864–75.

Barkhoudarian G, Hovda DA, Giza CC. The molecular pathophysiology of concussive brain injury—an update. Phys Med Rehabil Clin N Am 2016; 27: 373–93.

Barrow DW, Rhoads HT. Blast concussion injury. JAMA 1944; 125: 900–2.

Bazarian JJ, Zhu T, Zhong J, Janigro D, Rozen E, Roberts A, et al. Persistent, long-term cerebral white matter changes after sports-related repetitive head impacts. PLoS One 2014; 9: e94734.

Bell RD, Winkler EA, Sagare AP, Singh I, LaRue B, Deane R, et al. Pericytes control key neurovascular functions and neuronal phenotype in the adult brain and during brain aging. Neuron 2010; 68: 409–27.

Bhaskar K, Konerth M, Kokiko-Cochran ON, Cardona A, Ransohoff RM, Lamb BT. Regulation of tau pathology by the microglial fractalkine receptor. Neuron 2010; 68: 19–31.

Bieniek KF, Ross OA, Cormier KA, Walton RL, Soto-Ortolaza A, Johnston AE, et al. Chronic traumatic encephalopathy pathology in a neurodegenerative disorders brain bank. Acta Neuropathol 2015; 130: 877–89.

Blennow K, Hardy J, Zetterberg H. The neuropathology and neurobiology of traumatic brain injury. Neuron 2012; 76: 886–99.

Blumbergs PC, Scott G, Manavis J, Wainwright H, Simpson DA, McLean AJ. Staining of amyloid precursor protein to study axonal damage in mild head injury. Lancet 1994; 344: 1055–6.

Breedlove EL, Robinson M, Talavage TM, Morigaki KE, Yoruk U, O'Keefe K, et al. Biomechanical correlates of symptomatic and asymptomatic neurophysiological impairment in high school football. J Biomech 2012; 45: 1265–72.

Broglio SP, Schnebel B, Sosnoff JJ, Shin S, Fend X, He X, et al. Biomechanical properties of concussions in high school football. Med Sci Sports Exer 2010; 42: 2064–71.

Brooks SP, Dunnett SB. Tests to assess motor phenotype in mice: a user's guide. Nat Rev Neurosci 2009; 10: 519–29.

Cantu RC. Second-impact syndrome. Clin Sports Med 1998; 17: 37–44.

Carroll LJ, Cassidy JD, Holm L, Kraus J, Coronado VG. Methodological issues and research recommendations for mild traumatic brain injury: the WHO Collaborating Centre Task Force on Mild Traumatic Brain Injury. J Rehabil Med 2004 (43 Suppl): 113–25.

Cherry JD, Tripodis Y, Alvarez VE, Huber B, Kiernan PT, Daneshvar DH, et al. Microglial neuroinflammation contributes to tau accumulation in chronic traumatic encephalopathy. Acta Neuropathol Commun 2016; 4: 112.

Cheslow L, Alvarez JI. Glial-endothelial crosstalk regulates blood–brain barrier function. Curr Opin Pharmacol 2016; 26: 39–46.

Clavaguera F, Bolmont T, Crowther RA, Abramowski D, Frank S, Probst A, et al. Transmission and spreading of tauopathy in transgenic mouse brain. Nat Cell Biol 2009; 11: 909.

Cloots RJ, Gervaise HM, van Dommelen JA, Geers MG. Biomechanics of traumatic brain injury: influences of the morphologic heterogeneities of the cerebral cortex. Ann Biomed Eng 2008; 36: 1203–15.

Counotte DS, Li KW, Wortel J, Gouwenberg Y, Van Der Schors RC, Smit AB, et al. Changes in molecular composition of rat medial prefrontal cortex synapses during adolescent development. Eur J Neurosci 2010; 32: 1452–60.

Crawley JN. Behavioral phenotyping of transgenic and knockout mice: experimental design and evaluation of general health, sensory functions, motor abilities, and specific behavioral tests. Brain Res 1999; 835: 18–26.

Crisco JJ, Fiore R, Beckwith JG, Chu JJ, Brolinson PG, Duma S, et al. Frequency and location of head impact exposures in individual collegiate football players. J Athletic Train 2010; 45: 549–59.

Crisco JJ, Wilcox BJ, Beckwith JG, Chu JJ, Duhaime AC, Rowson S, et al. Head impact exposure in collegiate football players. J Biomech 2011; 44: 2673–8.

Critchley M. Punch-drunk syndromes: the chronic traumatic encephalopathy of boxers. In: Neurochirurgie: hommage a clovis vincent. Paris, France: Maloine; 1949.

Critchley M. Medical aspects of boxing, particularly from a neurological standpoint. BMJ 1957; 1: 357.

Davenport EM, Whitlow CT, Urban JE, Espeland MA, Jung Y, Rosenbaum DA, et al. Abnormal white matter integrity related to head impact exposure in a season of high school varsity football. J Neurotrauma 2014; 31: 1617–24.

David Y, Cacheaux LP, Ivens S, Lapilover E, Heinemann U, Kaufer D, et al. Astrocytic dysfunction in epileptogenesis: consequence of altered potassium and glutamate homeostasis? J Neurosci 2009; 29: 10588–99.

De Beaumont L, Tremblay S, Henry LC, Poirier J, Lassonde M, Théoret H. Motor system alterations in retired former athletes: the role of aging and concussion history. BMC Neurol 2013; 13: 109.

Denny-Brown D, Russell WR. Experimental cerebral concussion. Brain 1941; 64: 93–164.

Doherty CP, O'Keefe E, Wallace E, Loftus T, Keaney J, Kealy J, et al. Blood-brain barrier dysfunction as a hallmark pathology in chronic traumatic encephalopathy. J Neuropathol Exp Neurol 2016; 75: 656–62.

Dreier JP. The role of spreading depression, spreading depolarization and spreading ischemia in neurological disease. Nat Med 2011; 17: 439–47.

Dreier JP, Woitzik J, Fabricius M, Bhatia R, Major S, Drenckhahn C, et al. Delayed ischaemic neurological deficits after subarachnoid haemorrhage are associated with clusters of spreading depolarizations. Brain 2006; 129: 3224–37.

Evans RW. The postconcussion syndrome and the sequelae of mild head injury. In: Evans RW, editor. Neurology and trauma, 2nd edn. New York, NY: Oxford University Press; 2006. p. 95–128.

Fá M, Puzzo D, Piacentini R, Staniszewski A, Zhang H, Baltrons MA, et al. Extracellular tau oligomers produce an immediate impairment of LTP and memory. Sci Rep 2016; 6: 19393.

Faden AL, Demediuk P, Panter SS, Vink R. The role of excitatory amino acids and NMDA receptors in traumatic brain injury. Science 1989; 244: 798–800.

Fish R, Danneman PJ, Brown M, Karas A. Anesthesia and analgesia in laboratory animals. New York, NY: Academic Press; 2011.

Flurkey K, Currer M, Harrison DE. Mouse models in aging research. In: Fox JG, Barthold SW, Davisson MT, Newcomer CE, Quimby FW, Smith AL, editors. The mouse in biomedical research, 2nd edn. Burlington, VT: Elsevier; 2007. p. 637–72.

Gao Y-R, Ma Y, Zhang Q, Winder AT, Liang Z, Antinori L, et al. Time to wake up: Studying neurovascular coupling and brain-wide circuit function in the un-anesthetized animal. Neuroimage 2016; 153: 382–98.

Gardner RC, Yaffe K. Epidemiology of mild traumatic brain injury and neurodegenerative disease. Mol Cell Neurosci 2015; 66: 75–80.

Gavett BE, Stern RA, Cantu RC, Nowinski CJ, McKee AC. Mild traumatic brain injury: a risk factor for neurodegeneration. Alz Res Therap 2010; 2: 18.

Geissmann F, Jung S, Littman DR. Blood monocytes consist of two principal subsets with distinct migratory properties. Immunity 2003; 19: 71–82.

Gelman A, Hill J, Yajima M. Why we (usually) don't have to worry about multiple comparisons. J Res Educ Eff 2012; 5: 189–211.

Gennarelli TA, Thibault LE, Adams JH, Graham DI, Thompson CJ, Marcincin RP. Diffuse axonal injury and traumatic coma in the primate. Ann Neurol 1982; 12: 564–74.

Gennarelli TA, Thibault LE, Ommaya AK. Pathophysiologic responses to rotational and translational accelerations of the head. In: Backaitis SH, editor. Biomechanics of impact injury and injury tolerances of the head-neck complex. Warrendale, PA: Society of Automotive Engineers, Inc.; 1993. p. 411–23.

Gentleman S, Leclercq P, Moyes L, Graham D, Smith C, Griffin W, et al. Long-term intracerebral inflammatory response after traumatic brain injury. Forensic Sci Int 2004; 146: 97–104.

Ghajari M, Hellyer PJ, Sharp DJ. Computational modelling of traumatic brain injury predicts the location of chronic traumatic encephalopathy pathology. Brain 2017; 140: 333–43.

Giza CC, Hovda DA. The new neurometabolic cascade of concussion. Neurosurgery 2014; 75 (Suppl 4): S24–33.

Giza CC, Prins ML, Hovda DA. It's not all fun and games: sports, concussions, and neuroscience. Neuron 2017; 94: 1051–5.
Goedert M. Alzheimer's and Parkinson's diseases: the prion concept in relation to assembled Aβ, tau, and α-synuclein. Science 2015; 349: 1255555.
Goedert M, Masuda-Suzukake M, Falcon B. Like prions: the propagation of aggregated tau and α-synuclein in neurodegeneration. Brain 2017; 140: 266–78.
Goldstein H. Multilevel statistical models. Chichester, West Sussex, UK: John Wiley & Sons, Ltd.; 2011.
Goldstein LE, Fisher AM, Tagge CA, Zhang X-L, Velisek L, Sullivan JA, et al. Chronic traumatic encephalopathy in blast-exposed military veterans and a blast neurotrauma mouse model. Sci Transl Med 2012; 4: 134ra60.
Goldstein LE, McKee AC, Stanton PK. Considerations for animal models of blast-related traumatic brain injury and chronic traumatic encephalopathy. Alz Res Therap 2014; 6: 1–10.
Graham DI, Gennarelli TA, McIntosh TK. Trauma. In: Greenfield JG, Graham DI, Lantos PL, editors. Greenfield's neuropathology. 7th edn. New York, NY: Oxford University Press; 2002. p. 823–98.
Guerreiro R, Wojtas A, Bras J, Carrasquillo M, Rogaeva E, Majounie E, et al. TREM2 variants in Alzheimer's disease. N Eng J Med 2013; 368: 117–27.
Gurkoff GG, Shahlaie K, Lyeth BG. *In vitro* mechanical strain trauma alters neuronal calcium responses: implications for posttraumatic epilepsy. Epilepsia 2012; 53: 53–60.
Guskiewicz KM, Marshall SW, Bailes J, McCrea M, Cantu RC, Randolph C, et al. Association between recurrent concussion and late-life cognitive impairment in retired professional football players. Neurosurgery 2005; 57: 719–26; discussion 726.
Guskiewicz KM, Marshall SW, Bailes J, McCrea M, Harding HP, Matthews A, et al. Recurrent concussion and risk of depression in retired professional football players. Med Sci Sports Exercise 2007a; 39: 903–6.
Guskiewicz KM, McCrea M, Marshall SW, Cantu RC, Randolph C, Barr W, et al. Cumulative effects associated with recurrent concussion in collegiate football players: the NCAA Concussion Study. JAMA 2003; 290: 2549–55.
Guskiewicz KM, Mihalik JP. Biomechanics of sport concussion: quest for the elusive injury threshold. Exercise Sport Sci Rev 2011; 39: 4–11.
Guskiewicz KM, Mihalik JP, Shankar V, Marshall SW, Crowell DH, Oliaro SM, et al. Measurement of head impacts in collegiate football players: relationship between head impact biomechanics and acute clinical outcome after concussion. Neurosurgery 2007b; 61: 1244–52; discussion 1252–3.
Harmon KG, Drezner J, Gammons M, Guskiewicz K, Halstead M, Herring S, et al. American Medical Society for Sports Medicine position statement: concussion in sport. Clin J Sport Med 2013; 23: 1–18.
Hartings JA, Watanabe T, Bullock MR, Okonkwo DO, Fabricius M, Woitzik J, et al. Spreading depolarizations have prolonged direct current shifts and are associated with poor outcome in brain trauma. Brain 2011; 134: 1529–40.
Hay JR, Johnson VE, Young AM, Smith DH, Stewart W. Blood-brain barrier disruption is an early event that may persist for many years after traumatic brain injury in humans. J Neuropathol Exp Neurol 2015; 74: 1147–57.
Hedrich HJ. The laboratory mouse. London: Academic Press; 2012.
Heinemann U, Kaufer D, Friedman A. Blood-brain barrier dysfunction, TGFβ signaling, and astrocyte dysfunction in epilepsy. Glia 2012; 60: 1251–7.
Hemphill MA, Dauth S, Yu CJ, Dabiri BE, Parker KK. Traumatic brain injury and the neuronal microenvironment: a potential role for neuropathological mechanotransduction. Neuron 2015; 85: 1177–92.
Holbourn AHS. Mechanics of head injuries. Lancet 1943; 242: 438–41.
Holleran L, Kim JH, Gangolli M, Stein T, Alvarez V, McKee A, et al. Axonal disruption in white matter underlying cortical sulcus tau pathology in chronic traumatic encephalopathy. Acta Neuropathol 2017; 133: 367–80.
Huang L, Cichon J, Ninan I, Yang G. Post-anesthesia AMPA receptor potentiation prevents anesthesia-induced learning and synaptic deficits. Sci Transl Med 2016; 8: 344ra85.
Huber BR, Meabon JS, Martin TJ, Mourad PD, Bennett R, Kraemer BC, et al. Blast exposure causes early and persistent aberrant phospho- and cleaved-tau expression in a murine model of mild blast-induced traumatic brain injury. J Alz Dis 2013; 37: 309–23.
Ito U, Hakamata Y, Kawakami E, Oyanagi K. Temporary focal cerebral ischemia results in swollen astrocytic end-feet that compress microvessels and lead to focal cortical infarction. J Cereb Blood Flow Metab 2011; 31: 328–38.
Jay TR, Miller CM, Cheng PJ, Graham LC, Bemiller S, Broihier ML, et al. TREM2 deficiency eliminates TREM2+ inflammatory macrophages and ameliorates pathology in Alzheimer's disease mouse models. J Exp Med 2015; 212: 287–95.
Johnson VE, Stewart JE, Begbie FD, Trojanowski JQ, Smith DH, Stewart W. Inflammation and white matter degeneration persist for years after a single traumatic brain injury. Brain 2013a; 136: 28–42.
Johnson VE, Stewart W, Smith DH. Widespread tau and amyloid-beta pathology many years after a single traumatic brain injury in humans. Brain Pathol 2012; 22: 142–9.
Johnson VE, Stewart W, Smith DH. Axonal pathology in traumatic brain injury. Exp Neurol 2013b; 246: 35–43.
Jonsson T, Stefansson H, Steinberg S, Jonsdottir I, Jonsson PV, Snaedal J, et al. Variant of TREM2 associated with the risk of Alzheimer's disease. N Eng J Med 2013; 368: 107–16.
Jordan BD. The clinical spectrum of sport-related traumatic brain injury. Nat Rev Neurol 2013; 9: 222–30.
Jucker M, Walker LC. Self-propagation of pathogenic protein aggregates in neurodegenerative diseases. Nature 2013; 501: 45.
Jullienne A, Obenaus A, Ichkova A, Savona-Baron C, Pearce WJ, Badaut J. Chronic cerebrovascular dysfunction after traumatic brain injury. J Neurosci Res 2016; 94: 609–22.
Katayama Y, Becker DP, Tamura T, Hovda DA. Massive increases in extracellular potassium and the indiscriminate release of glutamate following concussive brain injury. J Neurosurg 1990; 73: 889–900.
Katz D, Cohen S, Alexander M. Mild traumatic brain injury. Handb Clin Neurol 2014; 127: 131–56.
Kawabori M, Kacimi R, Kauppinen T, Calosing C, Kim JY, Hsieh CL, et al. Triggering receptor expressed on myeloid cells 2 (TREM2) deficiency attenuates phagocytic activities of microglia and exacerbates ischemic damage in experimental stroke. J Neurosci 2015; 35: 3384–96.
Kay T, Harrington D, Adams R; American Congress of Rehabilitation Medicine, Head Injury Interdisciplinary Special Interest Group. Definition of mild traumatic brain injury. J Head Trauma Rehabil 1993; 8: 86–7.
Kenney K, Amyot F, Haber M, Pronger A, Bogoslovsky T, Moore C, et al. Cerebral vascular injury in traumatic brain injury. Exp Neurol 2016; 275: 353–66.
Kleinberger G, Yamanishi Y, Suárez-Calvet M, Czirr E, Lohmann E, Cuyvers E, et al. TREM2 mutations implicated in neurodegeneration impair cell surface transport and phagocytosis. Sci Transl Med 2014; 6: 243ra86.
Kobayashi T, Inman O, Buno W, Himwich HE. A multidisciplinary study of changes in mouse brain with age. Recent Adv Biol Psychiat 1963; 5: 293–308.
Kokiko-Cochran O, Ransohoff L, Veenstra M, Lee S, Saber M, Sikora M, et al. Altered neuroinflammation and behavior after traumatic

brain injury in a mouse model of Alzheimer's disease. J Neurotrauma 2016; 33: 625–40.
Kondo A, Shahpasand K, Mannix R, Qiu J, Moncaster J, Chen C-H, et al. Antibody against early driver of neurodegeneration cis P-tau blocks brain injury and tauopathy. Nature 2015; 523: 431–6.
Kristman VL, Borg J, Godbolt AK, Salmi LR, Cancelliere C, Carroll LJ, et al. Methodological issues and research recommendations for prognosis after mild traumatic brain injury: results of the International Collaboration on Mild Traumatic Brain Injury Prognosis. Arch Phys Med Rehabil 2014; 95 (3 Suppl): S265–77.
Langlois JA, Rutland-Brown W, Wald MM. The epidemiology and impact of traumatic brain injury: a brief overview. J Head Trauma Rehabil 2006; 21: 375–8.
Lau A, Tymianski M. Glutamate receptors, neurotoxicity and neurodegeneration. Pflüg Arch-Eur J Physiol 2010; 460: 525–42.
Lauffer RB, Parmelee DJ, Dunham SU, Ouellet HS, Dolan RP, Witte S, et al. MS-325: albumin-targeted contrast agent for MR angiography. Radiology 1998; 207: 529–38.
Laurer HL, Bareyre FM, Lee VM, Trojanowski JQ, Longhi L, Hoover R, et al. Mild head injury increasing the brain's vulnerability to a second concussive impact. J Neurosurg 2001; 95: 859–70.
Leestma JE, Thibault KL. Physical injury to the nervous system. In: Leestma JE, editor. Forensic neuropathology. 3rd edn. New York: CRC Press, Taylor & Francis Group; 2014. p. 417–594.
Lehman EJ, Hein MJ, Baron SL, Gersic CM. Neurodegenerative causes of death among retired National Football League players. Neurology 2012; 79: 1970–4.
Lewerenz J, Maher P. Chronic glutamate toxicity in neurodegenerative diseases—what is the evidence? Front Neurosci 2015; 9: 469.
Liddelow SA, Guttenplan KA, Clarke LE, Bennett FC, Bohlen CJ, Schirmer L, et al. Neurotoxic reactive astrocytes are induced by activated microglia. Nature 2017; 541: 481–7.
Liepmann HW, Roshko A. Elements of gasdynamics. New York, NY: John Wiley & Sons; 1957.
Lippmann K, Kamintsky L, Kim SY, Lublinsky S, Prager O, Nichtweiss JF, et al. Epileptiform activity and spreading depolarization in the blood-brain barrier-disrupted peri-infarct hippocampus are associated with impaired GABAergic inhibition and synaptic plasticity. J Cereb Blood Flow Metab 2017; 37: 1803–19.
Lu KP, Kondo A, Albayram O, Herbert MK, Liu H, Zhou XZ. Potential of the antibody against cis–phosphorylated tau in the early diagnosis, treatment, and prevention of Alzheimer disease and brain injury. JAMA Neurol 2016; 73: 1356–62.
Luethcke CA, Bryan CJ, Morrow CE, Isler WC. Comparison of concussive symptoms, cognitive performance, and psychological symptoms between acute blast-versus nonblast-induced mild traumatic brain injury. J Int Neuropsychol Soc 2011; 17: 36–45.
Luh C, Gierth K, Timaru-Kast R, Engelhard K, Werner C, Thal SC. Influence of a brief episode of anesthesia during the induction of experimental brain trauma on secondary brain damage and inflammation. PLoS One 2011; 6: e19948.
Mahan AL, Ressler KJ. Fear conditioning, synaptic plasticity and the amygdala: implications for posttraumatic stress disorder. Trends Neurosci 2012; 35: 24–35.
Major BP, Rogers MA, Pearce AJ. Using transcranial magnetic stimulation to quantify electrophysiological changes following concussive brain injury: a systematic review. Clin Exp Pharmacol Physiol 2015; 42: 394–405.
Maneshi MM, Sachs F, Hua SZ. A threshold shear force for calcium influx in an astrocyte model of traumatic brain injury. J Neurotrauma 2015; 32: 1020–9.
Mannix R, Meehan WP, Mandeville J, Grant PE, Gray T, Berglass J, et al. Clinical correlates in an experimental model of repetitive mild brain injury. Ann Neurol 2013; 74: 65–75.
Martland HS. Punch drunk. JAMA 1928; 91: 1103–7.
McCaffrey MA, Mihalik JP, Crowell DH, Shields EW, Guskiewicz KM. Measurement of head impacts in collegiate football players: clinical measures of concussion after high- and low-magnitude impacts. Neurosurgery 2007; 61: 1236–43.
McCrory P, Meeuwisse W, Dvorak J, Aubry M, Bailes J, Broglio S, et al. Consensus statement on concussion in sport—the 5th international conference on concussion in sport held in Berlin, October 2016. Br J Sports Med 2017; 51: 838–47.
McCrory P, Meeuwisse WH, Aubry M, Cantu B, Dvořák J, Echemendia RJ, et al. Consensus statement on concussion in sport: the 4th International Conference on Concussion in Sport held in Zurich, November 2012. Br J Sports Med 2013; 47: 250–8.
McDonald BC, Flashman LA, Saykin AJ. Executive dysfunction following traumatic brain injury: neural substrates and treatment strategies. Neurorehabilitation 2002; 17: 333–44.
McKee AC, Cairns NJ, Dickson DW, Folkerth RD, Keene CD, Litvan I, et al. The first NINDS/NIBIB consensus meeting to define neuropathological criteria for the diagnosis of chronic traumatic encephalopathy. Acta Neuropathol 2016; 131: 75–86.
McKee AC, Cantu RC, Nowinski CJ, Hedley-Whyte ET, Gavett BE, Budson AE, et al. Chronic traumatic encephalopathy in athletes: progressive tauopathy after repetitive head injury. J Neuropathol Exp Neurol 2009; 68: 709–35.
McKee AC, Daneshvar DH, Alvarez VE, Stein TD. The neuropathology of sport. Acta Neuropathol 2014; 127: 29–51.
McKee AC, Gavett BE, Stern RA, Nowinski CJ, Cantu RC, Kowall NW, et al. TDP-43 proteinopathy and motor neuron disease in chronic traumatic encephalopathy. J Neuropathol Exp Neurol 2010; 69: 918–29.
McKee AC, Stein TD, Kiernan PT, Alvarez VE. The neuropathology of chronic traumatic encephalopathy. Brain Pathol 2015; 25: 350–64.
McKee AC, Stein TD, Nowinski CJ, Stern RA, Daneshvar DH, Alvarez VE, et al. The spectrum of disease in chronic traumatic encephalopathy. Brain 2013; 136: 43–64.
Menon DK, Schwab K, Wright DW, Maas AI. Position statement: definition of traumatic brain injury. Arch Phys Med Rehabil 2010; 91: 1637–40.
Mez J, Daneshvar DH, Kiernan PT, Abdolmohammadi B, Alvarez VE, Huber BR, et al. Clinicopathological evaluation of chronic traumatic encephalopathy in players of American football. JAMA 2017; 318: 360–70.
Millspaugh J. Dementia pugilistica. US Naval Med Bull 1937; 35: 297–303.
Montenigro PH, Alosco ML, Martin BM, Daneshvar DH, Mez J, Chaisson CE, et al. Cumulative head impact exposure predicts later-life depression, apathy, executive dysfunction, and cognitive impairment in former high school and college football players. J Neurotrauma 2017; 34: 328–40.
Montenigro PH, Baugh CM, Daneshvar DH, Mez J, Budson AE, Au R, et al. Clinical subtypes of chronic traumatic encephalopathy: literature review and proposed research diagnostic criteria for traumatic encephalopathy syndrome. Alz Res Therap 2014; 6: 68.
Moss WC, King MJ, Blackman EG. Skull flexure from blast waves: a mechanism for brain injury with implications for helmet design. Phys Rev Lett 2009; 103: 108702.
Murray PJ, Wynn TA. Protective and pathogenic functions of macrophage subsets. Nat Rev Immunol 2011; 11: 723–37.
Nakamura K, Greenwood A, Binder L, Bigio EH, Denial S, Nicholson L, et al. Proline isomer-specific antibodies reveal the early pathogenic tau conformation in Alzheimer's disease. Cell 2012; 149: 232–44.
Namjoshi DR, Cheng WH, McInnes KA, Martens KM, Carr M, Wilkinson A, et al. Merging pathology with biomechanics using CHIMERA (Closed-Head Impact Model of Engineered Rotational Acceleration): a novel, surgery-free model of traumatic brain injury. Mol Neurodegen 2014; 9: 1.
Nayak D, Roth TL, McGavern DB. Microglia development and function. Ann Rev Immunol 2014; 32: 367–402.
Noble CR, Anderson AT, Barton NR, Bramwell JA, Capps A, Chang MH, et al. ALE3D: An arbitrary lagrangian-eulerian multi-physics

code (No. LLNL-TR-732040). Livermore, CA: Lawrence Livermore National Laboratory (LLNL); 2017.
Omalu B, Hammers JL, Bailes J, Hamilton RL, Kamboh MI, Webster G, et al. Chronic traumatic encephalopathy in an Iraqi war veteran with posttraumatic stress disorder who committed suicide. Neurosurg Focus 2011; 31: E3.
Omalu BI, DeKosky ST, Minster RL, Kamboh MI, Hamilton RL, Wecht CH. Chronic traumatic encephalopathy in a National Football League player. Neurosurgery 2005; 57: 128–34; discussion 134.
Ommaya AK, Gennarelli T. Cerebral concussion and traumatic unconsciousness. Brain 1974; 97: 633–54.
Oppenheimer DR. Microscopic lesions in the brain following head injury. J Neurol Neurosurg Psychiat 1968; 31: 299–306.
Østergaard L, Dreier JP, Hadjikhani N, Jespersen SN, Dirnagl U, Dalkara T. Neurovascular coupling during cortical spreading depolarization and–depression. Stroke 2015; 46: 1392–401.
Parker HL. Traumatic encephalopathy (Punch Drunk') of professional pugilists. J Neurol Psychopathol 1934; 1: 20–8.
Petraglia AL, Plog BA, Dayawansa S, Dashnaw ML, Czerniecka K, Walker CT, et al. The pathophysiology underlying repetitive mild traumatic brain injury in a novel mouse model of chronic traumatic encephalopathy. Surg Neurol Int 2014; 5: 184.
Phimister EG, Tanzi RE. TREM2 and risk of Alzheimer's disease—friend or foe? N Eng J Med 2015; 372: 2564–5.
Pietrobon D, Moskowitz MA. Chaos and commotion in the wake of cortical spreading depression and spreading depolarizations. Nat Rev Neurosci 2014; 15: 379.
Place R, Farovik A, Brockmann M, Eichenbaum H. Bidirectional prefrontal-hippocampal interactions support context-guided memory. Nat Neurosci 2016; 19: 992–4.
Planel E, Krishnamurthy P, Miyasaka T, Liu L, Herman M, Kumar A, et al. Anesthesia-induced hyperphosphorylation detaches 3-repeat tau from microtubules without affecting their stability *in vivo*. J Neurosci 2008; 28: 12798–807.
Planel E, Richter KE, Nolan CE, Finley JE, Liu L, Wen Y, et al. Anesthesia leads to tau hyperphosphorylation through inhibition of phosphatase activity by hypothermia. J Neurosci 2007; 27: 3090–7.
Post A, Hoshizaki TB. Mechanisms of brain impact injuries and their prediction: a review. Trauma 2012; 14: 327–49.
Povlishock JT. The pathophysiology of blood–brain barrier dysfunction due to traumatic brain injury. In: Pardridge WM, editor. Introduction to the blood–brain barrier: methodology, biology and pathology. Cambridge, UK: Cambridge University Press; 1998. p. 441–53.
Povlishock JT, Christman CW. The pathobiology of traumatically induced axonal injury in animals and humans: a review of current thoughts. J Neurotrauma 1995; 12: 555–64.
Prins ML, Alexander D, Giza CC, Hovda DA. Repeated mild traumatic brain injury: mechanisms of cerebral vulnerability. J Neurotrauma 2013; 30: 30–8.
Ravin R, Blank PS, Steinkamp A, Rappaport SM, Ravin N, Bezrukov L, et al. Shear forces during blast, not abrupt changes in pressure alone, generate calcium activity in human brain cells. PLoS One 2012; 7: e39421.
Rawson RA. The binding of T-1824 and structurally related diazo dyes by the plasma proteins. Am J Physiol 1943; 138: 708–17.
Richardson OC, Bane O, Scott ML, Tanner SF, Waterton JC, Sourbron SP, et al. Gadofosveset-based biomarker of tissue albumin concentration technical validation *in vitro* and feasibility *in vivo*. Mag Res Med 2015; 73: 244–53.
Rogers ML, Leong CL, Gowers SA, Samper IC, Jewell SL, Khan A, et al. Simultaneous monitoring of potassium, glucose and lactate during spreading depolarization in the injured human brain–proof of principle of a novel real-time neurochemical analysis system, continuous online microdialysis. J Cereb Blood Flow Metab 2017; 37: 1883–95.
Roozenbeek B, Maas AI, Menon DK. Changing patterns in the epidemiology of traumatic brain injury. Nat Rev Neurol 2013; 9: 231–6.
Ropper AH, Gorson KC. Concussion. N Eng J Med 2007; 356: 166–72.
Ruff RM, Iverson GL, Barth JT, Bush SS, Broshek DK. Recommendations for diagnosing a mild traumatic brain injury: a National Academy of Neuropsychology education paper. Arch Clin Neuropsychol 2009; 24: 3–10.
Russo MV, McGavern DB. Inflammatory neuroprotection following traumatic brain injury. Science 2016; 353: 783–5.
Saber M, Kokiko-Cochran O, Puntambekar S, Lathia J, Lamb B. TREM2 deficiency alters acute macrophage distribution and imparove recovery after TBI. J Neurotrauma 2016; 2016. p. A29–30.
Schmid CD, Sautkulis LN, Danielson PE, Cooper J, Hasel KW, Hilbush BS, et al. Heterogeneous expression of the triggering receptor expressed on myeloid cells-2 on adult murine microglia. J Neurochem 2002; 83: 1309–20.
Semple BD, Lee S, Sadjadi R, Fritz N, Carlson J, Griep C, et al. Repetitive concussions in adolescent athletes–translating clinical and experimental research into perspectives on rehabilitation strategies. Front Neurol 2015; 6: 69.
Sharp DJ, Fleminger S, Powell J. Traumatic brain injury. In: Husain M, Schott JM, editors. Oxford textbook of cognitive neurology and dementia. New York, NY: Oxford University Press; 2016.
Sharp DJ, Jenkins PO. Concussion is confusing us all. Pract Neurol 2015; 15: 172–86.
Shaw NA. The neurophysiology of concussion. Prog Neurobiol 2002; 67: 281–344.
Shenton M, Hamoda H, Schneiderman J, Bouix S, Pasternak O, Rathi Y, et al. A review of magnetic resonance imaging and diffusion tensor imaging findings in mild traumatic brain injury. Brain Imag Behav 2012; 6: 137–92.
Shively SB, Horkayne-Szakaly I, Jones RV, Kelly JP, Armstrong RC, Perl DP. Characterisation of interface astroglial scarring in the human brain after blast exposure: a post-mortem case series. Lancet Neurol 2016; 15: 944–53.
Sigurdsson T, Duvarci S. Hippocampal-prefrontal interactions in cognition, behavior and psychiatric disease. Front Syst Neurosci 2015; 9: 190.
Smith C, Gentleman SM, Leclercq PD, Murray LS, Griffin WST, Graham DI, et al. The neuroinflammatory response in humans after traumatic brain injury. Neuropathol Appl Neurobiol 2013a; 39: 654–66.
Smith DH, Johnson VE, Stewart W. Chronic neuropathologies of single and repetitive TBI: substrates of dementia? Nat Rev Neurol 2013b; 9: 211–21.
Smith IT, Townsend LB, Huh R, Zhu H, Smith SL. Stream-dependent development of higher visual cortical areas. Nat Neurosci 2017; 20: 200–8.
Spear LP. Adolescent brain development and animal models. Ann N Y Acad Sci 2004; 1021: 23–6.
Stamm JM, Bourlas AP, Baugh CM, Fritts NG, Daneshvar DH, Martin BM, et al. Age of first exposure to football and later-life cognitive impairment in former NFL players. Neurology 2015; 84: 1114–20.
Statler KD, Alexander H, Vagni V, Dixon CE, Clark RS, Jenkins L, et al. Comparison of seven anesthetic agents on outcome after experimental traumatic brain injury in adult, male rats. J Neurotrauma 2006; 23: 97–108.
Stein TD, Alvarez VE, McKee AC. Concussion in chronic traumatic encephalopathy. Curr Pain Headache Rep 2015a; 19: 47.
Stein TD, Montenigro PH, Alvarez VE, Xia W, Crary JF, Tripodis Y, et al. Beta-amyloid deposition in chronic traumatic encephalopathy. Acta Neuropathol 2015b; 130: 21–34.
Strich SJ. Diffuse degeneration of the cerebral white matter in severe dementia following head injury. J Neurol Neurosurg Psychiatry 1956; 19: 163–85.

Strich SJ. Shearing of nerve fibres as a cause of brain damage due to head injury: a pathological study of twenty cases. Lancet 1961; 2: 443–8.

Strich SJ. Lesions in the cerebral hemispheres after blunt head injury. J Clin Pathol Suppl (R Coll Pathol) 1970; 4: 166–71.

Suarez SD, Gallup GG. An ethological analysis of open-field behavior in rats and mice. Learn Motiv 1981; 12: 342–63.

Sukoff Rizzo SJ, Crawley JN. Behavioral phenotyping assays for genetic mouse models of neurodevelopmental, neurodegenerative, and psychiatric disorders. Ann Rev Anim Biosci 2017; 5: 371–89.

Sunderkötter C, Nikolic T, Dillon MJ, Van Rooijen N, Stehling M, Drevets DA, et al. Subpopulations of mouse blood monocytes differ in maturation stage and inflammatory response. J Immunol 2004; 172: 4410–7.

Sweatt JD. Neural plasticity and behavior–sixty years of conceptual advances. J Neurochem 2016; 139 (Suppl 2), 179–99.

Sydow A, Van der Jeugd A, Zheng F, Ahmed T, Balschun D, Petrova O, et al. Tau-induced defects in synaptic plasticity, learning, and memory are reversible in transgenic mice after switching off the toxic Tau mutant. J Neurosci 2011; 31: 2511–25.

Talavage TM, Nauman EA, Breedlove EL, Yoruk U, Dye AE, Morigaki KE, et al. Functionally-detected cognitive impairment in high school football players without clinically-diagnosed concussion. J Neurotrauma 2014; 31: 327–38.

Terwilliger VK, Pratson L, Vaughan CG, Gioia GA. Additional post-concussion impact exposure may affect recovery in adolescent athletes. J Neurotrauma 2016; 33: 761–5.

Tomkins O, Friedman O, Ivens S, Reiffurth C, Major S, Dreier JP, et al. Blood-brain barrier disruption results in delayed functional and structural alterations in the rat neocortex. Neurobiol Dis 2007; 25: 367–77.

Ulrich JD, Holtzman DM. TREM2 Function in Alzheimer's disease and neurodegeneration. ACS Chem Neurosci 2016; 7: 420–7.

Vazana U, Veksler R, Pell GS, Prager O, Fassler M, Chassidim Y, et al. Glutamate-mediated blood-brain barrier opening: Implications for neuroprotection and drug delivery. J Neurosci 2016; 36: 7727–39.

Veksler R, Shelef I, Friedman A. Blood-brain barrier imaging in human neuropathologies. Arch Med Res 2014; 45: 646–52.

Walker AE, Kollros JJ, Case TJ. The physiological basis of concussion. J Neurosurg 1944; 1: 103–16.

Walsh RN, Cummins RA. The open-field test: a critical review. Psychol Bull 1976; 83: 482–504.

Wang Y, Cella M, Mallinson K, Ulrich JD, Young KL, Robinette ML, et al. TREM2 lipid sensing sustains the microglial response in an Alzheimer's disease model. Cell 2015; 160: 1061–71.

Weissberg I, Veksler R, Kamintsky L, Saar-Ashkenazy R, Milikovsky DZ, Shelef I, et al. Imaging blood-brain barrier dysfunction in football players. JAMA Neurol 2014; 71: 1453–5.

Weissberg I, Wood L, Kamintsky L, Vazquez O, Milikovsky DZ, Alexander A, et al. Albumin induces excitatory synaptogenesis through astrocytic TGF-β/ALK5 signaling in a model of acquired epilepsy following blood–brain barrier dysfunction. Neurobiol Dis 2015; 78: 115–25.

Whittington RA, Bretteville A, Dickler MF, Planel E. Anesthesia and tau pathology. Prog Neuropsychopharmacol Biol Psychiat 2013; 47: 147–55.

Woerman AL, Aoyagi A, Patel S, Kazmi SA, Lobach I, Grinberg LT, et al. Tau prions from Alzheimer's disease and chronic traumatic encephalopathy patients propagate in cultured cells. Proc Nat Acad Sci USA 2016; 113: 8187–96.

Wojnarowicz MW, Fisher AM, Minaeva O, Goldstein LE. Considerations for experimental animal models of concussion, traumatic brain injury, and chronic traumatic encephalopathy—these matters matter. Front Neurol 2017; 8: 1–14.

Wu JW, Hussaini SA, Bastille IM, Rodriguez GA, Mrejeru A, Rilett K, et al. Neuronal activity enhances tau propagation and tau pathology *in vivo*. Nat Neurosci 2016; 19: 1085–92.

Xu W, Südhof TC. A neural circuit for memory specificity and generalization. Science 2013; 339: 1290–5.

Yoshino A, Hovda DA, Kawamata T, Katayama Y, Becker DP. Dynamic changes in local cerebral glucose utilization following cerebral concussion in rats: evidence of a hyper-and subsequent hypometabolic state. Brain Res 1991; 561: 106–19.